PHYSICAL OCEANOGRAPHIC MEASUREMENTS IN THE NORTHEASTERHN CHUKCHI SEA: 2012

Prepared for

ConocoPhillips, Inc.
P.O. Box 100360
Anchorage, AK 99510-0360

Shell Exploration & Production Company
3601 C Street, Suite 1000
Anchorage, AK 99503

and

Statoil USA E&P, Inc.
3800 Centerpoint Drive, Suite 920
Anchorage, AK 99502

FINAL REPORT

Prepared by

Thomas Weingartner, Seth Danielson, Liz Dobbins, and Rachel Potter

Institute of Marine Science
University of Alaska
Fairbanks, AK 99775

July 2013

Introduction

This report provides a partial synopsis of the data set collected in summer 2012 from the northeastern Chukchi Sea in areas potentially subject to and influenced by offshore oil exploration activities. Prior years' data and interpretations were summarized in previous reports and most recently by the synthesis of Weingartner et al. (2013a) and will not be repeated in detail herein.

As noted previously seasonal changes in Chukchi Sea water properties are established by the annual cycles of sea-ice formation and ablation, air-sea heating/cooling and wind mixing, and transport of waters from Bering Strait. In summer and early fall, the Strait transport is northward on average and includes three major water masses, which following the nomenclature of Coachman et al. (1975) and Walsh et al. (1989) are: cold, salty, nutrient-rich Anadyr Water; warm, fresh, nutrient-poor Alaskan Coastal Water (ACW); and Bering Shelf Water (BSW). The latter has properties intermediate between, but nonetheless distinct from, the Anadyr and Alaskan Coastal water masses. Coachman et al. (1975) maintain that the Anadyr and Bering Shelf water masses mix to form BSW north of the Strait, whereas ACW maintains its properties on the Chukchi shelf. In summer and fall, Chukchi bottom waters often include near-freezing, saline (dense) waters that formed in winter by freezing over both the Bering and Chukchi seas. In addition, shallow plumes of cool, dilute, surface waters, formed by ice melt, may also be present.

Figure 1 illustrates the mean circulation over the shelf based on the model of Spall (2007), which largely agrees with the inferences drawn from the observations. Although the mean flow is nominally northward over much of the shelf, the bulk of the transport proceeds along three principal pathways with each pathway associated with a distinct bathymetric feature; Herald Canyon, the Central Channel, and Barrow Canyon. The troughs are separated from one another by shoals: Herald Shoal separates Herald Canyon from the Central Channel and Hanna Shoal lies between Barrow Canyon and the Central Channel.

BSW is transported to the northwest Chukchi, over the central shelf, and northward through the Central Channel (Fig. 1a; Weingartner et al., 2005; Woodgate et al., 2005). Weingartner et al. (2005) and Weingartner et al. (2013a) suggest that, south of Hanna Shoal, some central-shelf waters flow eastward toward the coast, in agreement with the circulation models of Winsor and Chapman (2004) and Spall (2008). North of the Central Channel, where there are no long-term current measurements, both models suggest the average flow follows the bathymetry around the western and northern flanks of Hanna Shoal before turning southward along the eastern side of the Shoal before eventually entering Barrow Canyon. However, the models also predict that some of the water along the eastern flank of Hanna Shoal penetrates southwestward along the southern flank of the Shoal before turning eastward towards the coast. ACW flows northeastward within the Alaskan Coastal Current toward the head of Barrow Canyon. Here it merges with waters flowing eastward from the central shelf to form the canyon outflow. Hence in summer and fall, the canyon outflow contains a horizontally- and vertically-structured complex of water masses (Pickart et al., 2005; Shroyer and Plueddemann, 2012) that include ACW, meltwater, dense residual winter waters, BSW, and mixtures of each.

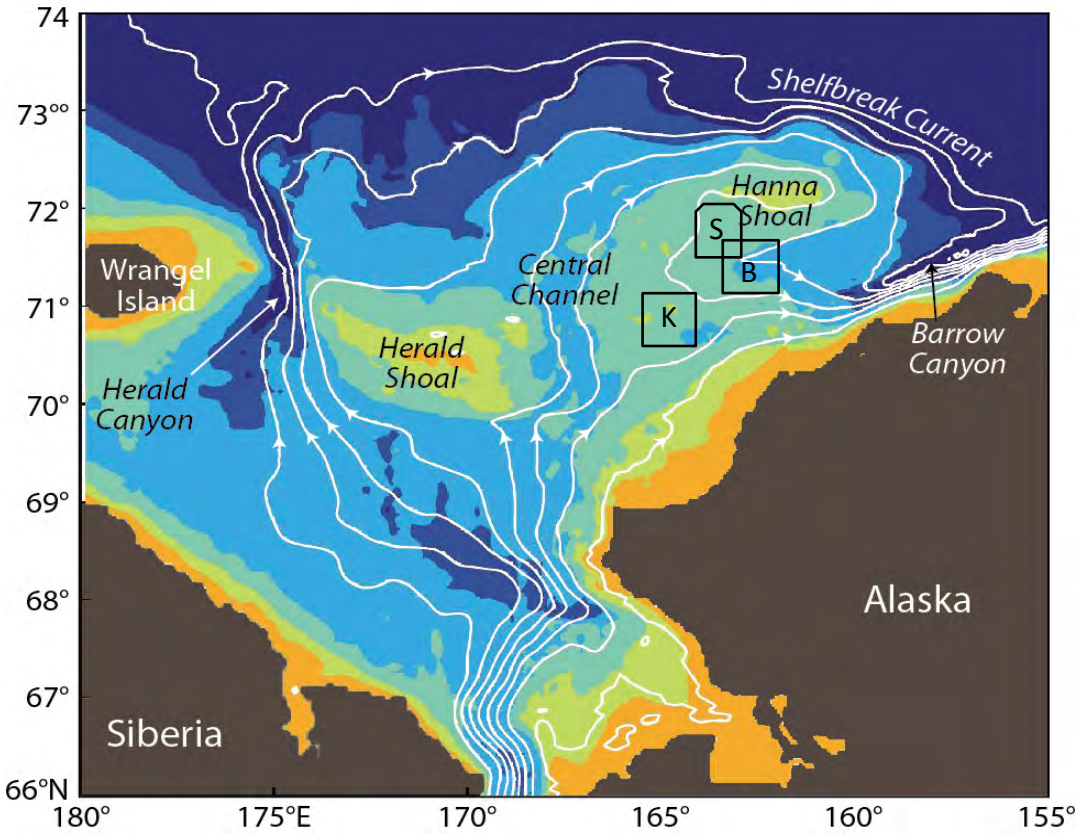

Figure 1. Mean depth-integrated streamlines (white lines) in the Chukchi Sea, after Spall, (2007). The bathymetry is colored and major bathymetric features are labeled. The lettered boxes denote the approximate locations of the Klondike (K), Burger (B), and Statoil (S) survey areas.

Two further aspects of the circulation depicted in Figure 1 deserve further emphasis. First, note the streamline intersecting the Statoil survey area. The model results indicate that the flow here is southward through Statoil before veering eastward along the northern edge of the Klondike survey area. Weingartner et al. (2013a) suggest that the flow across Statoil is southeastward at least over the western half of Statoil, with this flow then merging with an eastward flow emanating from Klondike. It appears that these flows converge along the southern half of Burger. Second, the acute curvature of the streamline in Burger implies that water is being carried from the eastern side of Hanna Shoal into Burger before turning back eastward toward the coast. That flow would advect meltwater in the upper water column as well as dense, winter water in the lower portion of the water column. Weingartner et al. (2013a) infer that this model prediction is correct, at least intermittently. The implications of these findings are that in summer BSW flows eastward from the Central Channel across both Klondike and the western half of Statoil. This flow then converges with the waters entering Burger from the northeast. Eventually all of these water masses flow eastward and enter Barrow Canyon. The conclusions of Weingartner et al. (2013a) are, to some extent further supported by the data collected in summer 2012 and discussed below.

Methods

The sampling discussed in this report was in the northeast Chukchi Sea and included repeated surveys in the Klondike, Burger and Statoil study areas and over a much broader region surrounding these areas (**Figure 2**). Note that the Klondike study area lies to the east of the Central Channel, whereas Statoil is along the southwest flank of Hanna Shoal and Burger is on the southern flank of this shoal. Water depths in the region are ~40 – 45 m.

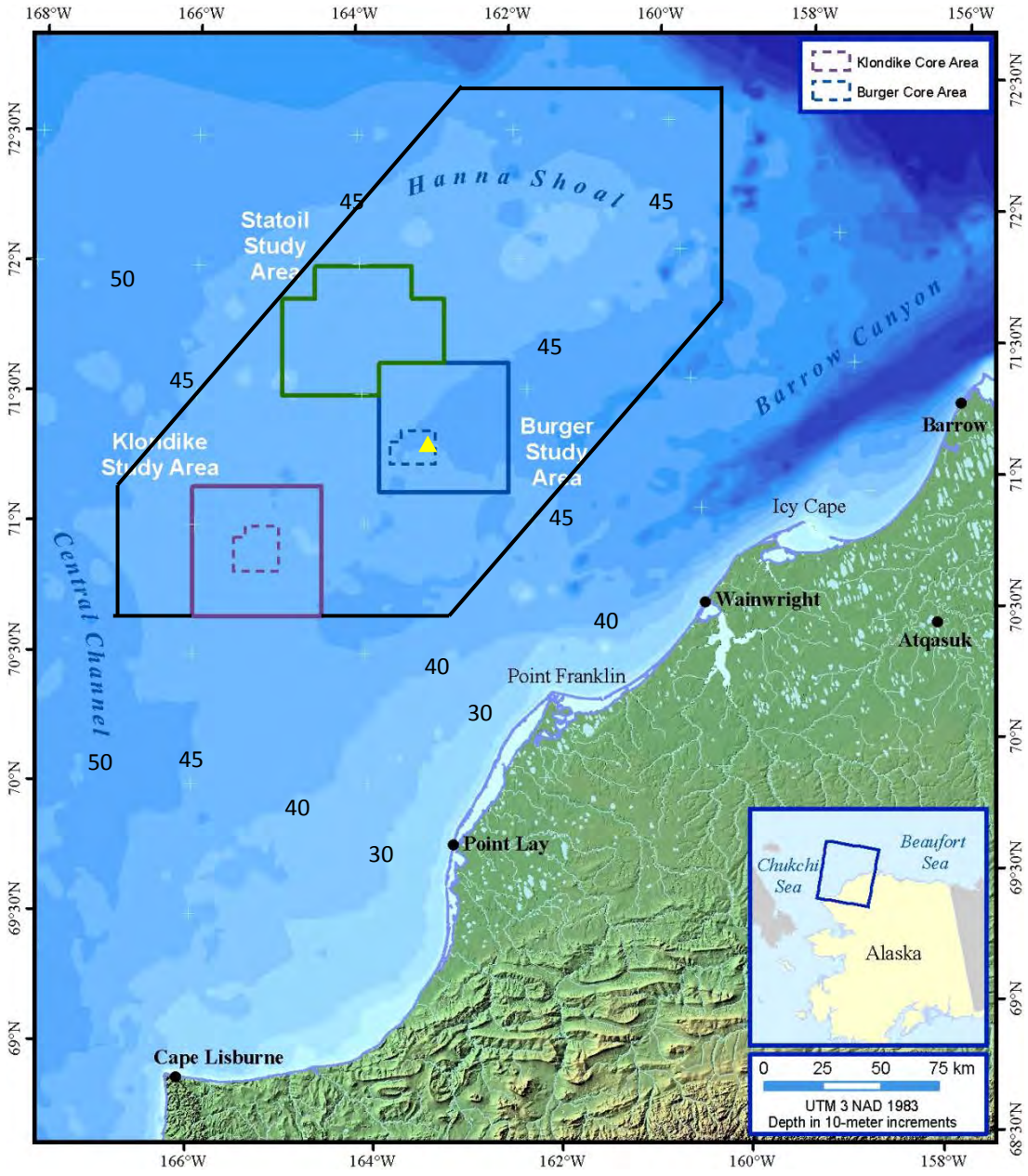

Figure 2. Map showing locations of the Klondike, Burger, and Statoil study areas in relation to the Alaskan coast. The yellow triangle shows the approximate location of the NCEP-NARR meteorological grid point used to assess the regional winds. The black line encompasses the sampling conducted within the regional survey between 31 August and 4 October 2012.

Conductivity-temperature-depth (pressure) data were collected with a Seabird, Inc. SBE-19+V2 CTD sampling at 4 Hz. The system also included a fluorometer and transmissometer. The instrument was lowered throughout the water column at a rate of ~0.5m min^{-1} so that ~480 samples m^{-1} was obtained. Measured variables include pressure, temperature, conductivity, beam transmission, and fluorescence. Derived variables include depth, salinity, density and speed of sound. The data were processed according to the manufacturer's recommended procedures [provided in the SBE Data Processing manual) and further screened for anomalous spikes, dropouts and density inversions. Data were averaged to 1 decibar (approximately 1 meter) vertical profiles. Post-season calibrations of the temperature and conductivity cells were performed at the manufacturer's calibration facility. Comparison of the pre- and post-calibration values indicated that the temperature data are accurate to better than 0.005 °C and salinity to 0.02.

The stations occupied during the two survey cruises are shown in **Figure 3**, with the color shading indicating the Julian day of the sampling. The 16 26 August survey sampling (Cruise T2) began at Klondike, then moved to Burger for a few days before returning to Klondike. Afterwards the ship began sampling in Statoil. However, ice advance (and retreat) required that the ship move opportunistically back and forth between Burger and Statoil to complete the sampling. The broad-scale survey commenced on August 31 at the eastern end of Klondike and then captured stations at the western end before heading north into Statoil. Sampling then proceeded eastward along the southern limit of the ice edge and then into the western half of Burger. Thereafter the remaining stations were occupied as ice conditions permitted. Stations along the northern side of the broader region were occupied toward the end of the cruise. Thus sampling was followed by a return to Klondike and Burger to sample the remaining stations. We present these sampling times to emphasize that the results cannot be considered synoptic given

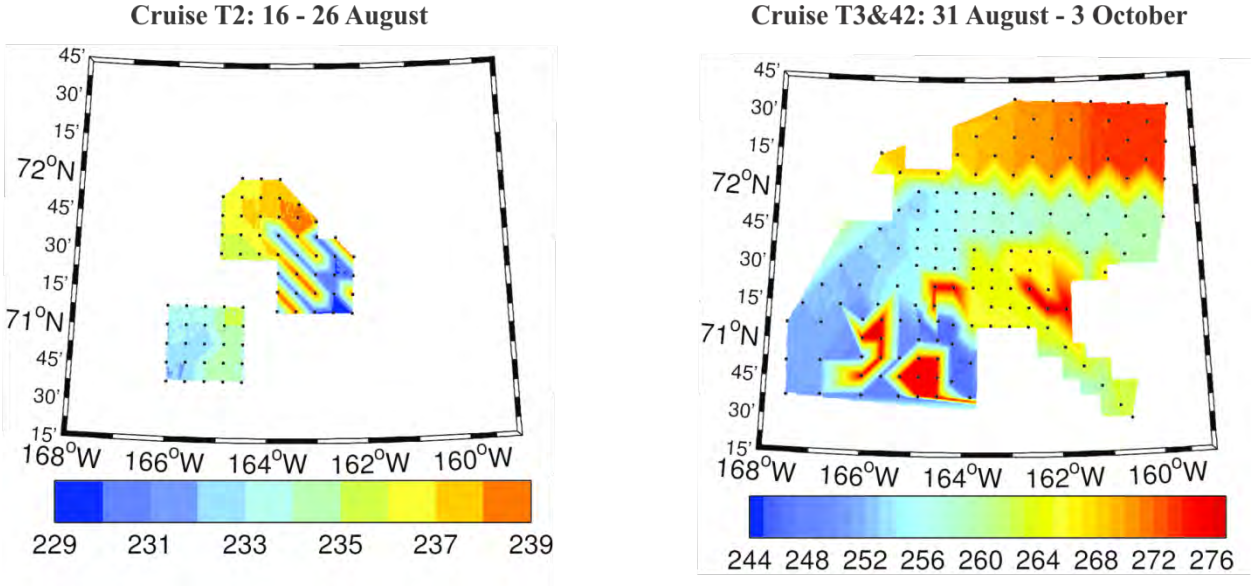

Figure 3. Contours showing the Julian day of year of CTD station occupations during the 2012 cruises.

the time differences in the sampling. This holds especially for the second cruise, in which the last station was occupied 32 days after the first station. The results presented below may be temporally aliased because of the lack of synopticity. Thus interpretations should be viewed with respect to this caveat.

Winds

We used 3-hourly winds produced by the National Center for Environmental Prediction North American Regional Re-analysis (NARR) model hindcasts (Mesinger et al., 2006). The NARR wind grid point used in our analysis is taken from within Klondike and is representative of conditions over the northeastern Chukchi Sea shelf.

ADCP data quality and processing summary

A 600-KHz Teledyne-RDI acoustic Doppler current profiler (ADCP) was operated during the 2012 Chukchi field season. Setup, operating parameters, transformations and error-screening procedures are listed in the **Tables 1** and **2**. Initial data screenings were performed using the TRDI software package VmDAS. Final data assessment and transformations were made in the MATLAB programming language with custom software. Data QA/QC parameters are listed in **Table 3**. *Note that unlike previous years, the system was not set to collect data in the bottom-track mode in 2012.* This shipboard operations oversight resulted in having to reference all water velocities to the GPS navigation, rather than the ADCP's own measurement of motion relative to the bottom. Additionally, the lack of bottom track pings resulted in no water depth measurements by the ADCP. Data quality was not strongly affected because the GPS feed was generally of good quality through the season. However, the change in approach required us to apply somewhat more conservative limits in identifying and rejecting suspicious data. After evaluating each 1-minute ensemble, consisting of 60 1-second pings, the data were averaged into 6-hour

Table 1. ADCP Setup and Navigation parameters.

System	Teledyne RDI Workhorse
Frequency	600KHz
Installation	Vessel-attached pole-mount
Orientation	Downward
Operating mode	Broadband
Bottom Track	***No***
Time per ping	1 s
Number of bins:	25
Bin size	2 m
Blanking Distance	0.88 m
Transducer Depth	3 m
Ship position	NMEA1 GGA
Ship speed	NMEA2 VTG
Tilt source	ADCP internal tilt sensor
Heading source:	NMEA1 HDT
Alignment Error:	45^{o}

bins and plotted. **Figure 4** shows the temporal distribution of the 6-hourly averaged ensembles for the 10 August - 4 October period. In order to form a 6-hour average we require that at least 25% of the ensembles collected during that 6-hour period have good data. Time series of the percent good, error and vertical velocity time series as a function of depth and 6-hour averaged ensemble are shown in **Figure 5.** Inspection of these data suggested that the first depth bin which yielded reliably acceptable data was 11 m below the surface. Velocities were also depth-averaged into 2-m deep bins.

Overall data quality was good, although there were periods with data gaps (**Figures 4 and 5**) caused by rough seas or other interruptions in data collection. This can result in loss of bottom-tracking and/or interference due to bubble entrainment below the transducer. Vessel speed and orientation with respect to direction of the surface wave field may also impact data quality. In general, data quality decreases if the vessel is heading into heavy seas. Again, the interpretation of these data is hampered by the lack of synopticity.

Table 2. VmDAS averaging and data screening thresholds.

STA average interval	60s
Profile Ping Normalization reference layer	Bins 3 - 10
Water Current Profile Received Signal Strength Indicator	30 counts
Water Current Profile Correlation	180 counts
Water Current Profile Error Velocity	1 m/s
Water Current Profile Vertical Velocity	1 m/s
Water Current Profile Fish target	50 counts
Water Current Profile Percent Good	50%

Table 3. QA/QC thresholds and corrections applied to 1-minute STA ensembles.

Minimum correlation	64
Minimum percent-good 4-beam + 3-beam solutions	80%
Minimum percent-good bottom track pings	25%
Blanking above bottom (% of distance to transducer)	6%
Maximum heading standard deviation	3
Maximum change in speed	0.2 m/s
Minimum speed	1.5 m/s
Maximum vertical velocity	0.1 m/s
Maximum error velocity	0.05 m/s
Minimum good fraction of water profile allowed	2/3
Individual ensemble cross-track magnitude/direction corrections	Yes
Transducer mis-alignment correction	4.05°
Ensembles removed with unrealistically large mean velocity (> 1.5 m/s)	Yes
Removed adjacent ensembles with unrealistically large change in velocity	Yes
Truncated bins based on largest/smallest	0.25% outliers
Maximum bin depth	35 m

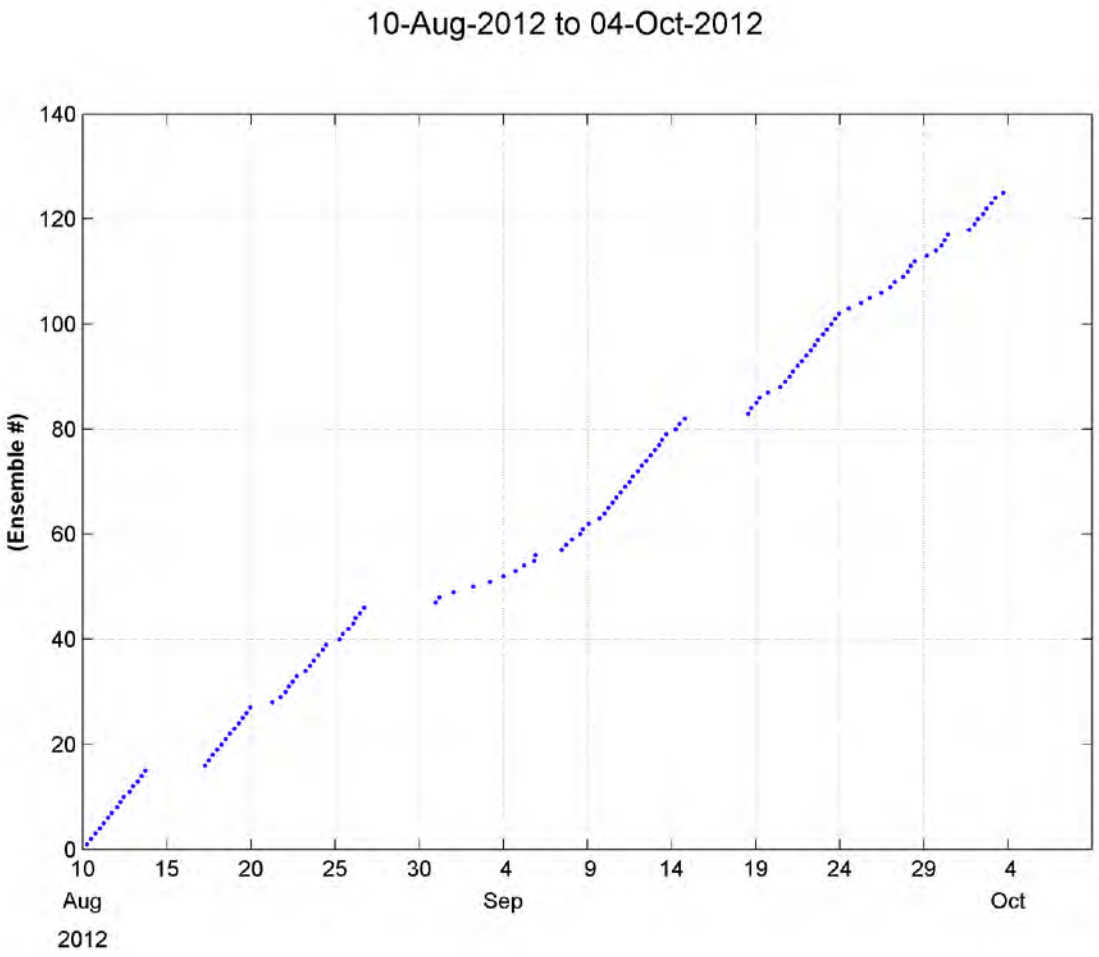

Figure 4. Temporal distribution of final 6-hourly averaged vessel-mounted ADCP data ensembles for the period 10 August through 4 October. Data gaps are indicated by the absence of dots and are associated with poor data quality due to heavy seas, GPS interruptionss, and/or sampling downtime between cruises.

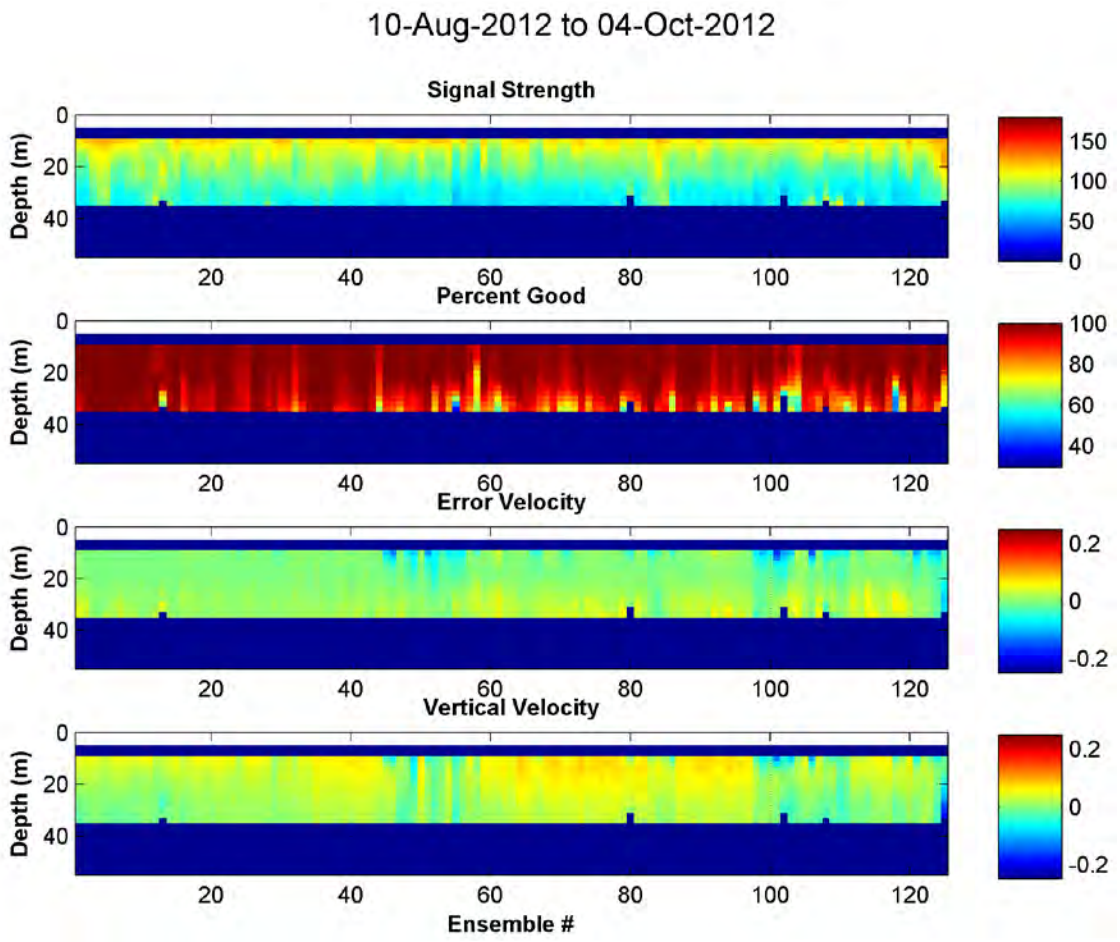

Figure 5. From top-to-bottom, ADCP signal strength, percent good, error velocity and vertical velocity of the 6-hourly averaged ensembles for 10 August – 4 October, 2012.

Results

Winds 2008 - 2012

Figure 6 shows time series of the 3-hourly wind vectors from 1 June through 15 October from 2008 – 2012 from the NARR gridpoint within Klondike (similar results hold for both Klondike and Statoil). In 2008 winds were from the northeast at 5 - 10 m s^{-1} (10 – 20 kts) from early July through early October except for a brief period of southwest winds in late July. In 2009, winds were from the northeast through July and then generally mild or from the southwest through early September. However, strong northeasterlies developed by the second week of September and these remained strong until mid-October. In 2010, moderate northeasterlies prevailed in June, but in comparison to the other years, the winds from July through September were variable and weaker. In 2011, winds were primarily from the northeast from June through mid-October with only brief interludes of winds from the southern quadrant. By contrast, the winds from June through August 2012 blew primarily from southerly quadrants with speeds of between 5 and 10 m s^{-1}. Only in early September 2012 did the winds become northeasterly with wind speeds between 5 and 10 m s^{-1}.

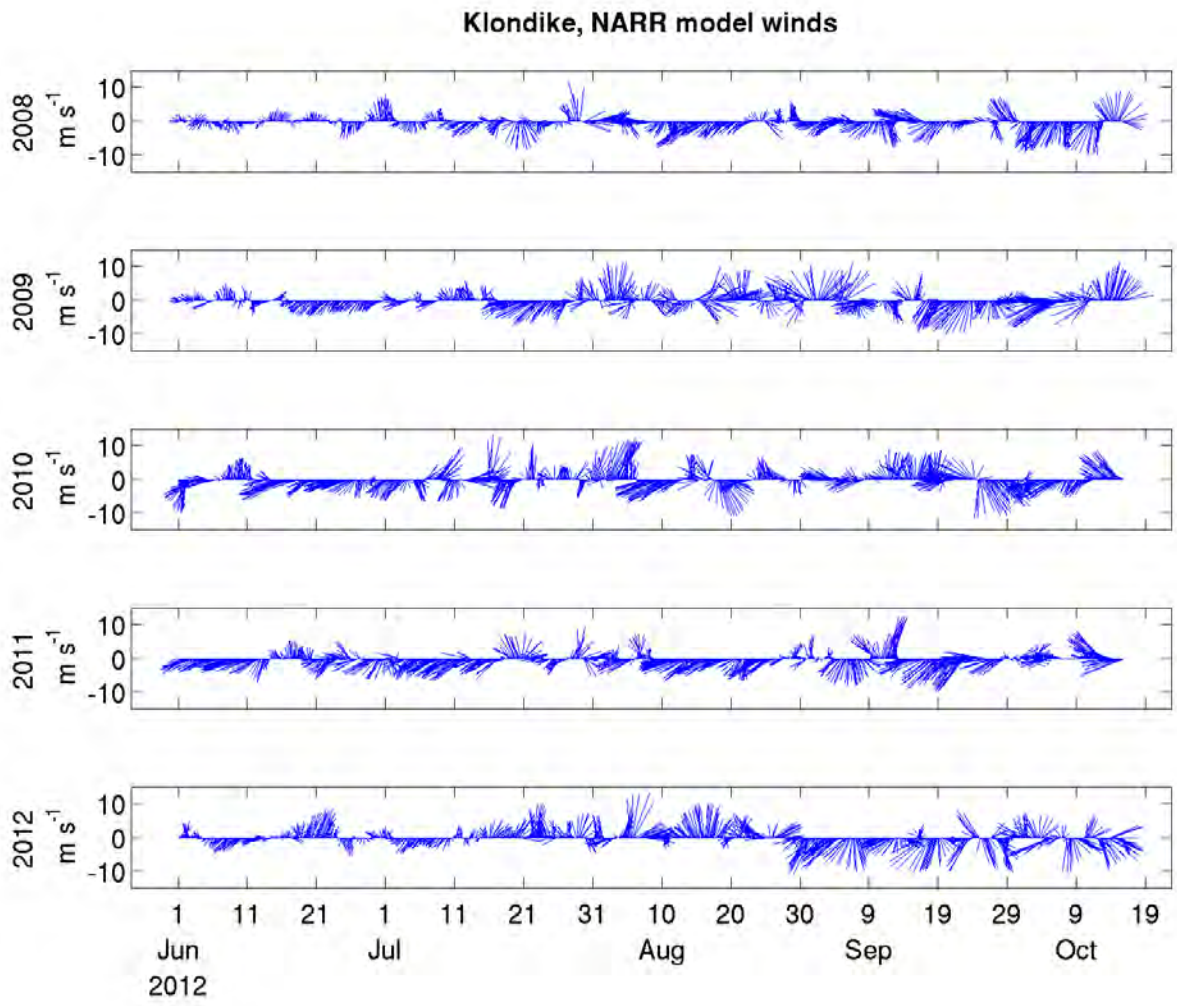

Figure 6. Time series of 3-hourly wind vectors for 2008 (top) through 2012 (bottom). The vectors are oriented in the direction toward which the wind is blowing, with True North toward the top of the page. The length of the vector is proportional to the wind speed.

Sea-ice concentrations

The seasonal distribution and retreat of sea ice also varied among the years. In 2008 and 2010, ice first began retreating off the northwest coast of Alaska in early May due to strong westward winds. This retreat subsequently merged with a retreat that propagated northward from Bering Strait so that the two open water areas joined in late June. In 2009, the retreat started from Bering Strait and spread northwestward along the Chukotkan coast and into the central Chukchi Sea, with ice only retreating from the northwest coast of Alaska in late June. The 2011 ice retreat involved coincidental retreats from both the Bering Strait region and the northwest coast of Alaska, although the northward rate of retreat in 2011 was more rapid across the Chukchi Sea compared to previous years.

We have explored these retreat patterns in a climatological sense by examining statistical patterns of ice concentration (based on empirical orthogonal modes, EOFs) for each month of the year since 1979 (when daily satellite-derived sea ice concentration maps first became available

routinely). Our findings, while preliminary, indicate three principal modes of May ice retreat and their variation through time (**Figure 7**). The dominant mode (which accounts for 48% of the variance in May ice concentrations) corresponds to northward ice retreat and/or disintegration from Bering Strait. The next mode (accounting for 27% of the variance) yields a pattern in which changes in ice concentration along the northwest coast of Alaska are out-of-phase with concentrations along the Chukotkan coast. This is as expected because as westward winds drive ice offshore of northwest Alaska the same winds pile it up along the Chukotkan coast. The third mode (~7% of the variance) indicates that ice concentrations offshore of the Chukotkan and Alaskan coasts are in-phase with one another, but out-of-phase with ice concentrations north of Bering Strait. The time-amplitude function (lower panel of **Figure 7**) indicates that mode 2 had large amplitudes in 2008 and 2010 (with reduced ice concentrations along the Alaskan coast), whereas this mode was large in 2009 (heavy ice concentrations in Alaska, but light concentrations along Siberia). Both modes 1 and 2 contributed in 2011. When viewed over the entire record, the amplitudes of Mode 2 in the 2008 – 2010 period were among the largest observed, while the largest amplitudes in Mode 1 occurred in the periods from 1980 – 1985 and 19955 - 2005. Note however that in 2012 the first three modes all had small weights, suggesting that the ice retreat in May 2012 was substantially different when compared to the entire record. We illustrate this further using ice concentration data in May, June, and July 2012 (**Figure 8)** using the Special Sensor Microwave Imager (SSMI) satellite sensor and processed according to Spreen et al., (2008). The sequence of maps provides a broader perspective of the seasonal evolution in sea ice retreat over the Chukchi shelf prior to the 2012 vessel surveys.

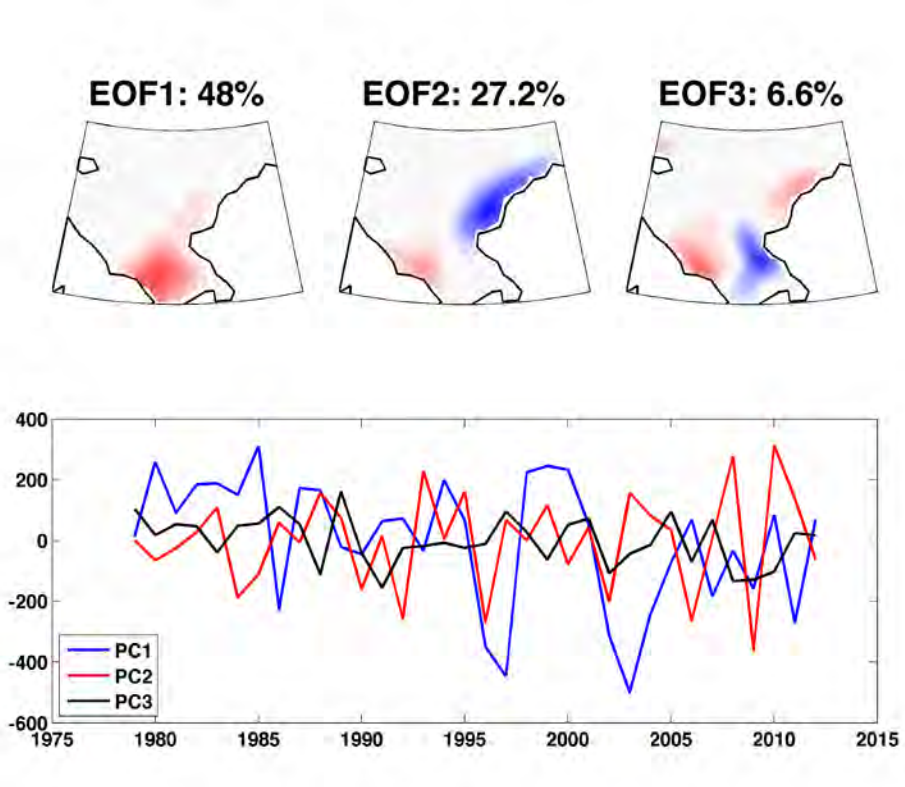

Figure 7. The upper panels shows the structure of the first three empirical orthogonal modes of May sea ice concentrations in the Chukchi Sea based on 1979 – 2012 satellite-derived sea ice concentration maps. The lower panel shows the temporal variation in mode weights.

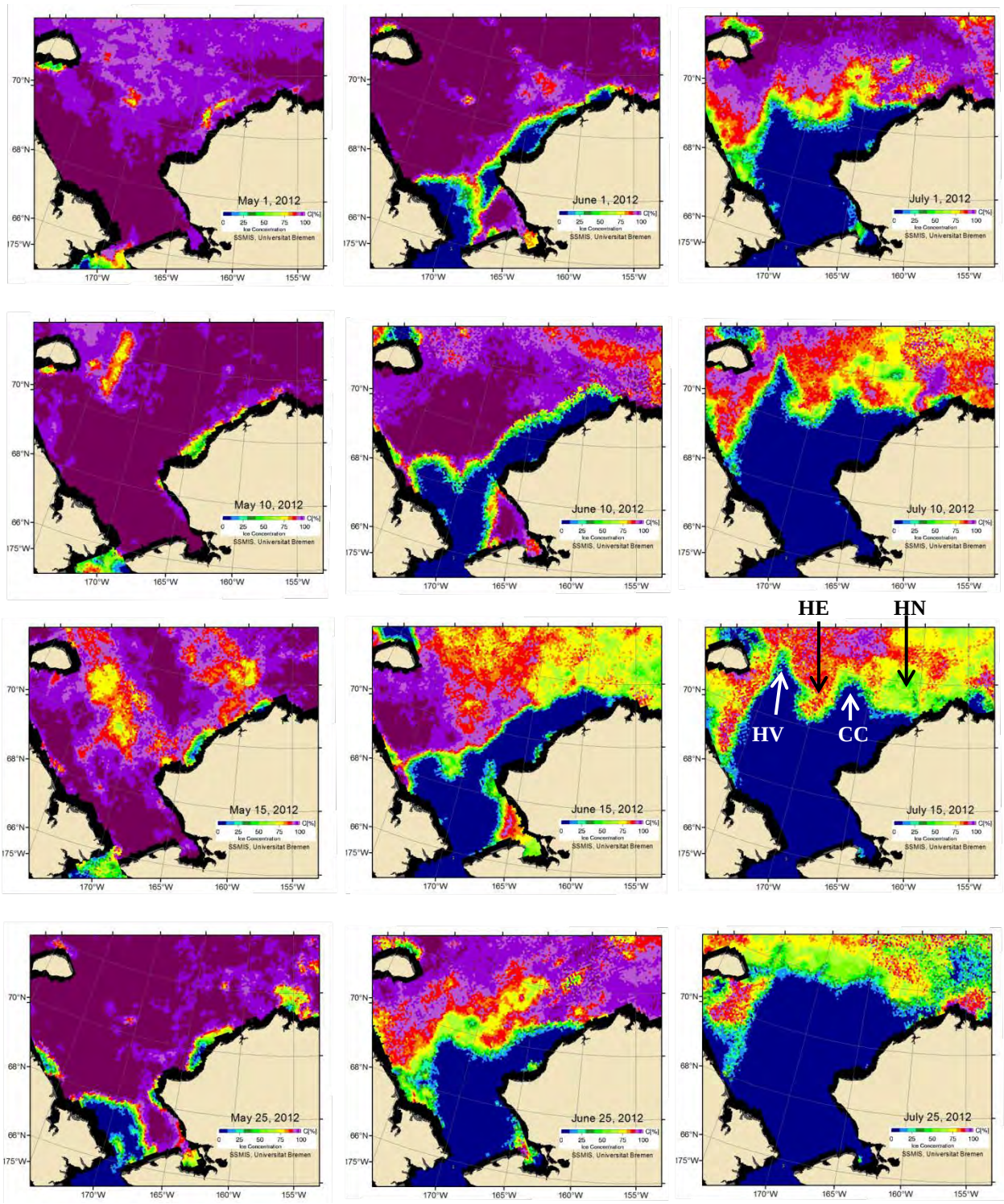

Figure 8. Sea ice concentration maps in 2012 for May (left), June (middle), and July (right). The labels on the July 15 map refer to Hanna (HN) and Herald (HE) shoals, the Central Channel (CC), and Herald Valley (HV).

In 2012, substantial ice retreat only began in Bering Strait in late May; ~2 weeks later than in the previous survey years. This delay may have been due to the extensive ice cover formed over the Bering Sea during the previous winter. It appears that the sluggish onset of retreat in May 2012 is responsible for the apparenlty low EOF weights (cf. **Figure 7**). Ice retreat through June continued at a much slower rate than in previous years, with the retreat occurring primarily along both the northwest coast of Alaska and north of Bering Strait (with the exception of the bight between the Seward and Lisburne peninsulas). There was, in fact, relatively little overall retreat between June 10 and June 25 even though the winds were weak and, on average, from the south (**Figure 6**). Ice retreat accelerated in July with the formation of the typical ice edge embayments forming over Herald Valley and the Central Channel by mid-July, while heavy ice concentrations remained over Herald and Hanna shoals.

We next consider the evolution of sea-ice concentrations over the northeast Chukchi Sea, including the survey areas, for the period of late July – late September 2012. This discussion is based on the ice concentration maps shown in **Figures 9 – 16** (all prepared by R. Zawislak and courtesy of Fairweather Science). Overlain on the ice maps are the sampling regions occupied in August and early October 2012. **Figure 9** includes two maps from July which show that ice concentrations >90% occupied most of the sampling areas as well as Herald and Hanna Shoal. Reduced ice concentrations occurred in the Central Channel. Note that this heavy ice cover was limited to the Chukchi Sea as there was very little ice to the east in the Beaufort Sea. Although not shown in these maps, heavy ice also extended to the west (at least as far as Wrangel Island) based on proprietary synthetic aperture radar imagery (available to the lead author during an August 2012 cruise aboard the USCG *Healy*). By late July ice concentrations diminished over Herald Shoal and the Central Channel and Klondike, whereas Hanna Shoal, Statoil, and Burger still had concentrations > 70% (**Figure 10**). Ice continued to diminish through mid-August (**Figure 11**), albeit slowly, with Burger and Statoil having concentrations of 10 – 50%. By 21 August (**Figure 12**) Herald Shoal and the survey areas were nearly ice-free, although heavy concentrations of ice occasionally drifted southward over both Statoil and Burger. During this same period ice concentrations in the western Beaufort Sea were 10 - 30% and that these concentrations moved westward through time. (The eastern Beaufort Sea was ice-free by this time.) By late August (**Figure 13**), the heaviest ice concentrations were confined to Hanna Shoal (and to the northern portion of the shelf west of the Central Channel) and along the northern boundaries of Statoil and Burger. Thereafter, ice rapidly decayed (**Figures 14 and 15**), although modest concentrations remained over Hanna Shoal until late September (**Figure 16**). The 2012 seasonal evolution of sea ice contrasted markedly with the previous years surveyed in which ice was virtually absent over Hanna Shoal by mid- to late August.

This difference in summer ice retreat over the northeast Chukchi Sea between 2012 and previous years appears related to a large mass of multi-year ice that moved into the northern Chukchi Sea and grounded over Hanna Shoal during the 2011/2012 winter. We suggest that over the winter the grounded ice accumulated first-year ice that drifted onto the Chukchi Sea shelf through winter and subsequently deformed and attached to the grounded ice. Hence relative to prior survey years, the 2012 summer sea ice was less mobile, thicker, present in substantially higher concentrations and therefore persisted longer.

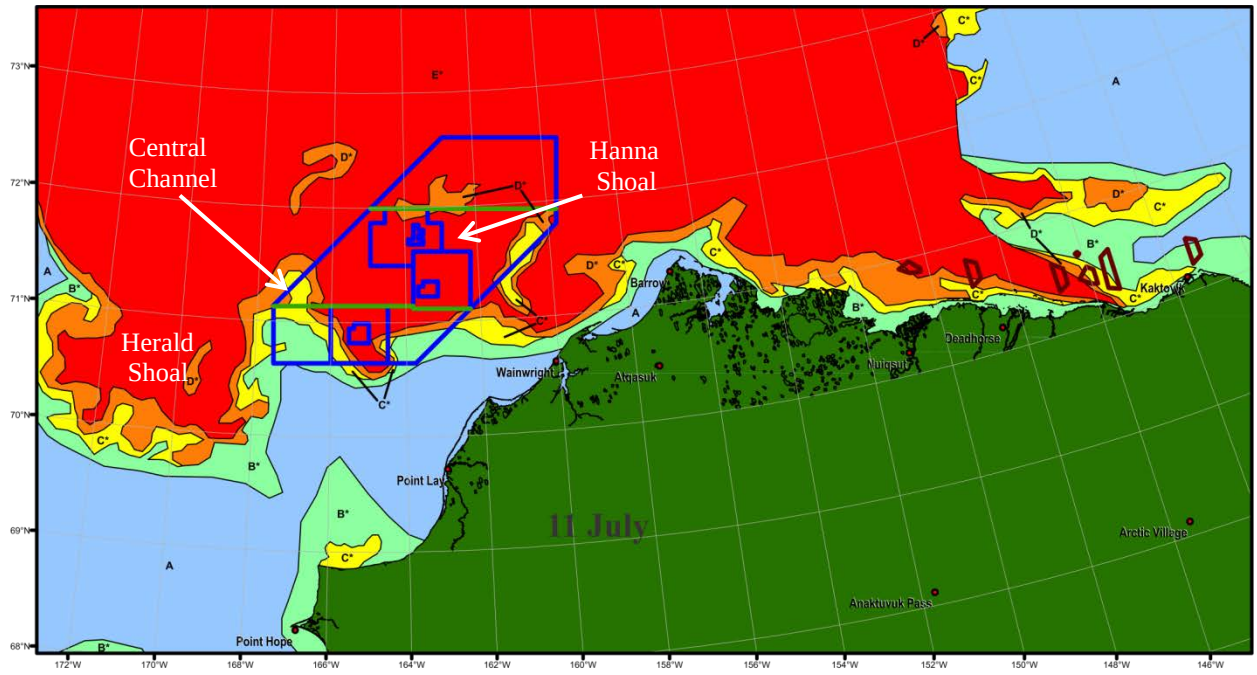

Ice concentrations: "A" <10%, "B" 10 - 30%, "C" 40 - 60%, "D" 70 - 80%, "E" 90 - 100%

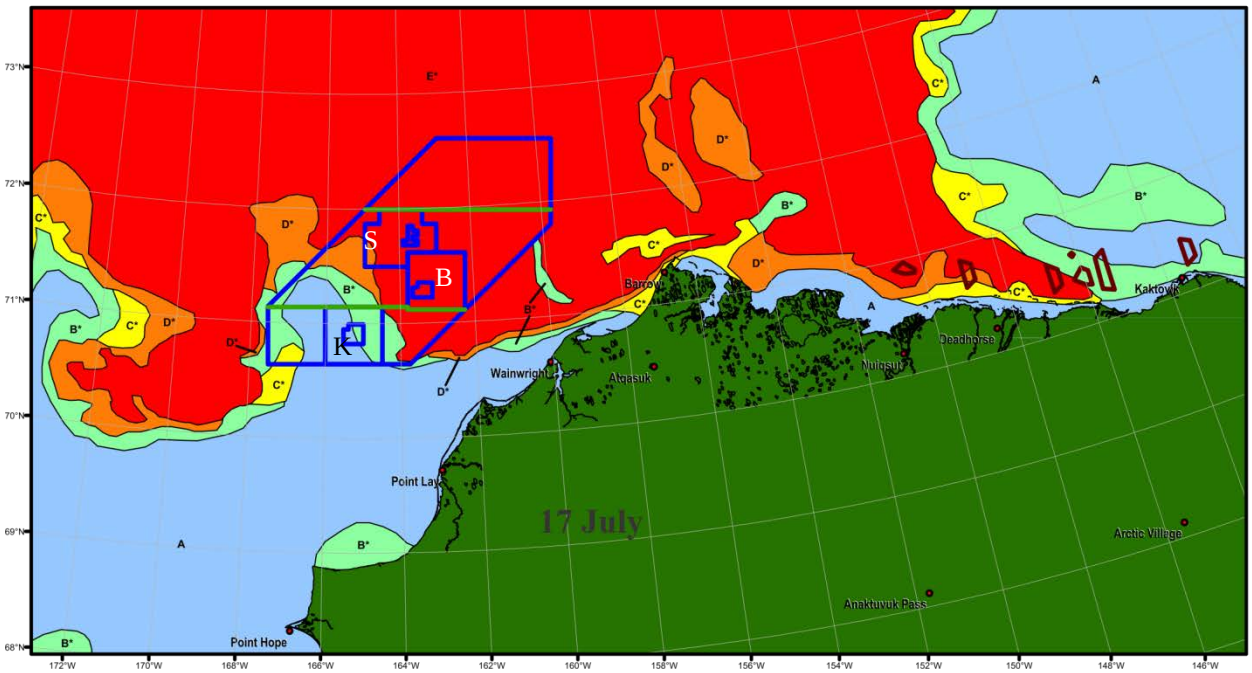

Figure 9. Sea ice concentrations maps for 11 (top) and 17 (bottom) July 2012, derived from MODIS imagery. The Statoil (S), Burger (B), and Klondike (K) survey areas are also noted. Areas outlined in purple in the Beaufort Sea represent industry study regions there.

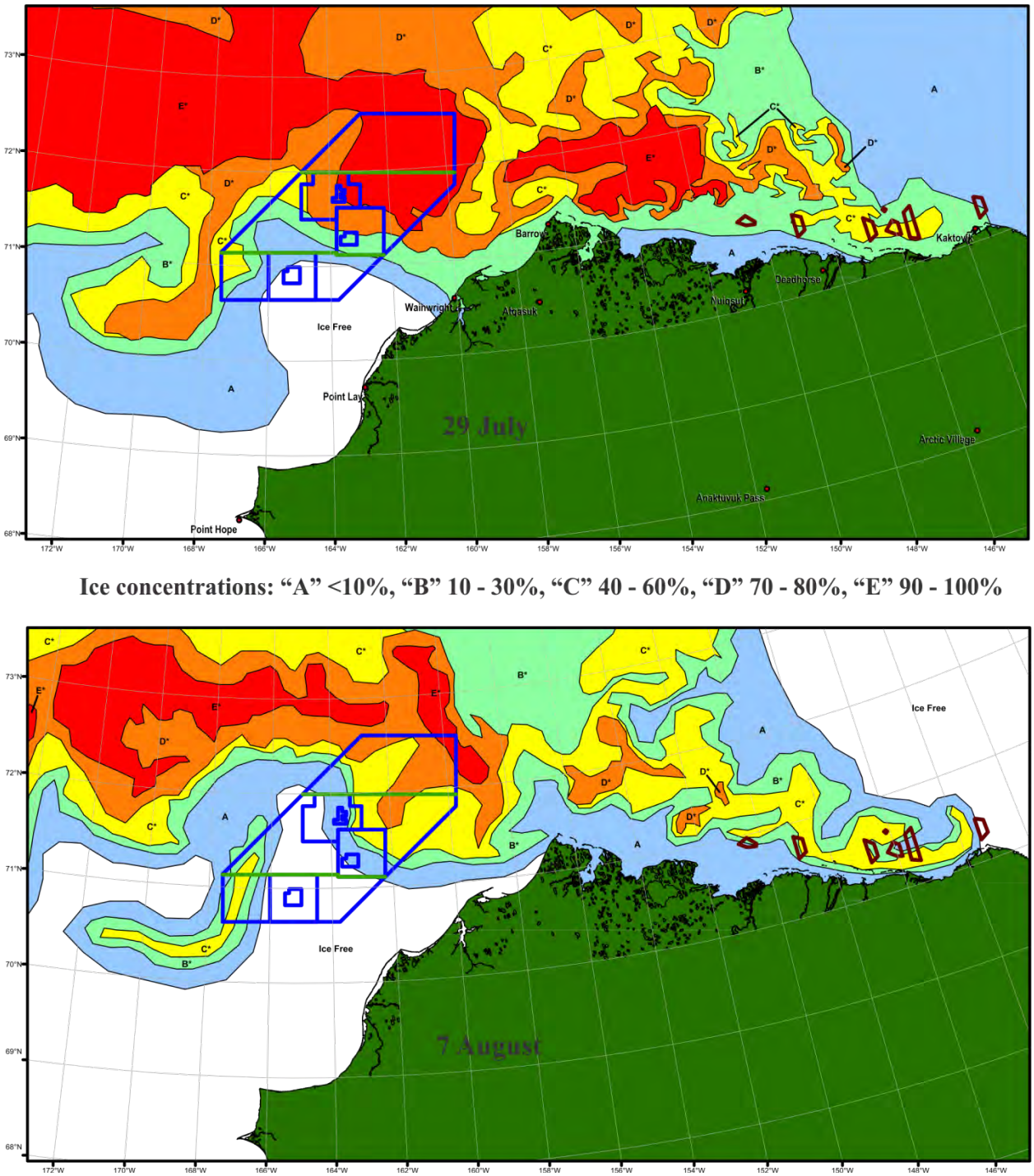

Figure 10. Sea ice concentrations maps for 29 July (top) and 7 August (bottom) 2012, derived from MODIS imagery. The Statoil (S), Burger (B), and Klondike (K) survey areas are also noted. Areas outlined in purple in the Beaufort Sea represent industry study regions there.

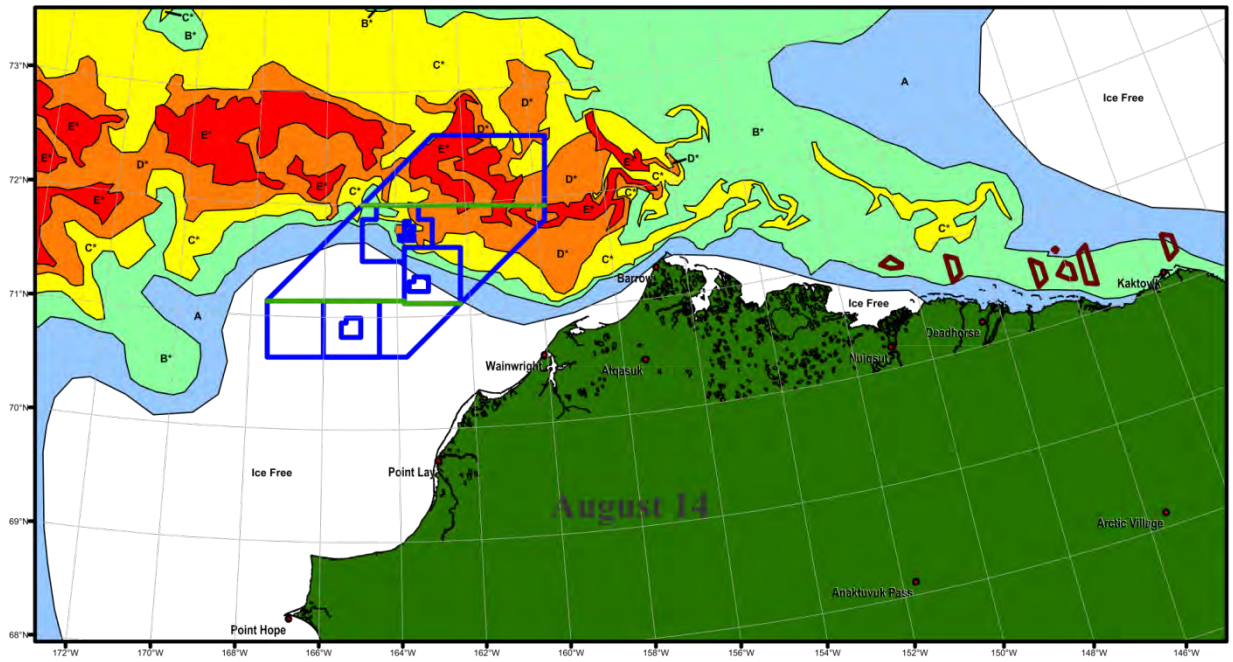

Ice concentrations: "A" <10%, "B" 10 - 30%, "C" 40 - 60%, "D" 70 - 80%, "E" 90 - 100%

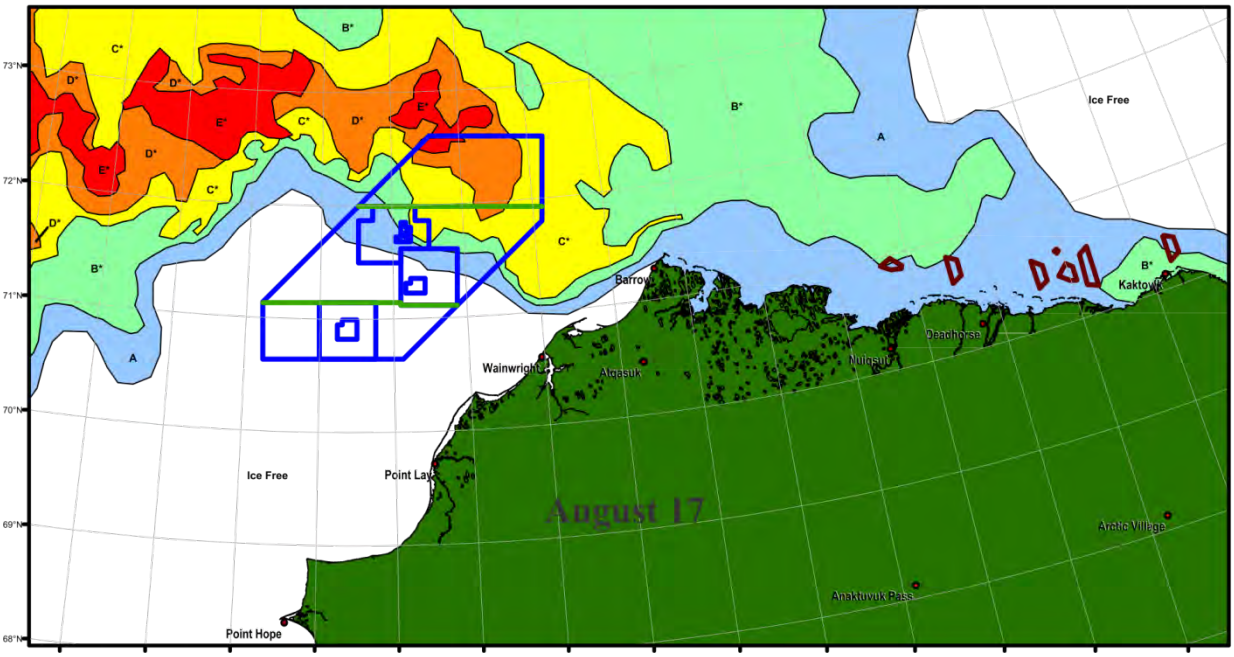

Figure 11. Sea ice concentrations maps for 14 (top) and 17 (bottom) August 2012, derived from MODIS imagery. The Statoil (S), Burger (B), and Klondike (K) survey areas are also noted. Areas outlined in purple in the Beaufort Sea represent industry study regions there.

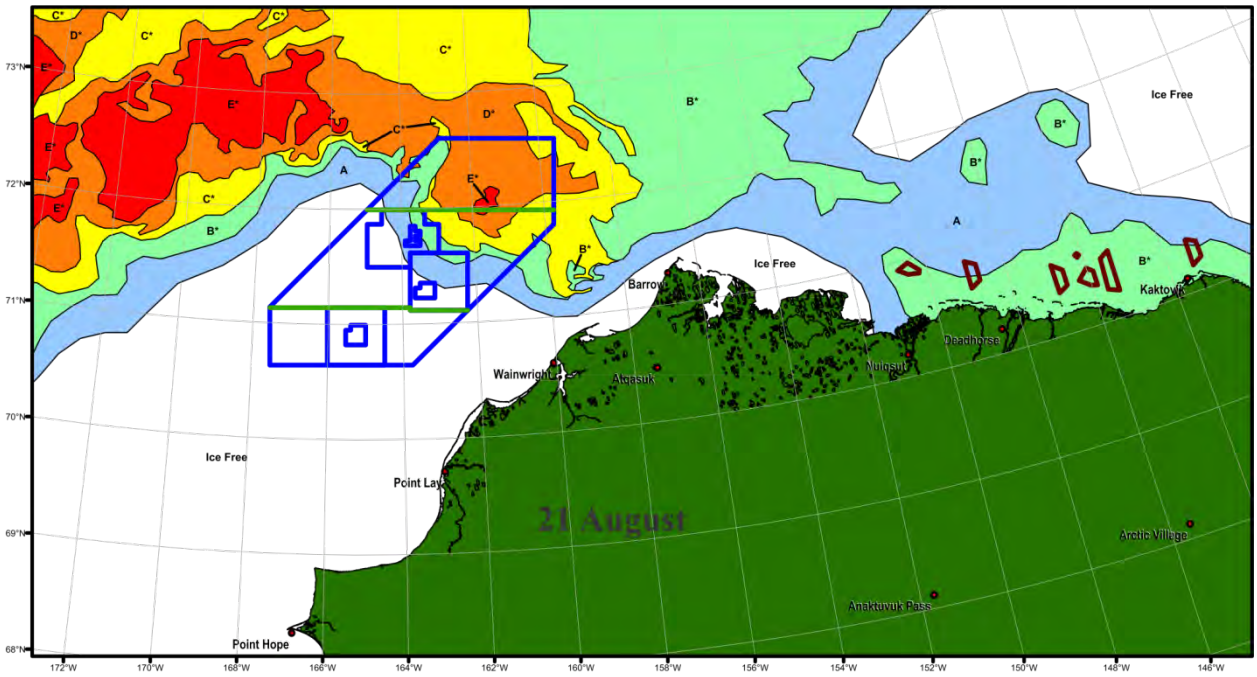

Ice concentrations: "A" <10%, "B" 10 - 30%, "C" 40 - 60%, "D" 70 - 80%, "E" 90 - 100%

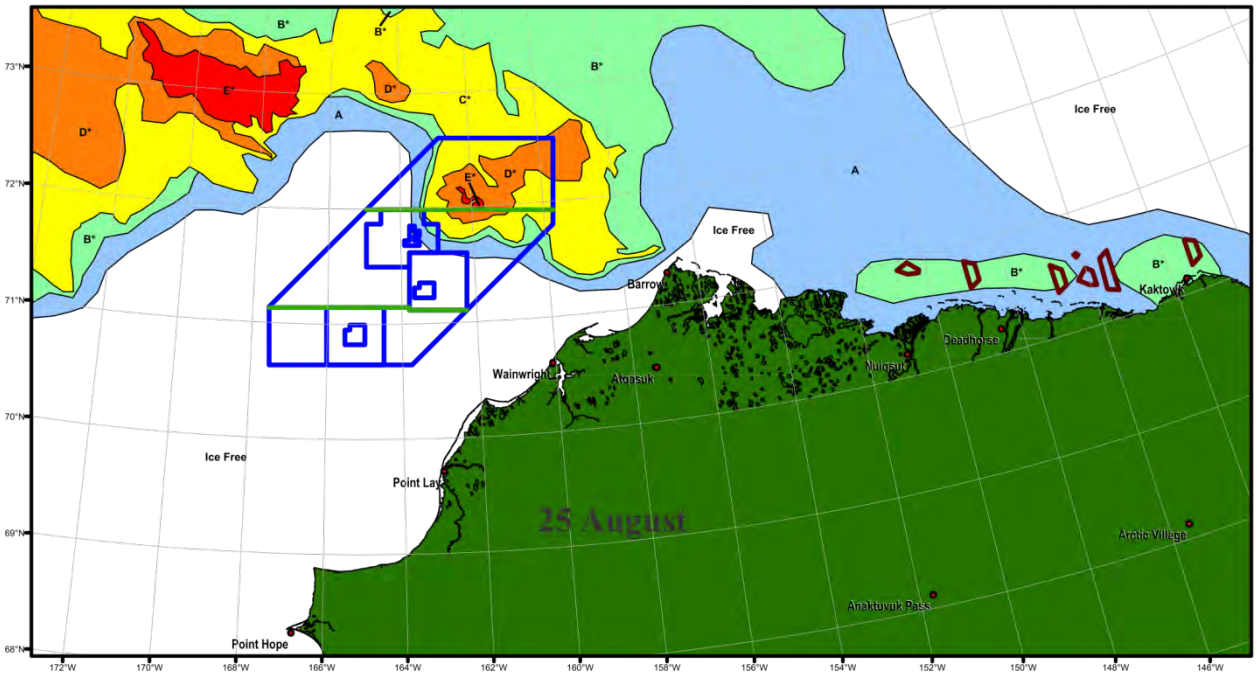

Figure 12. Sea ice concentrations maps for 21 (top) and 25 (bottom) August 2012, derived from MODIS imagery. The Statoil (S), Burger (B), and Klondike (K) survey areas are also noted. Areas outlined in purple in the Beaufort Sea represent industry study regions there.

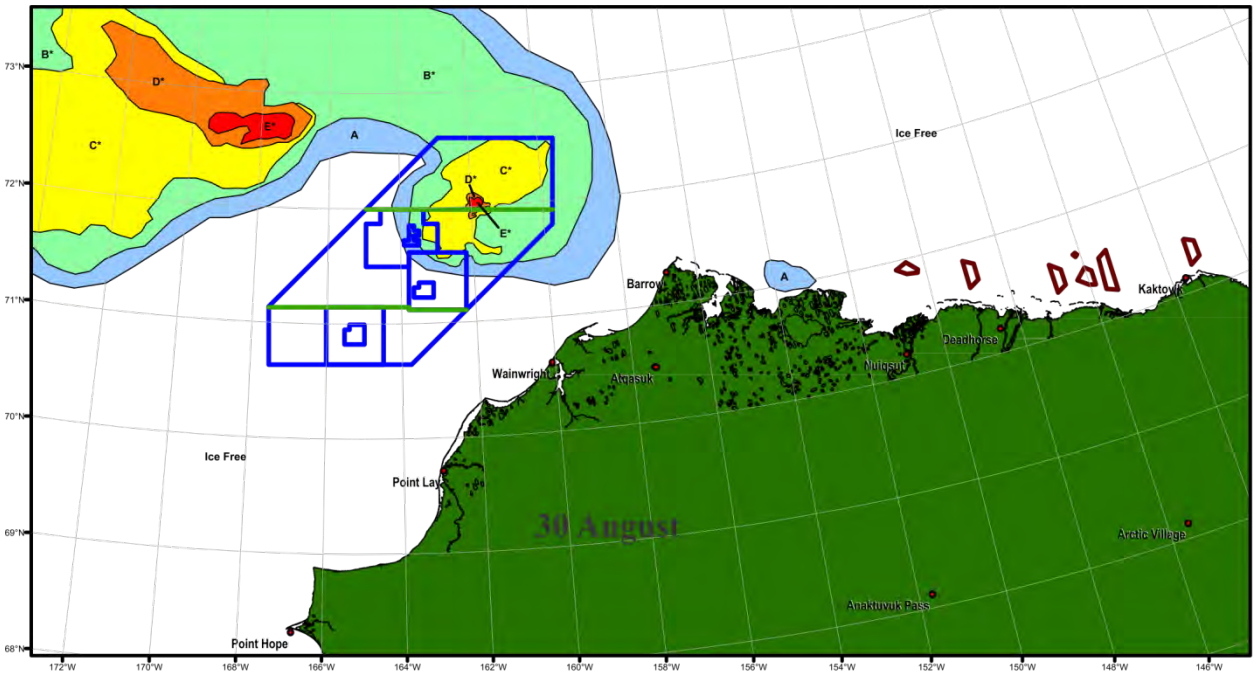

Ice concentrations: "A" <10%, "B" 10 - 30%, "C" 40 - 60%, "D" 70 - 80%, "E" 90 - 100%

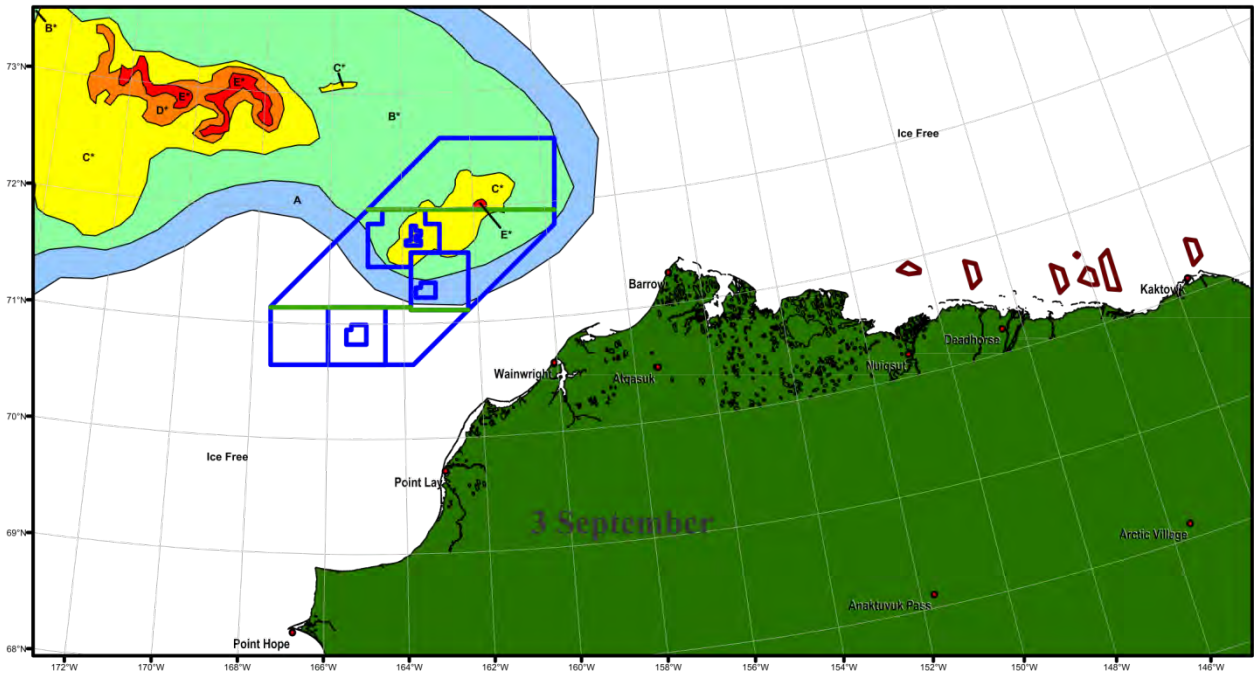

Figure 13. Sea ice concentrations maps for 30 August (top) and 3 September (bottom) 2012, derived from MODIS imagery. The Statoil (S), Burger (B), and Klondike (K) survey areas are also noted. Areas outlined in purple in the Beaufort Sea represent industry study regions there.

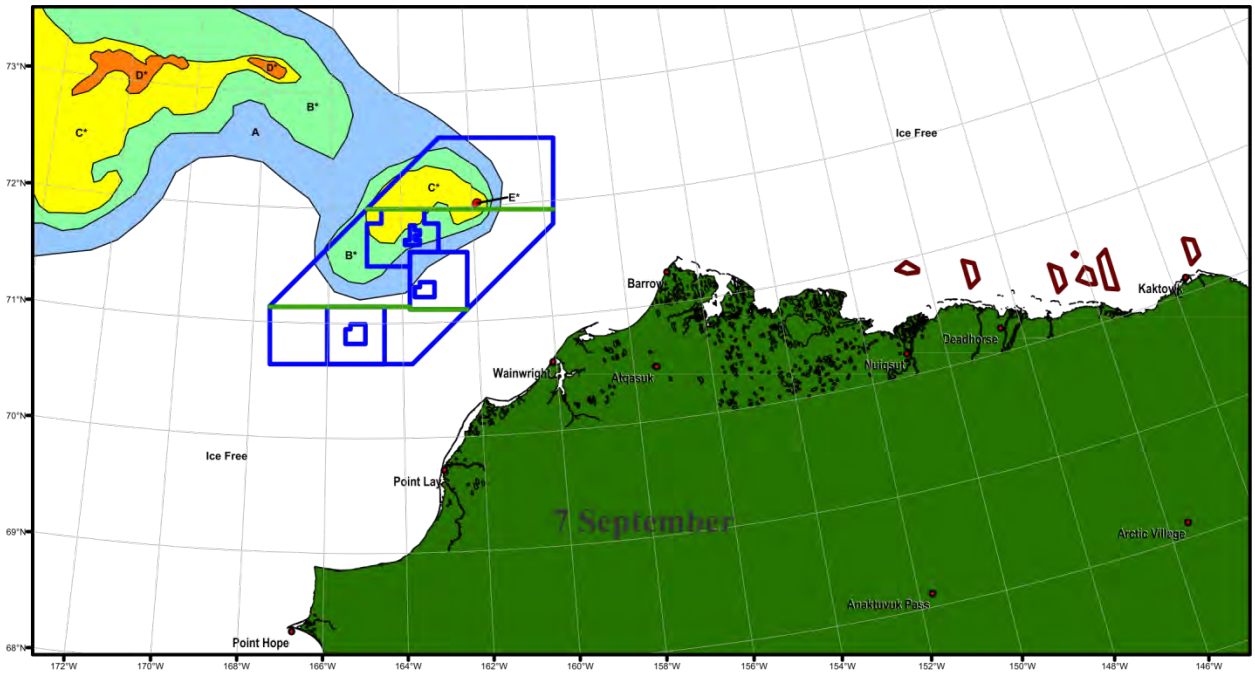

Figure 14. Sea ice concentrations maps for 7 (top) and 11 (bottom) September 2012, derived from MODIS imagery. The Statoil (S), Burger (B), and Klondike (K) survey areas are also noted. Areas outlined in purple in the Beaufort Sea represent industry study regions there.

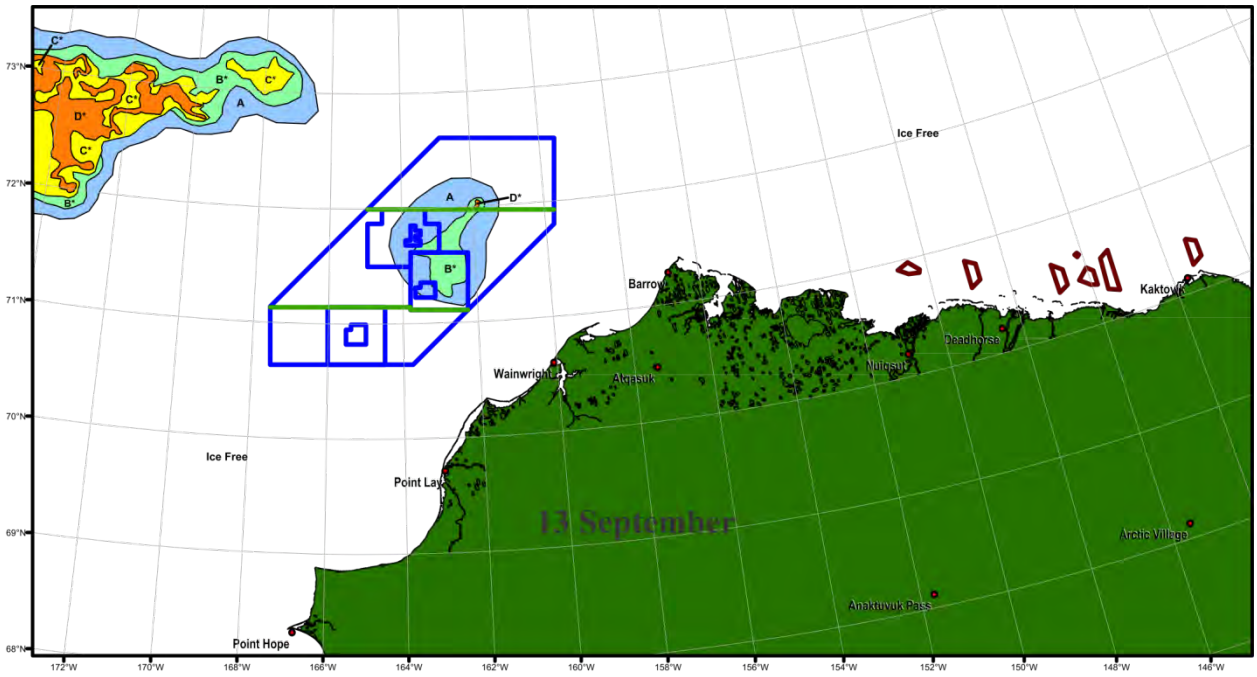

Ice concentrations: "A" <10%, "B" 10 - 30%, "C" 40 - 60%, "D" 70 - 80%, "E" 90 - 100%

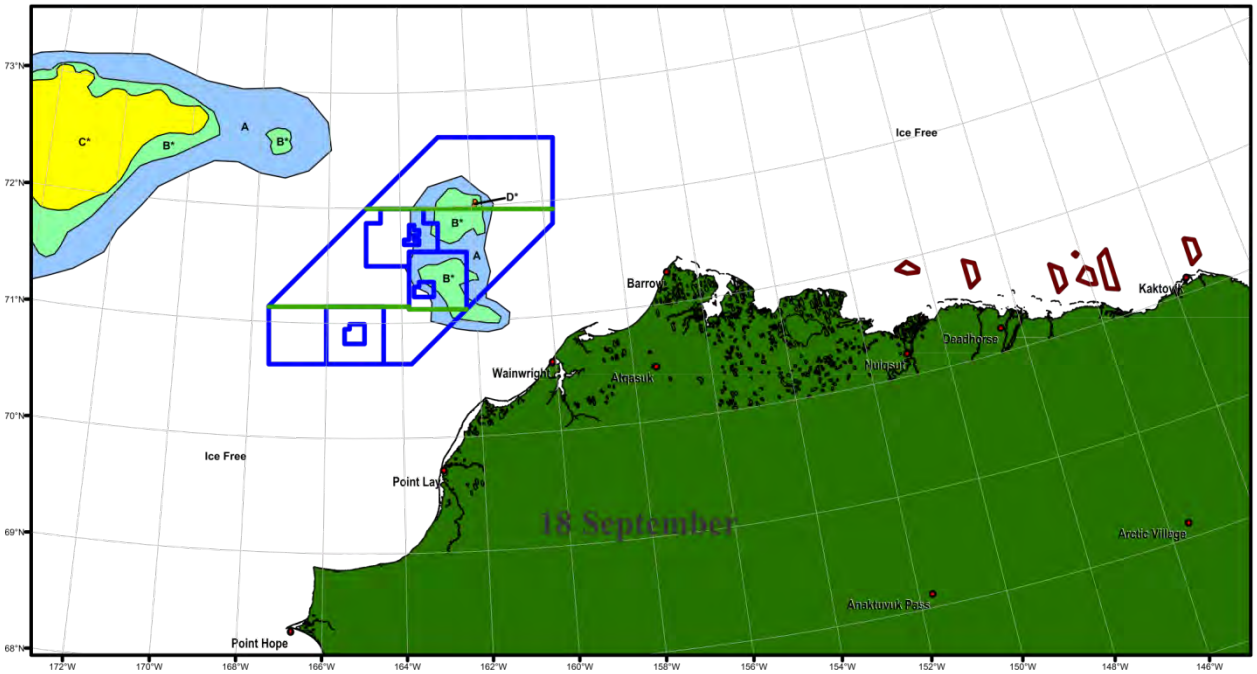

Figure 15. Sea ice concentrations maps for 13 (top) and 18 (bottom) September 2012, derived from MODIS imagery. The Statoil (S), Burger (B), and Klondike (K) survey areas are also noted. Areas outlined in purple in the Beaufort Sea represent industry study regions there.

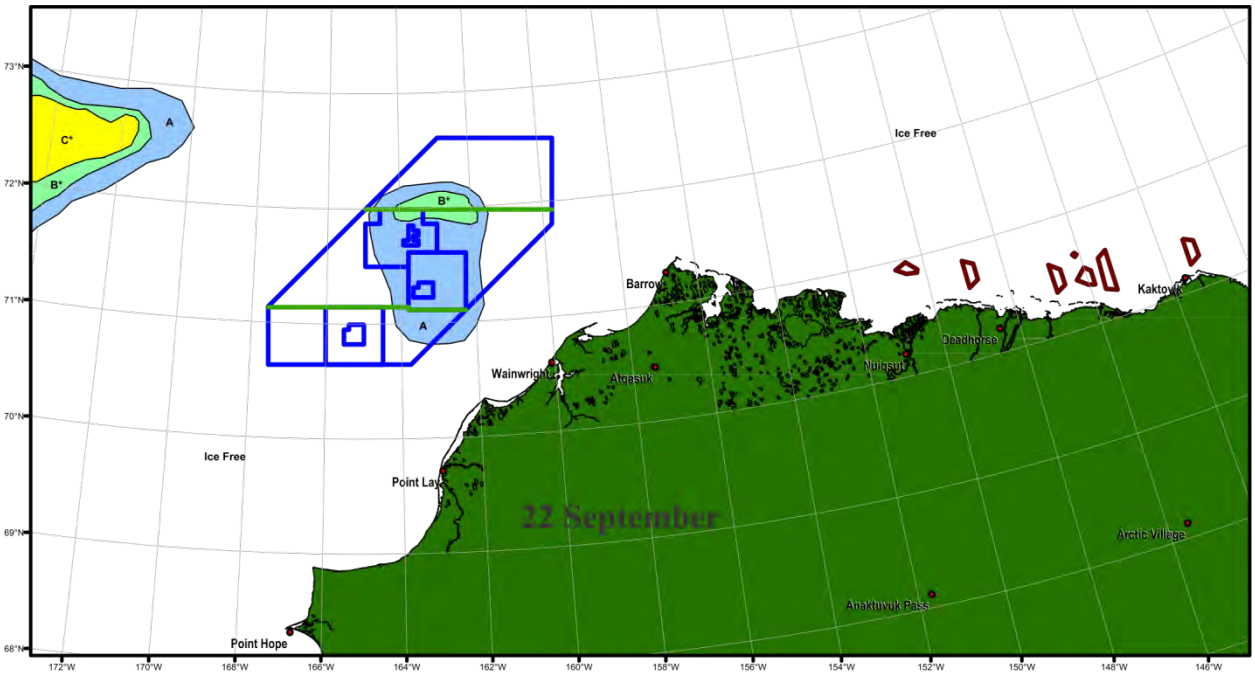

Ice concentrations: "A" <10%, "B" 10 - 30%, "C" 40 - 60%, "D" 70 - 80%, "E" 90 - 100%

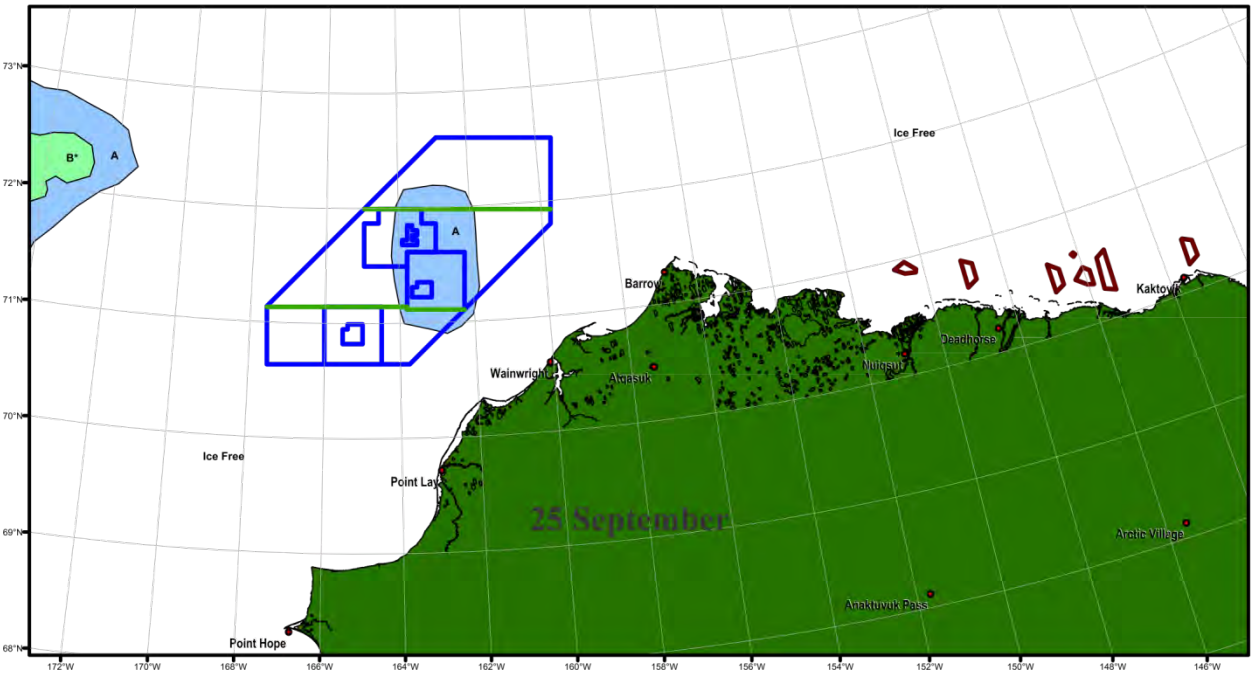

Figure 16. Sea ice concentrations maps for 22 (top) and 25 (bottom) September 2012, derived from MODIS imagery. The Statoil (S), Burger (B), and Klondike (K) survey areas are also noted. Areas outlined in purple in the Beaufort Sea represent industry study regions there.

Hydrography 2012

Temperature and salinity

Before presenting the spatial distribution of temperature (T) and salinity (S) along the CTD transects we first describe the various water masses found in the survey areas, based on T/S diagrams. These are scatterplots that depict the T and S characteristics at each 1-meter averaged CTD sample from all casts in the standard study area (Klondike, Burger, and Statoil stations; **Figure 17**). In addition **Figure 18** are the T/S diagrams for stations outside of these areas occupied over the broader sampling grid only on Cruises 3 and 4 (T34). The data are segregated into stations during the second (16 – 26 August), third (31 August – 16 September), and fourth (16 September – 3 October) cruises in the standard study areas. In **Figure 18**, the stations are further delineated into those south and north of Hanna Shoal, those located between these two groupings, and those (DF) that are at the extreme end of the longest CTD transect.

The overall distribution of data points is similar to that found in 2008 – 2010 in consisting of cool ($<2^oC$), fresh (<30) meltwater, very cold ($<2^oC$) and salty (<32.5) waters remnant from ice formation during the previous winter, and an intermediate grouping of warm ($>2^oC$), moderately saline (30<S<32.5) waters, which have recently arrived from the Bering Sea. There are also water types having characteristics between these basic groupings, indicative of mixtures of the basic water masses. These same groupings are evident also over the broader sampling domain (**Figure 18**). There are several general patterns that emerge. First, during the August cruise, Klondike consisted of meltwater, BSW, and mixtures of the two. Samples from stations in the Burger and Statoil contain mainly meltwaters and winter waters. Over the broader survey region, the BSW mass is mainly found in the SOUTH region and at the southeastern DF stations. Stations within the CENTRAL and NORTH domains consisted largely of meltwater, winter water, and mixtures between these two. The other point of interest is that the meltwaters and winter waters persist throughout the entire season at all locations, except in Klondike. In previous years (except 2008) there was a gradual decrease through the season in the frequency of occurrence of meltwater and winter water as these water masses were replaced by BSW. Finally we note that in 2012 the waters were slightly cooler than those in previous years (except 2008), the maximum temperatures were ~6.5^oC in 2012, whereas in earlier years temperatures exceeding 7^oC were not uncommon. As a further contrast among years, we include the T/S diagram from the 2011 survey, when virtually no meltwater was present. As noted in last year's report, 2011 was unusual insofar as stratification over the shelf was generally established by vertical temperature gradients given the narrow salinity range of ~30 – 32.5 (**Figure 19**). In 2012, the stratification was largely determined by vertical salinity gradients (this stratification dependence on salinity is typical of the Chukchi shelf), except in Klondike and the SOUTH region.

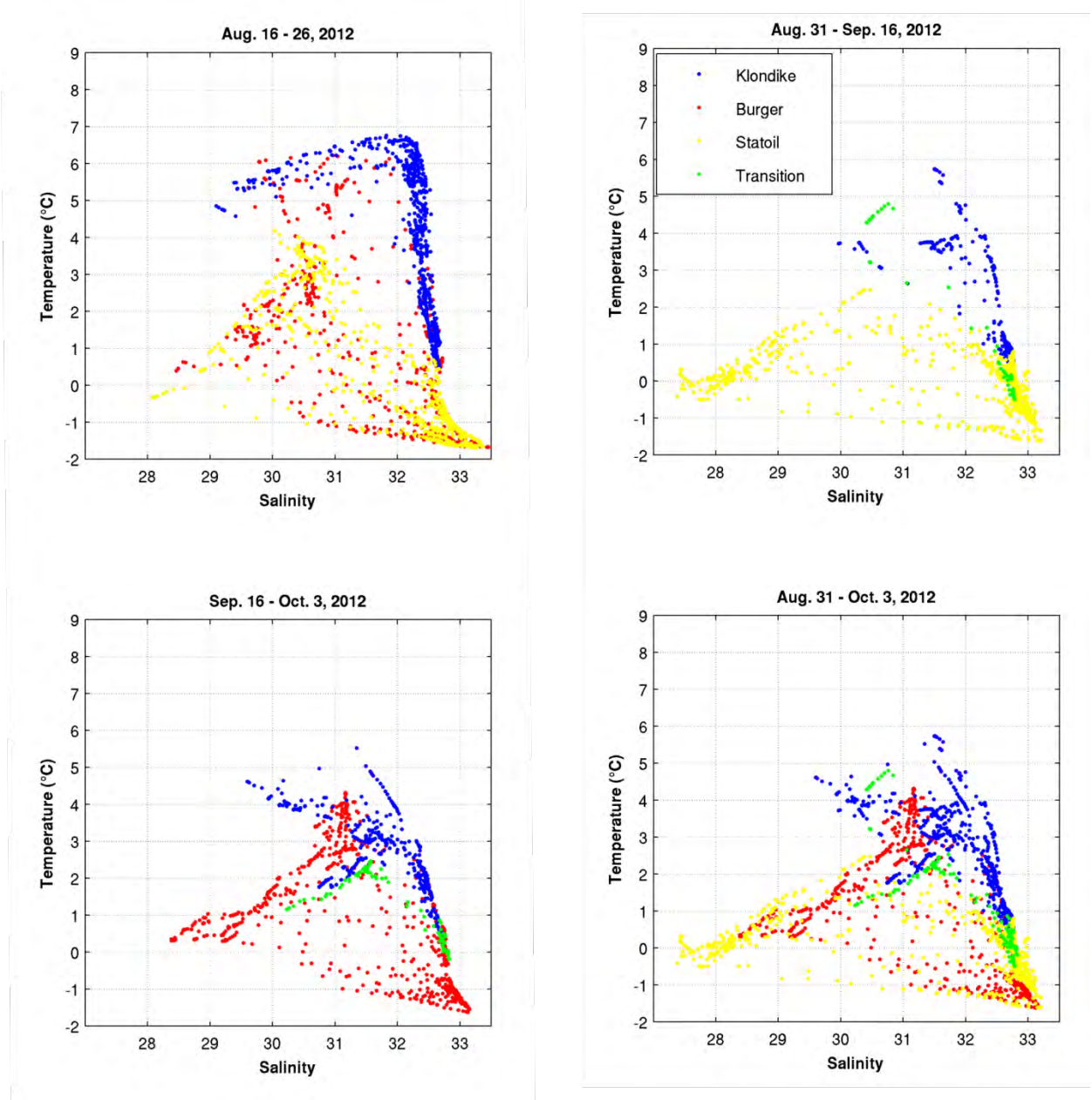

Figure 17. Temperature-salinity diagrams for the Klondike, Burger, and Statoil stations for each cruise, including the combined data for the 31 August – 3 October 2012 period.

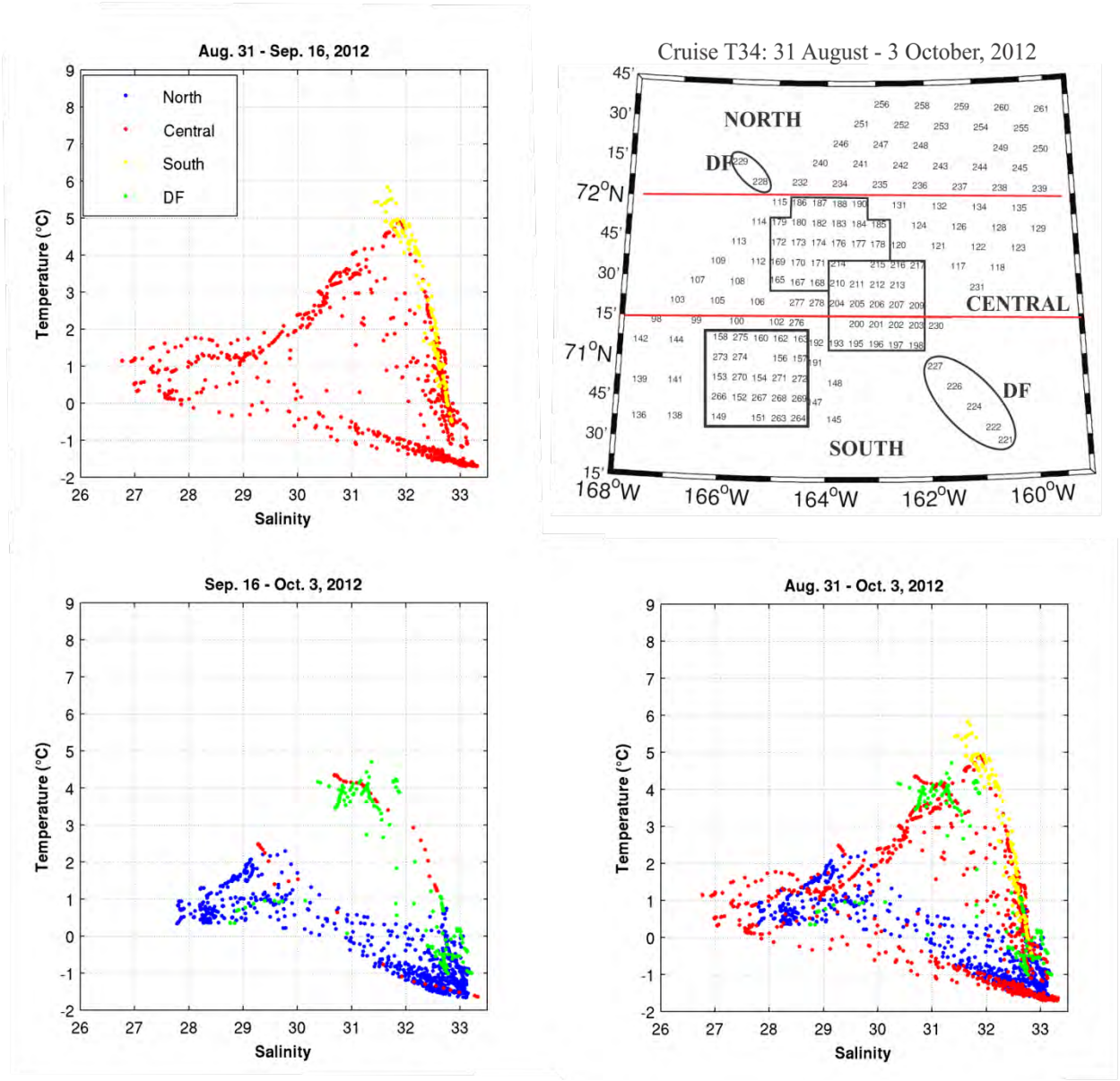

Figure 18. Temperature-salinity diagram from all stations on Cruise T34 (upper right) except those in Klondike, Burger, and Statoil (indicated by boxes). "SOUTH" stations are all south of 71° 15'N, "CENTRAL" stations are those between 72 °N and 71° 15'N, "NORTH" stations are north of 72 °N and "DF" stations are enclosed by ovals. The bottom right panel is the T/S diagram based on the entire period between 31 August and 3 October, 2012.

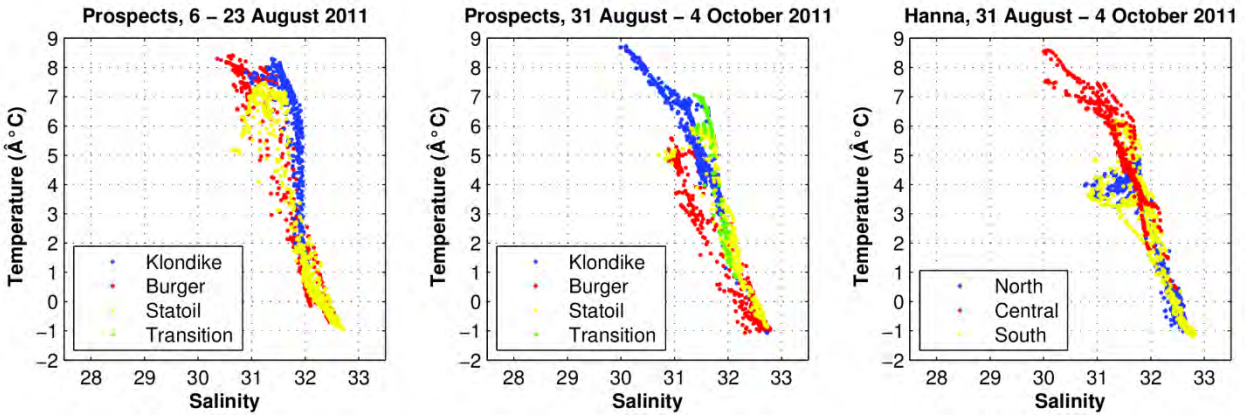

Figure 19. Temperature-salinity diagrams for each survey conducted in 2011. The left and middle panels are the T/S plots for the survey areas only. The rightmost panels are data collected during the second cruise from stations outside of the survey areas.

Water Property Distributions

We next investigate the temperature, salinity, density, fluorescence, and beam transmission distributions as a function of distance and depth (pressure) along a number of transects across the region. **Figure 20 s**hows the nomenclature and locations of the various transects presented herein.

Vertical sections showing the spatial distributions of water mass properties in 2012 for the 16 – 26 August (Cruise T2) and from 31 August – 3 October (Cruise T34) were constructed along the transects shown in **Figure 20**. **Figures 21 – 31** show property distributions along standard sections (denoted by a either the suffix "1" or no suffix) and their spatial extensions (denoted by suffix "2" or higher). These include T2we (west-east), T34we1, T34we2, T2sn1 (south-north), T2sn2, T34sn1, T34sn2, T2 and T34 (southwest-northeast across Klondike and Burger), T2BS, T34BS1 (southeast to northwest from Burger to Statoil) and T34BS2 (southeast from the coast and then across Burger and Statoil). To the extent possible we have attempted to construct these transects to conform to those described in previous reports. Indeed many of the shorter transects are only included to facilitate easier comparison with past transects. Following the presentation of the standard transects, we examine several southwest to northeast sections that are organized from west to east across the region. These transects include SWNE1, SWNE2, SWNE3, T34-3, and SWNE4. Several of these match similar transects occupied in 2011. In aggregate all provide a comprehensive depiction of the spatial distribution of water properties over the entire region sampled in 2012.

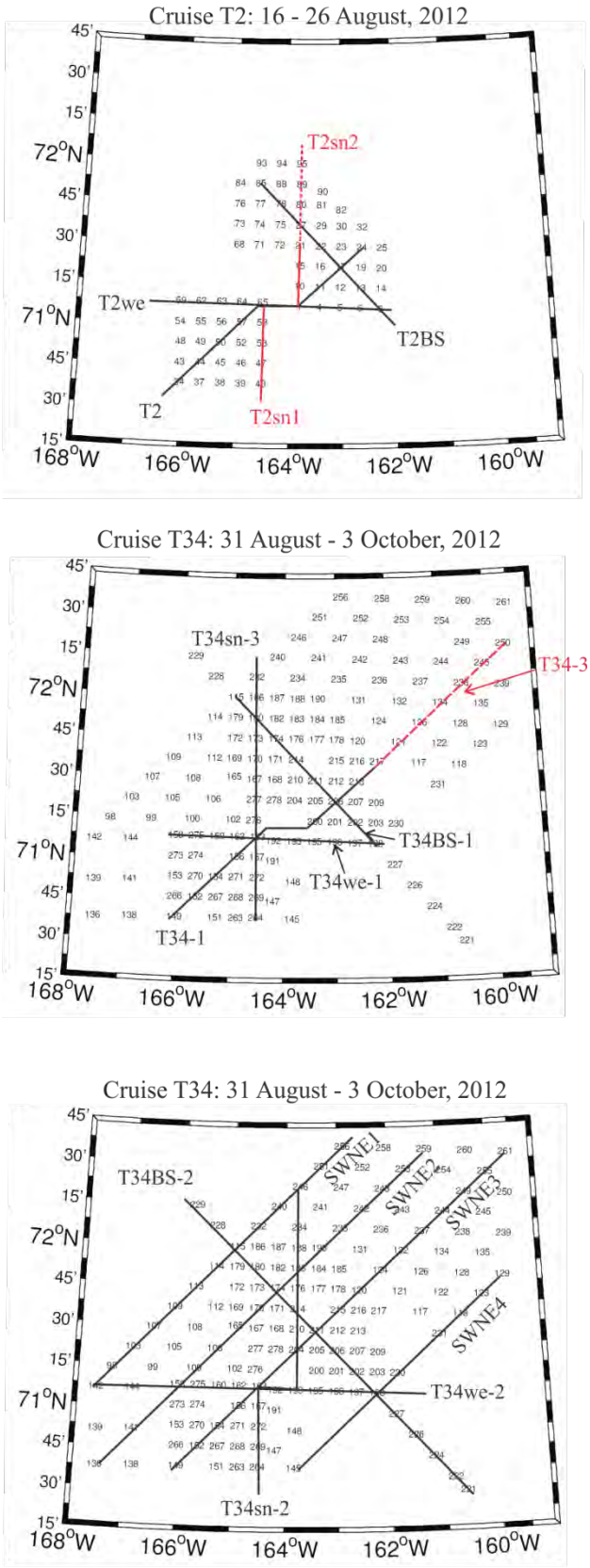

Figure 20. The location and nomenclature of transects used herein.

The T2we section (**Figure 21**) consisted of a strongly stratified pycnocline at 10 – 15 m deep, capped by a well-mixed surface layer with temperatures of ~5^{o}C and salinities of $\leq$ 31. Below the pycnocline the water column was well-mixed with temperatures ranging from 0 – 1 ^{o}C and with salinities of ~32.5. There were no strong horizontal temperature or salinity gradients (fronts) along this section, hence horizontal density gradients were also weak. Fluorescence was weak except for a small patch on the western end of the section (within Klondike) below the pycnocline. The beam transmission was high everywhere (indicating clear water), with the lowest values (~80 - 90%) below the pycnocline. The T34we sections (**Figure 22 and 23**) differed from T2 in several ways. The pycnocline was ~10 m deeper, the surface temperatures were ~ 2 - 3^{o}C cooler and there was greater horizontal variability in surface temperature and salinity as evidenced by the banding structure in these fields. These bands may be filaments or pockets of meltwaters that were slowly eroding by becoming saltier (through vertical diffusion) and warmer (chiefly through solar radiation) over time. Another point of difference between T2 and T34 is that the transmission had decreased substantially on T34 (in some places by ~50%) within about 10 m of the bottom. Presumably these lower transmission values were due to an increase in near-bottom currents and/or storm wave energy. The T34we2 (**Figure 23**) section includes two stations to the west of the origin of the T2we1 transect. These stations, which lie to the west of Klondike and within the Central Channel, are of particular interest because they contain a pool of warm (>5 ^{o}C), moderately saline water (>31.5) water in the upper 25 m, which was separated by a thin thermocline from cooler (~2 ^{o}C) bottom waters where the salinity was ~32.5. We think that Central Channel waters were moving northward as well as eastward across Klondike based on prior measurements (Weingartner et al., 2005; Weingartner et al., 2013a).

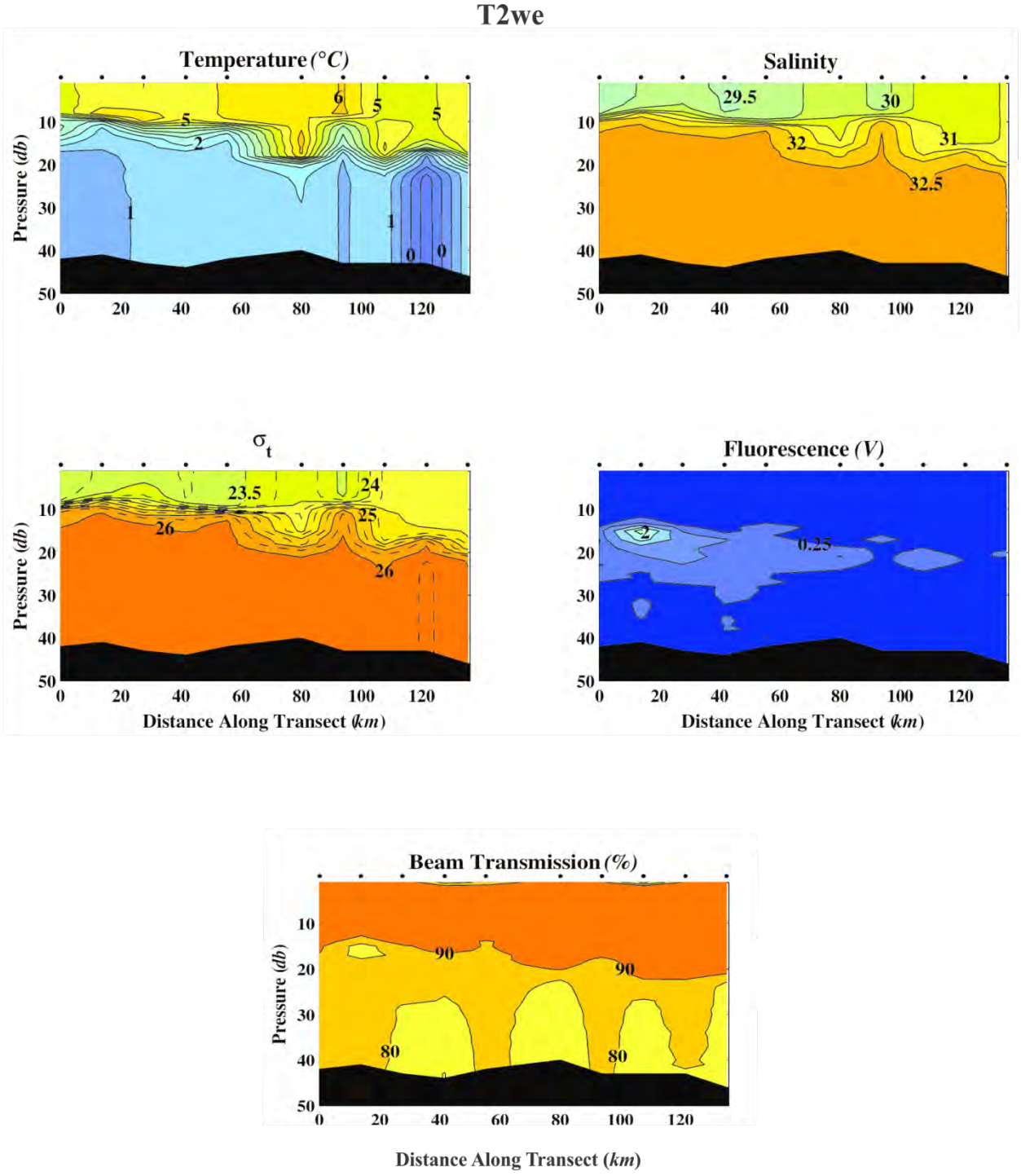

Figure 21. West-east (T2we) section (per **Figure 20**) of temperature, salinity, sigma-t, fluorescence and beam transmission from the 16 – 26 August 2012 survey.

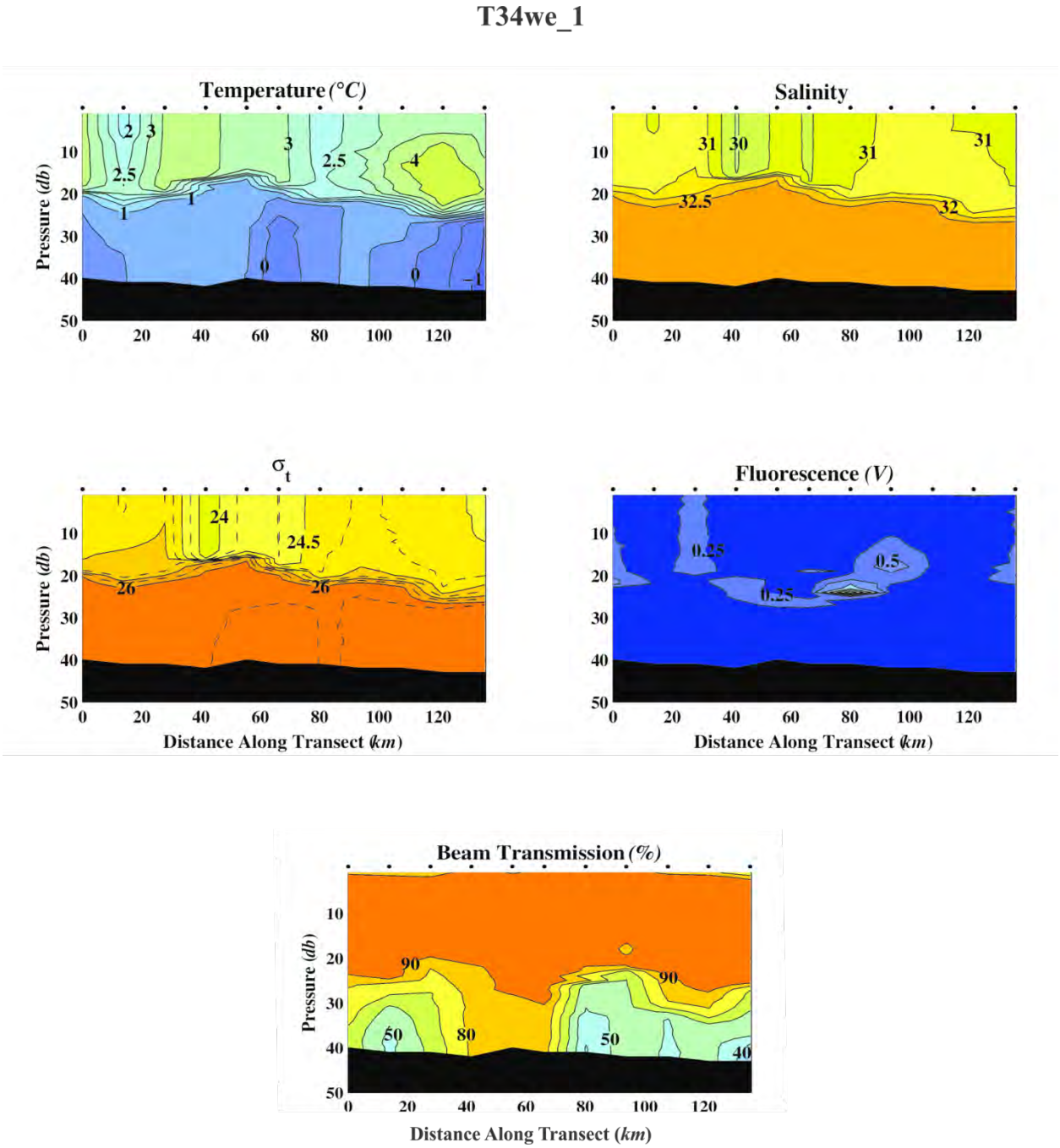

Figure 22. West-east (T4we_1) section (per **Figure 20**) of temperature, salinity, sigma-t, fluorescence and beam transmission from the 31 August – 3 October3 2012 survey.

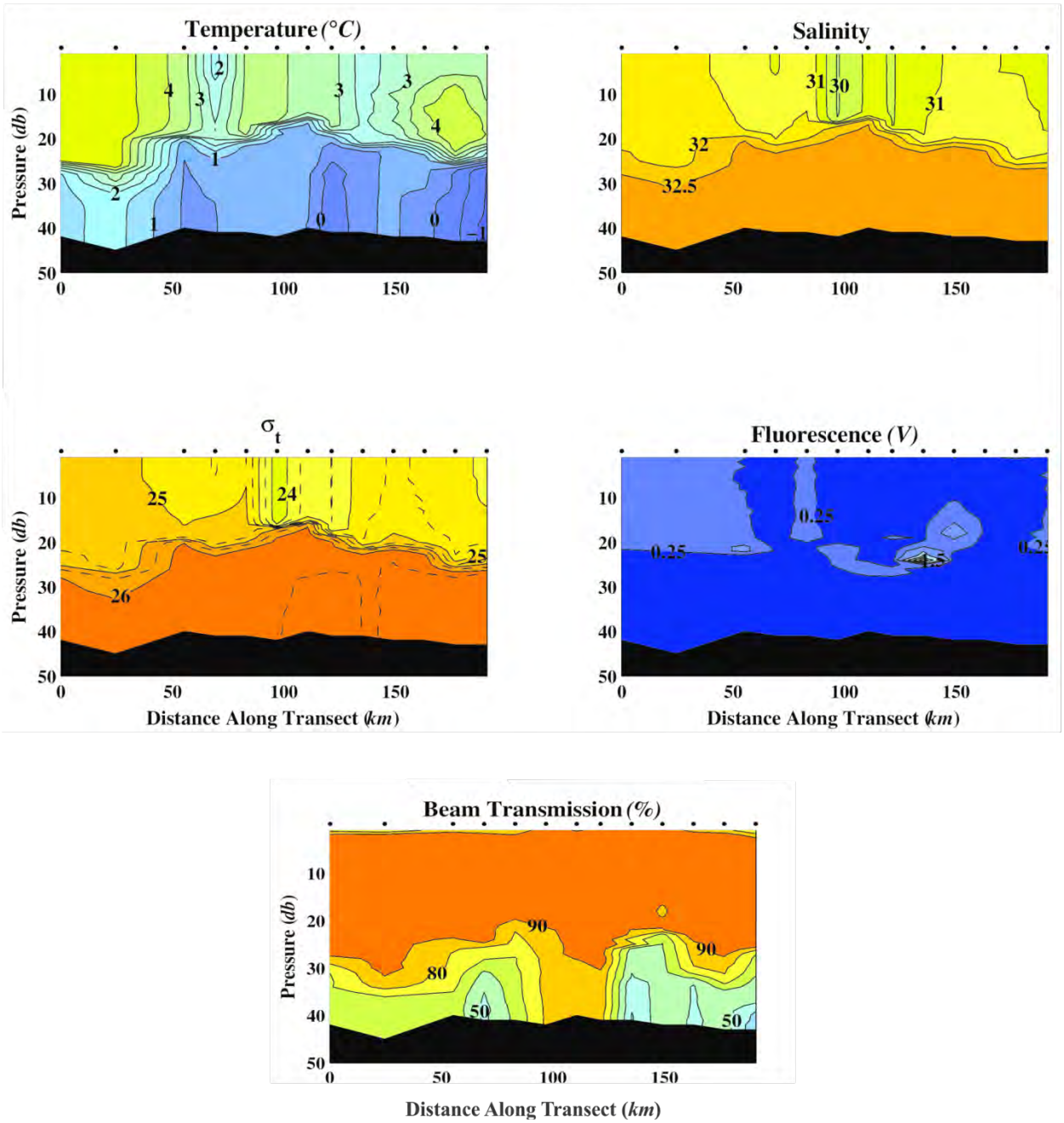

Figure 23. West-east (T4we_2) section (per **Figure 20**) of temperature, salinity, sigma-t, fluorescence and beam transmission from the 31 August – 3 October3 2012 survey.

We next consider the north-south sections. During T2 (**Figures 24 and 25**), the pycnocline was 10 – 15 m deep everywhere. However, surface temperatures varied from >6 ^{o}C in the south to ~1 ^{o}C in the north. Deeper temperatures also varied being >3 ^{o}C in the south but <-1.5 ^{o}C in the north and coincident with very saline (>33) water. (Note that the northern end of the section terminates on the south side Hanna Shoal.) Although the largest horizontal temperature gradients occurred below the pycnocline, the south – north density gradients were weak, as density varied by only ~1 kg m^{-3} over 100 km. Instead the largest horizontal density gradients were in the surface layer and associated with salinity variations. The salinity was nearly 32 in the south but <30 in the north. The picture that emerges from this section is that BSW occupied the southern end of the section and spread northward in the upper 10 m, where it encountered a 10m thick plume of meltwater. Waters beneath the pycnocline included cooler and saltier BSW (in the south) which graded into cold, salty water in the north. The coldest (<-1.5 ^{o}C) and saltiest (33) of these waters were at the northern end of the transect, contained in a 15-m thick bottom plume that extended 50 km to the south. Fluoresence was weak and patchy, with the largest signal occurring beneath the pycnocline, but above the coldest water at the northern end of the section. Beam transmission was >90% above the pycnocline and ranged between 70 and 80% within 10 of the bottom.

The south-north sections constructed from Cruise T34 (**Figures 26 and 27)** indicate that the pycnocline had weakened slightly in the south, but had strengthened considerably in the north. This strengthening was largely due to the pool of very low salinity (<29.5) water that extended southward ~60 km from the northern end of transect T34sn3 (**Figure 27**). The southern limit of this plume consisted of a strong horizontal salinity (and density) gradient across which salinity (density) increased by ~2 (2.5 kg m^{-3}) over 15 km. Such large density gradients can support geostrophic jets. Based on the thermal wind relation (which provides only a relative estimate of velocity), the water in this surface jet was flowing westward at 10 cm s^{-1}, *relative* to the water below the pycnocline. As suggested by the arrows in **Figure 27**, there appears to be a subduction zone slightly south of this front wherein surface waters (with temperatures of 1 - 2^{o}C and salinities of 30.5 – 31.5) were sinking beneath the plume**.** Fluorescence signals were extremely weak on T34.

In comparison to the T2sn sections, water column temperatures at the southern end of the T34sn sections were ~1 ^{o}C cooler. On the other hand, subsurface temperatures over the northern half of the section were 1 – 2 ^{o}C warmer and there was marked decrease in waters with salinities > 33. These changes are consistent with the notion that eastward advection of warmer, moderately saline water was replacing the dense winter water. Although there were no changes in transmission in the upper half of the water column between T2sn and T34sn, it had decreased substantially within the bottom 10 m (from ~70% on T2sn to from 30 – 60% on T34sn).

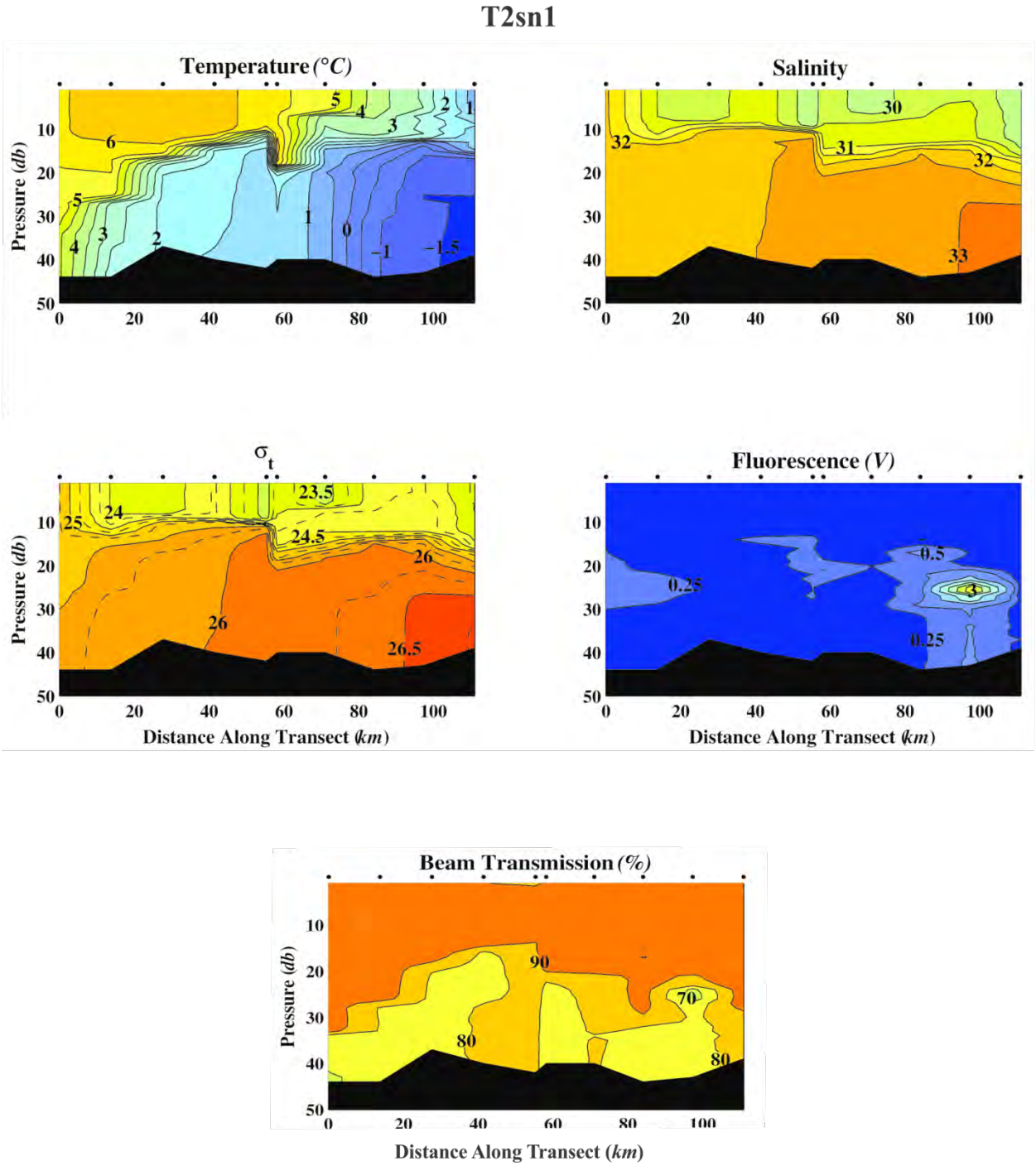

Figure 24. South-north (T2sn1) section (per **Figure 20**) of temperature, salinity, sigma-t, fluorescence and beam transmission from the 16 – 26 August 2012 survey.

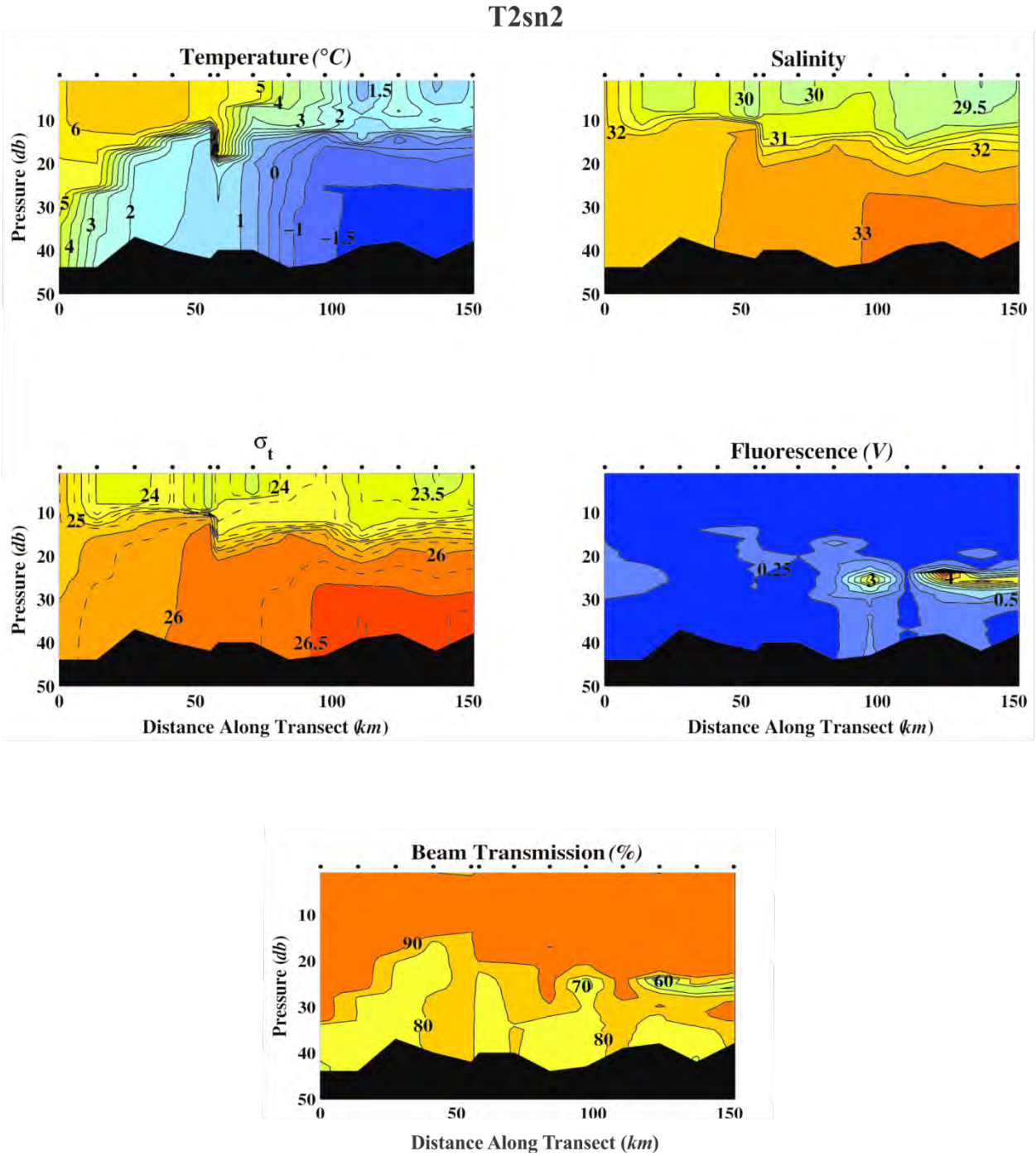

Figure 25. South-north (T2sn2) section (per **Figure 20**) of temperature, salinity, sigma-t, fluorescence and beam transmission from the 31 August – 3 October 2012 survey.

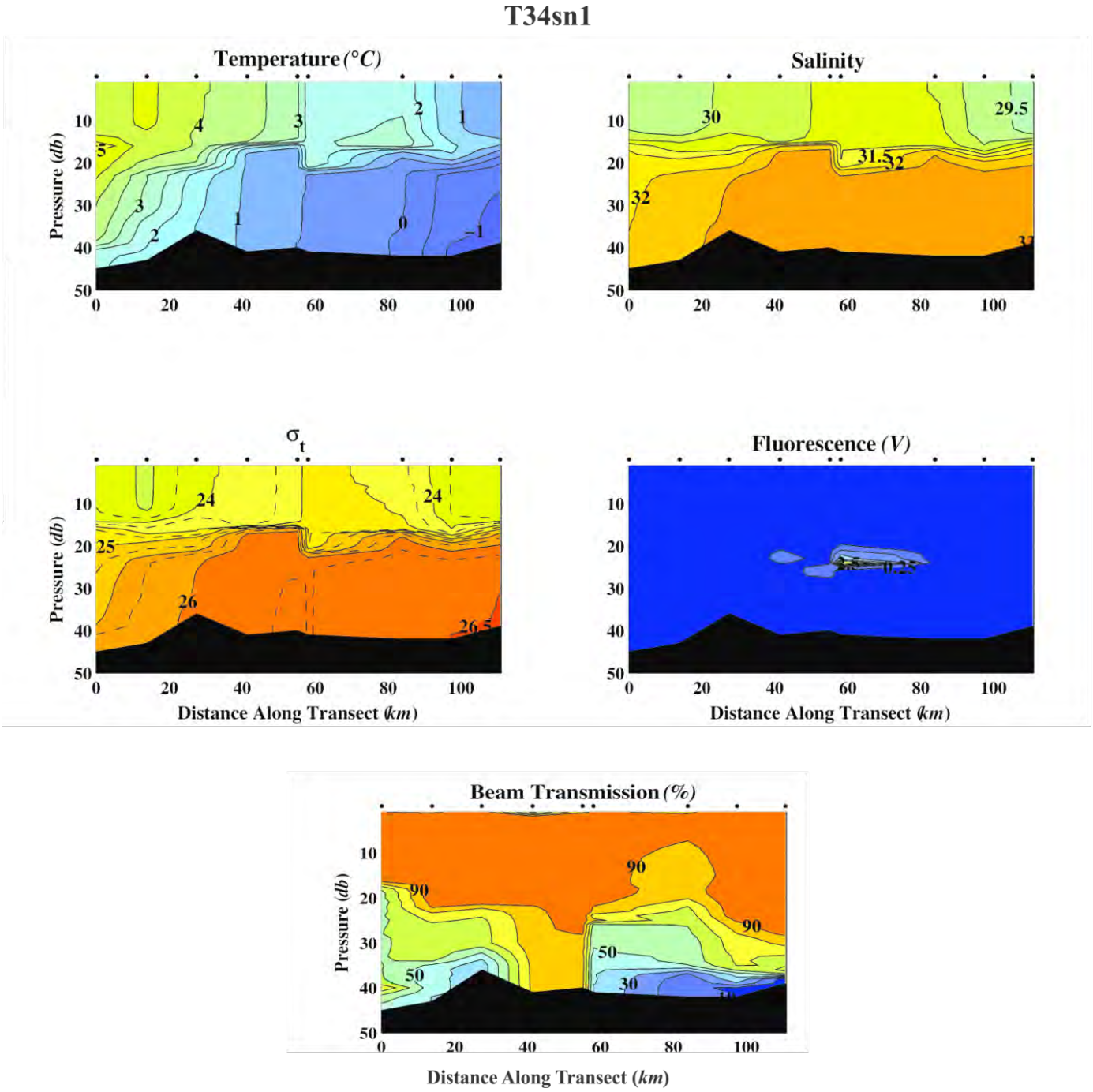

Figure 26. South-north (T34sn1) section (per **Figure 20**) of temperature, salinity, sigma-t, fluorescence and beam transmission from the 31 August – 3 October 2012 survey.

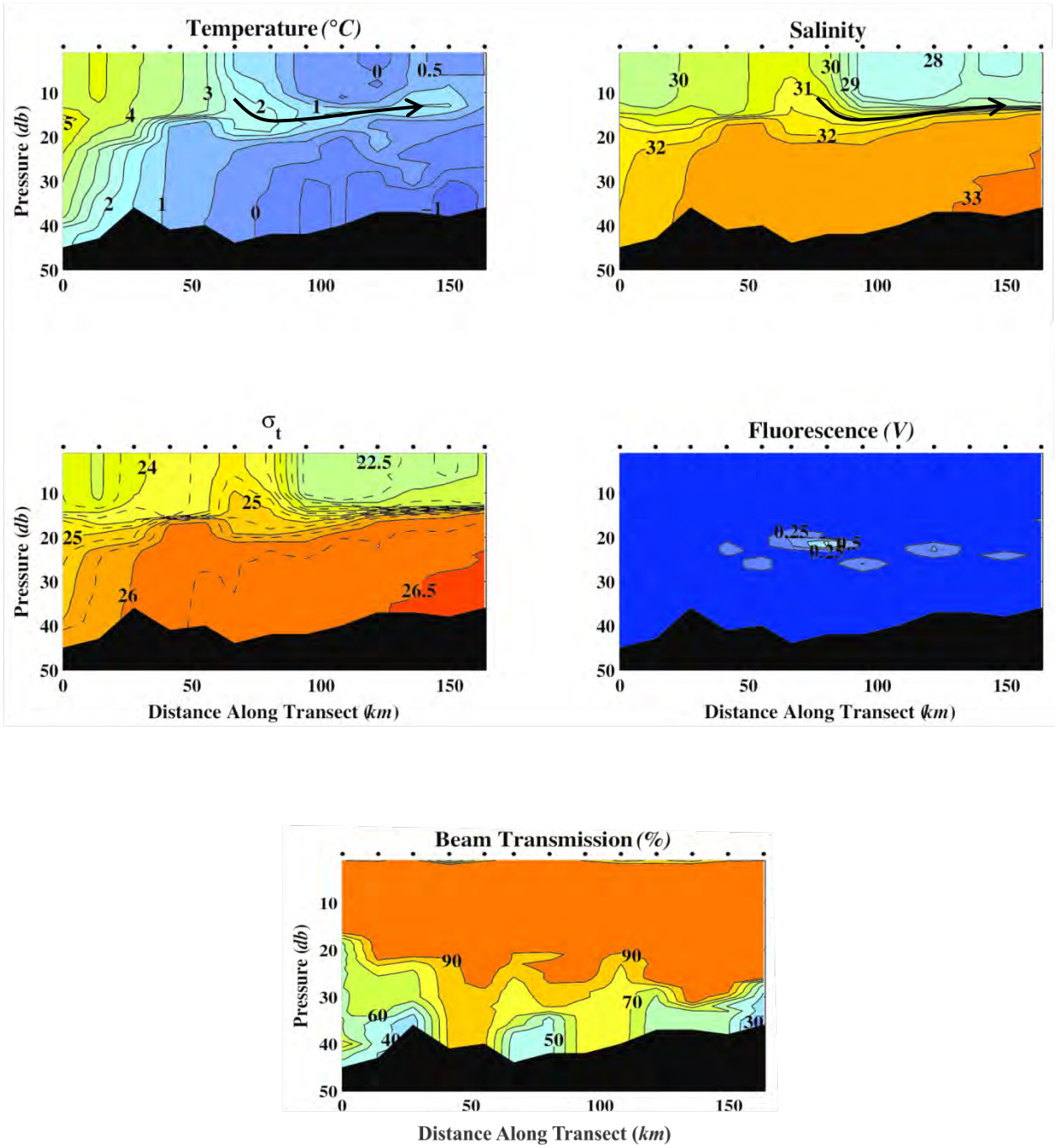

Figure 27. South-north (T34sn3) section (per **Figure 20**) of temperature, salinity, sigma-t, fluorescence and beam transmission from the 31 August – 3 October 2012 survey. The arrows on the temperature and salinity transect suggests a subduction zone whereby surface waters (temperatures of 1 -2 ^{o}C and salinities of 30.5 – 31.5) from the southern half of the transect were sinking beneath cooler, fresher surface waters at this time.

The T2 and T34_1 sections (**Figures 28 and 29**) run northeast from the southwest corner of Klondike to the northeast corner of Burger. During T2, the southwest corner of Klondike was virtually unstratified because salinities (~32) were nearly uniform over the water column. Temperatures varied vertically, however, and were ~6 ^{o}C at the surface and ~4^{o}C at the bottom. A shallow pycnocline was present farther to the northeast, which separated a 10 m deep low-salinity (<31) surface layer from more saline (>32.5) waters at depth. At the northeast end of this section deep temperatures were <-1 ^{o}C and salinities were >33. The highest fluorescence levels occurred at this location at ~35 m depth. Transmission values were >90% in the surface and decreased below the pycnocline from ~90% to 60 – 80% along the bottom.

Along section T34 (**Figure 29**) conditions over the southwestern half of the transect were similar to those on T2, although temperatures in the upper half of the water column had cooled by ~2 ^{o}C and a somewhat stronger pycnocline had developed due to surface freshening. At the northwest end of the transect there was a prominent surface freshening as more meltwater (relative to T2) had moved into the area. Two prominent features on this section were the bolus of 3 ^{o}C, ~31.5 water, which appears to be subducting beneath the meltwater plume, and the elevated fluorescence levels in the northeast corner of Burger. As with the previous sections, transmission values within 10 m of the bottom had decreased substantially (to <70%). This region of low transmission is generally within 10 m of the bottom and very likely defines the thickness of the bottom boundary layer of the shelf.

Sections T2BS, T34BS-1 and T34BS-2 extend from the southeast to the northwest and cut across Burger and Statoil. T34BS-2 includes four additional stations extending from the southeast corner of Burger toward the coast and two additional stations extending to the northwest of Statoil. As found for the other T2 sections, the water column contained a heavily stratified pycnocline at 10 – 20 m depth. The surface waters over the central portion of the transect included a pond of meltwater. Warmer and slightly saltier surface waters occurred on either side of the pond, suggesting that the meltwater pond was being "squeezed" by summer water from the Bering Sea infiltrating from the northwest and southeast. The coldest and saltiest bottom waters were below the pycnocline and centered beneath the meltwater pool. Bottom temperatures increased to the southeast and were >0 ^{o}C in the southeast corner of Statoil. Fluorescence was patchy and transmissivity was high above the pycnocline but lower within the bottommost 20 m.

Although the T34BS-1 section is generally similar in several respects to T2BS there are two substantial differences. First, the water found at the surface on the northwest end of T2BS was replaced by meltwater (this is also evident on the T34BS-2 section). Second, a considerable amount of meltwater moved into the region, as evidenced by the increase across the transect in the area of waters having temperatures < 1 ^{o}C and salinities < 30.5. Note also that this intrusion of meltwater was colder and fresher than observed on T2BS. Third, the thickness of the dense bottom water layer decreased between the two occupations and the densest bottom waters shifted southeast relative to their position on T234. Transect T34BS-2 also shows that conditions near the coast showed quite warm temperatures >4 ^{o}C and moderate salinities suggesting continuity in the water properties from the southeast corner of Burger to the coast. The coastal waters had relatively high fluorescence and low transmission; the latter due to the shoaling depths.

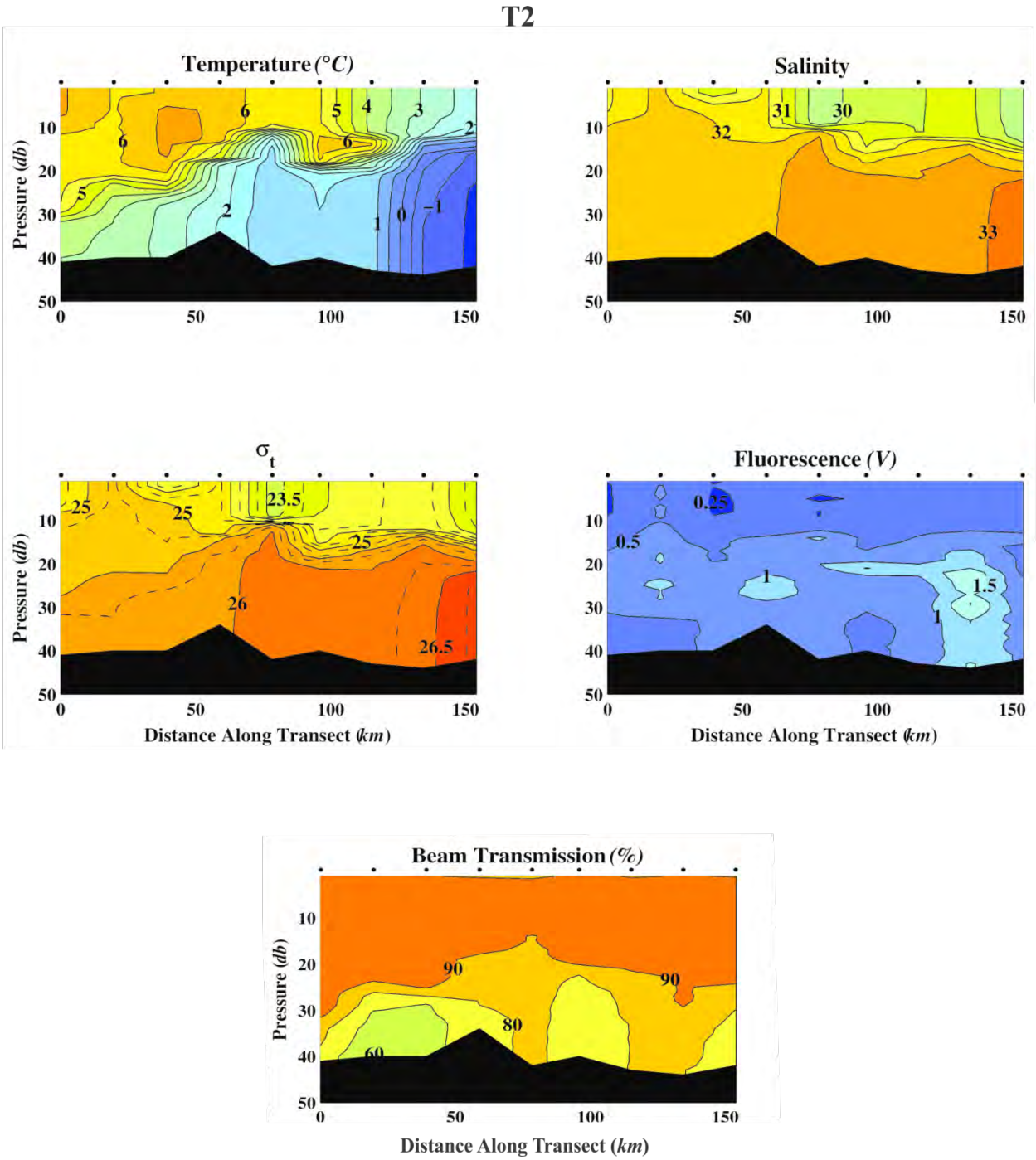

Figure 28. Southwest-northeast (T2) section (per **Figure 20**) of temperature, salinity, sigma-t, fluorescence and beam transmission from the 16 - 26 August 2012 survey.

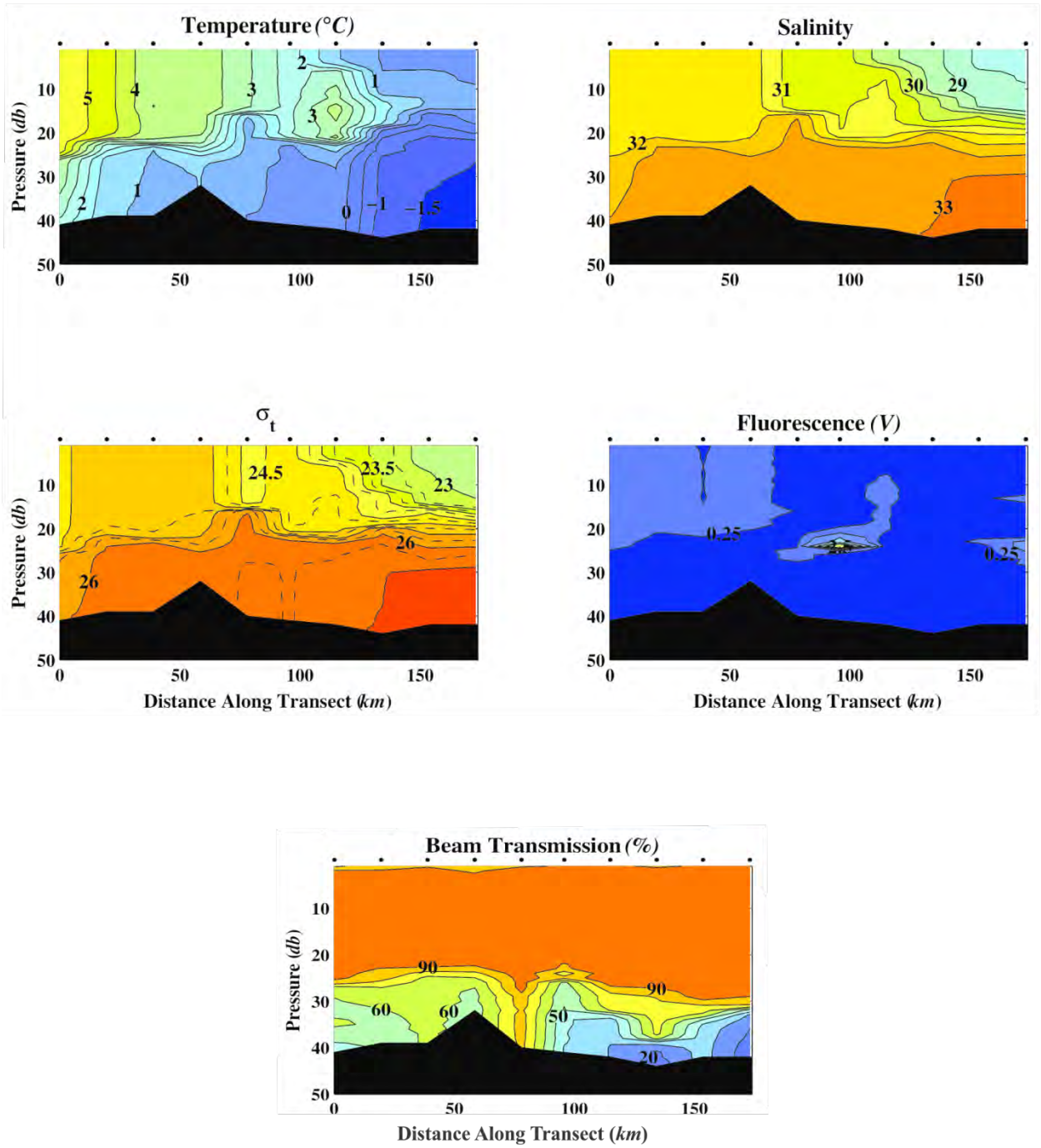

Figure 29. Southwest-northeast (T34_1) section (per **Figure 20**) of temperature, salinity, sigma-t, fluorescence and beam transmission from the 31 August – 3 October 2012 survey.

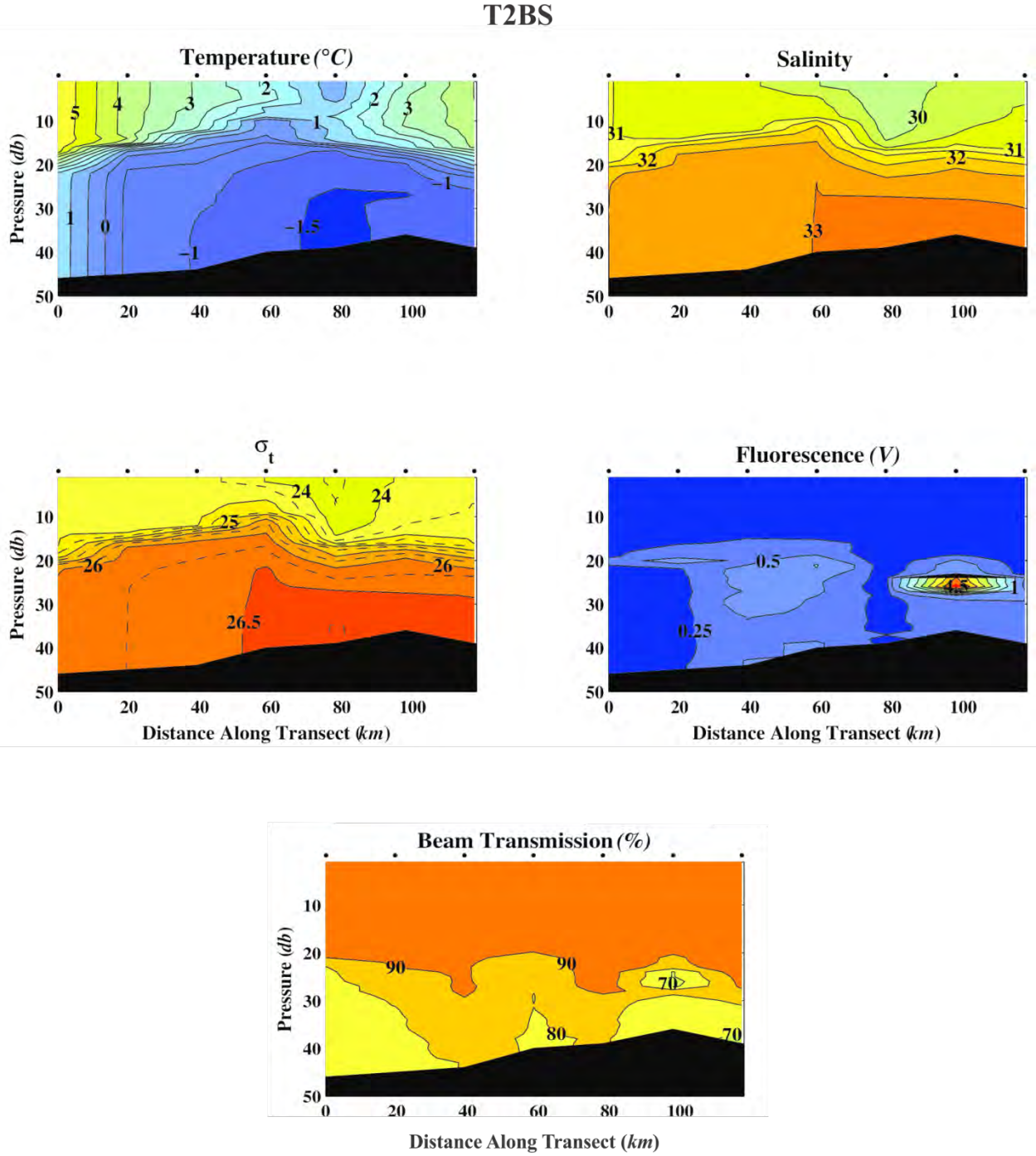

Figure 30. Southeast-northwest (T2BS) section (per **Figure 20**) of temperature, salinity, sigma-t, fluorescence and beam transmission from the 16 – 26 August 2012 survey. Burger stations are on the left side of each panel and Statoil stations are on the right side of each panel.

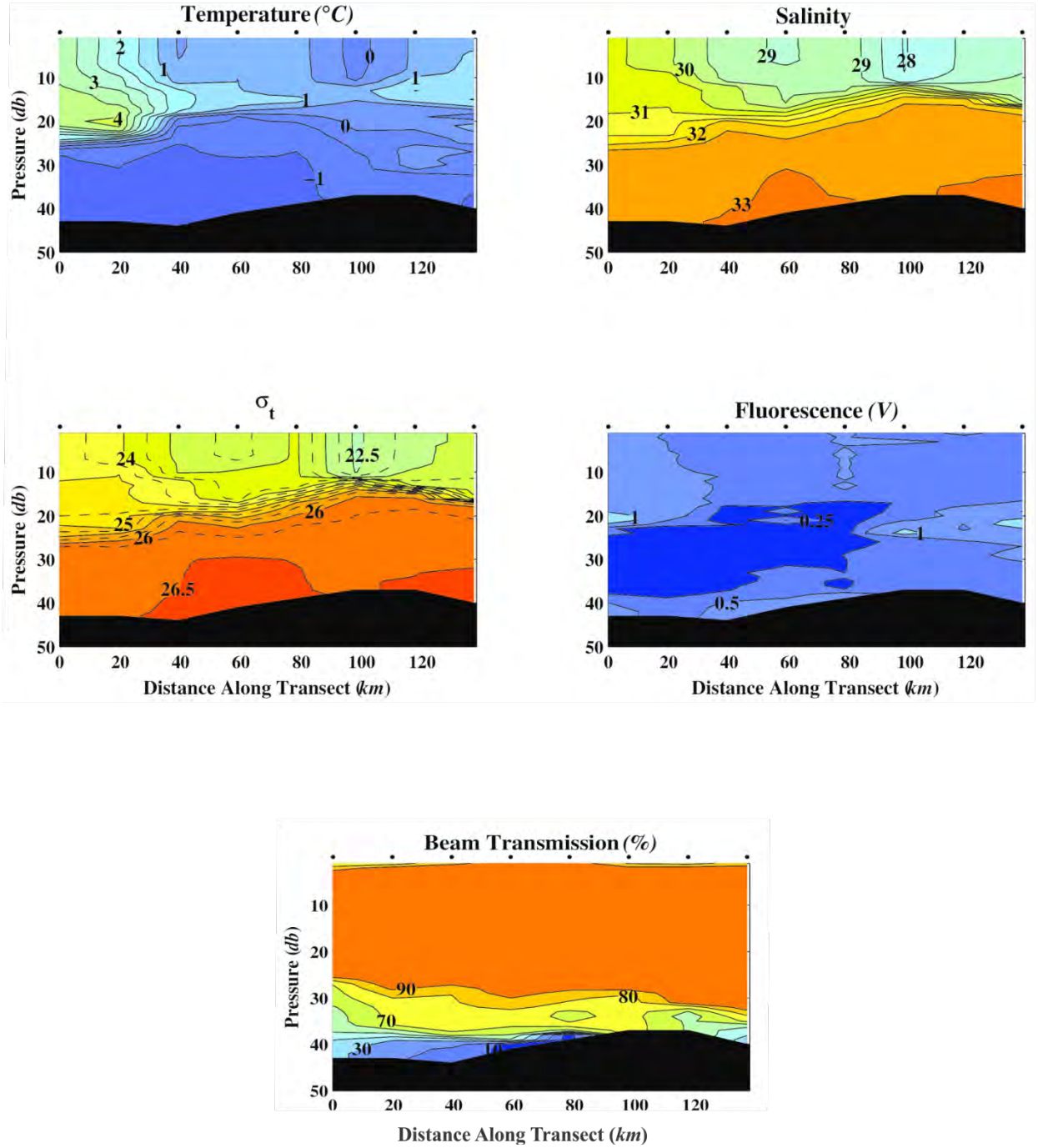

Figure 31. Southeast-northwest (T34BS1) section (per **Figure 20**) of temperature, salinity, sigma-t, fluorescence and beam transmission from the 31 August - 3 October 2012 survey. Burger stations are on the left side of each panel and Statoil stations are on the right side of each panel.

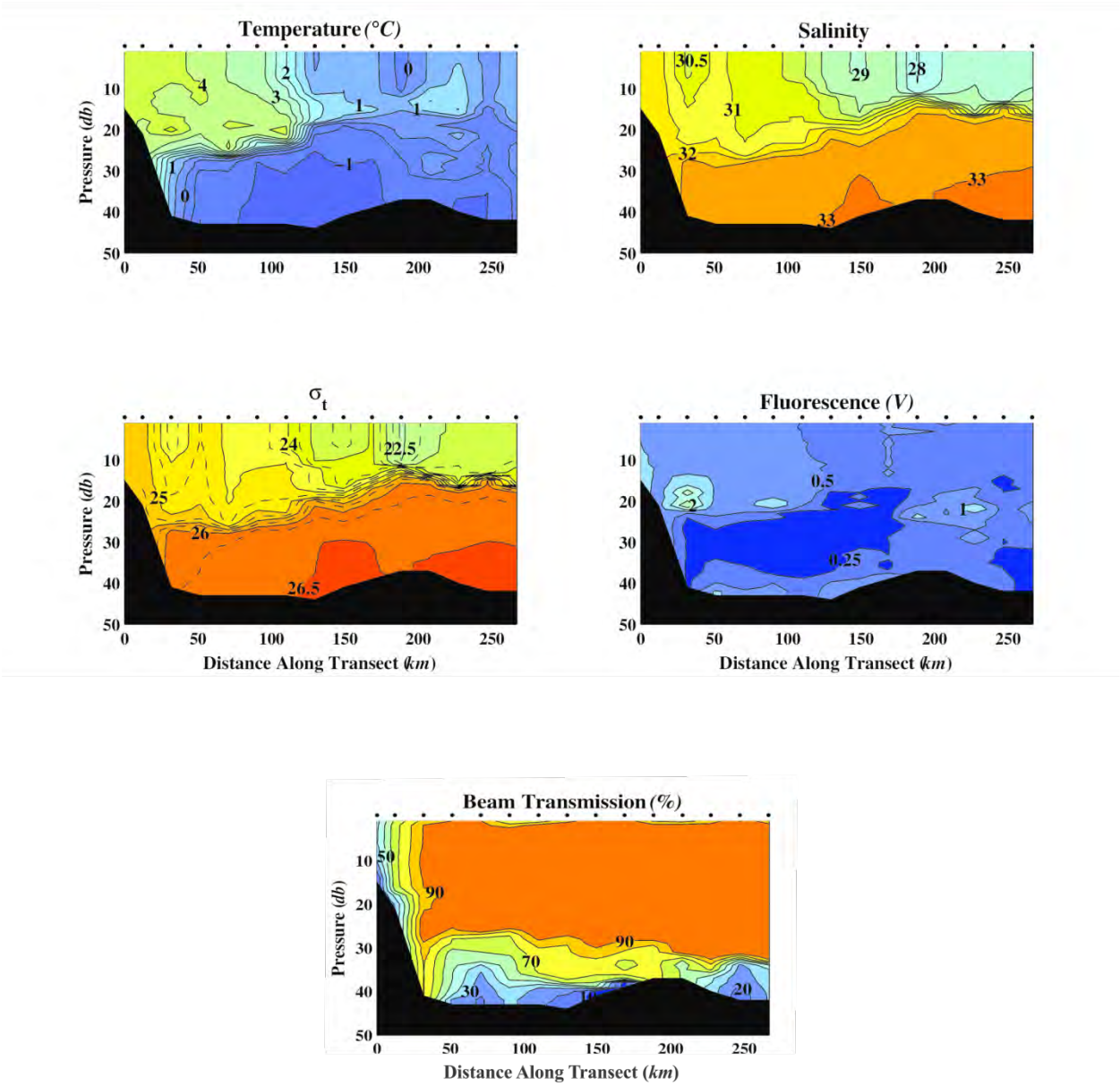

Figure 32. Southeast-northwest (T34BS2) section (per figure 23) of temperature, salinity, sigma-t, fluorescence and beam transmission from the 31 August - 3 October 2012 survey. Burger stations are on the left side of each panel and Statoil stations are on the right side of each panel.

Figures 33 – 37 show a sequence of five transects that run from the southwest to the northeast across the sampling grid. The figures are organized with the westernmost transect (T34_SWNE1) in **Figure 33** and the easternmost transect (T34_SWNE4) in **Figure 37**. On all transects transmission values ranged between 50 and 80% within 15 m of the bottom and were ≥90% above this depth. Fluorescence values are also small throughout the area except on the southernmost portions of SWNE1 and SWNE2, where these values are ~1.5; the highest values observed in 2012. Meltwater occupies the upper 15 m over the northern 150 km half of each section. However, the front separating meltwater from Bering waters to the south strengthened progressing from west to east (at least as far east as T34-3) and the meltwaters in the east were more dilute than those to the west. Winter waters were observed along the bottom over the northern half of each section, although the densest waters (temperatures ≤ -1.5 C and salinities ≥ 33) were more abundant to the east. As a consequence of these zonal gradients in meltwater and bottom waters, the pycnocline strengthened from west to east. Note also that the temperatures were warmer and salinities higher the northernmost portion of each meltwater pool on transects SWNE1, SWNE2, SWNE3 and T34-3. These sections either bracket or cross over Hanna Shoal. Hence the meltwater distribution is consistent with the ice maps, which indicated that Hanna Shoal was the last place within the survey grid that became ice-free.

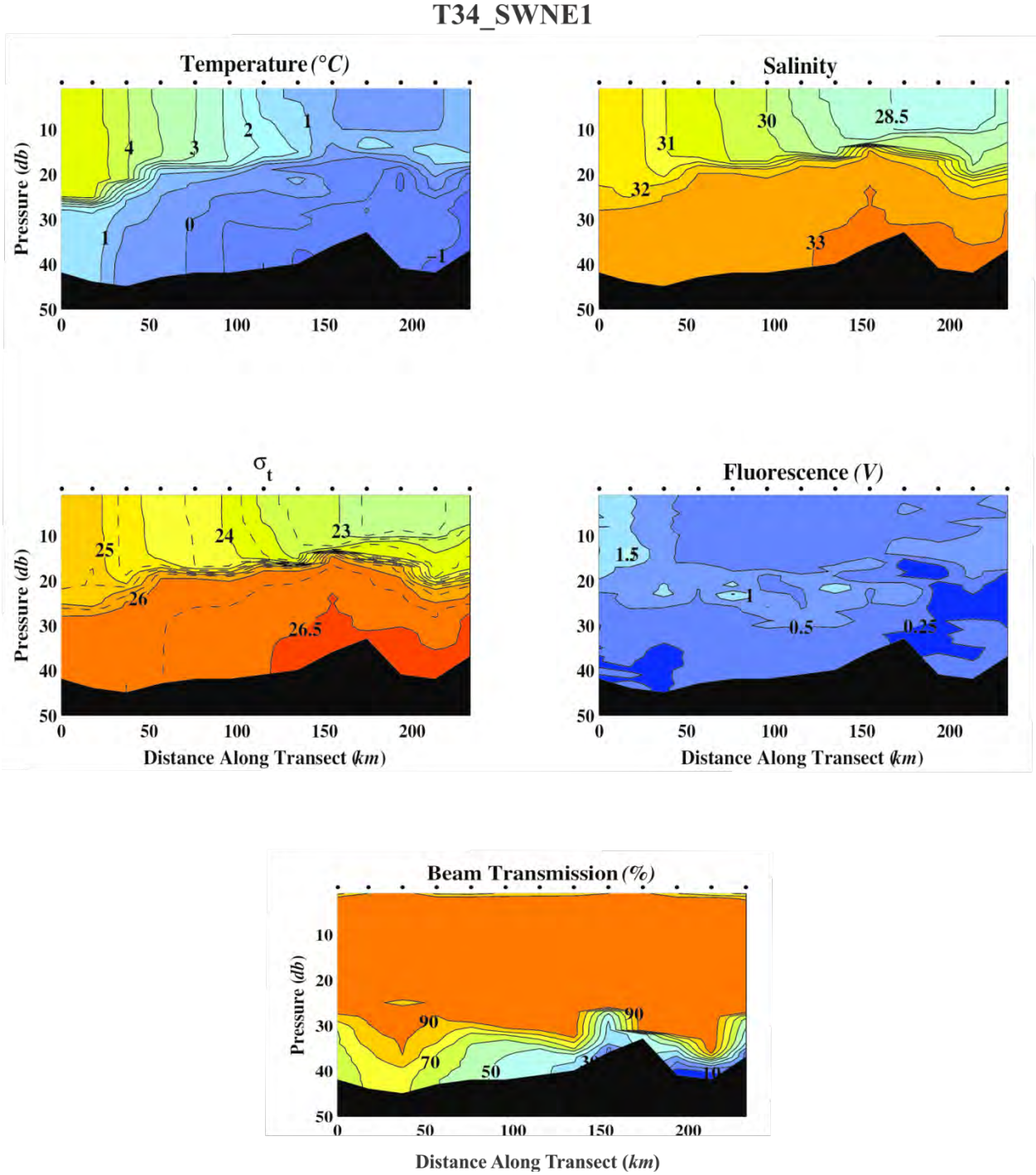

Figure 33. Southwest-northeast (SWNE1) section (per **Figure 20**) of temperature, salinity, sigma-t, fluorescence and beam transmission from the 31 August - 3 October 2012 survey.

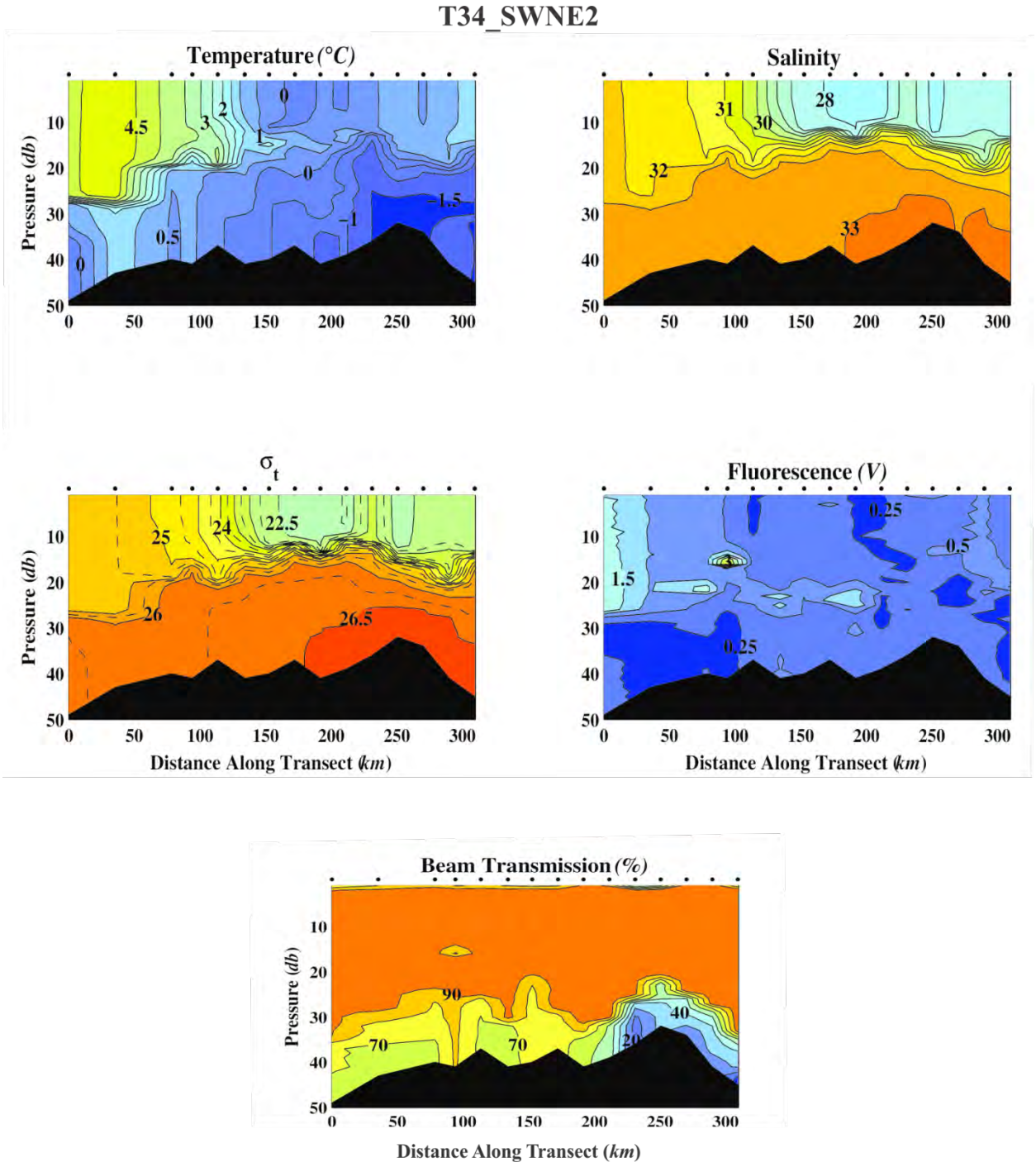

Figure 34. Southwest-northeast (SWNE2) section (per **Figure 20**) of temperature, salinity, sigma-t, fluorescence and beam transmission from the 31 August - 3 October 2012 survey.

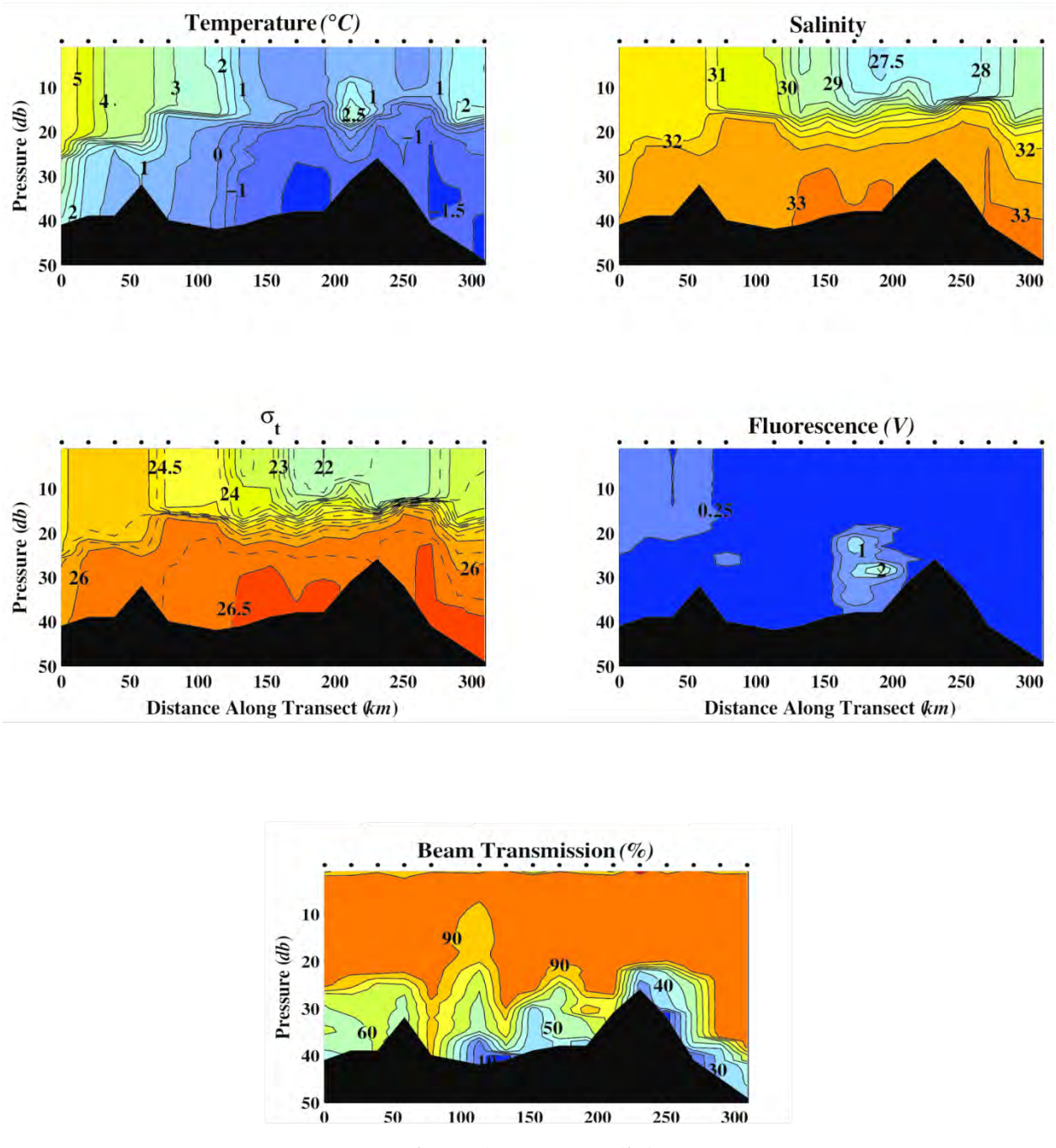

Figure 35. Southwest-northeast (SWNE3) section (per **Figure 20**) of temperature, salinity, sigma-t, fluorescence and beam transmission from the 31 August - 3 October 2012 survey.

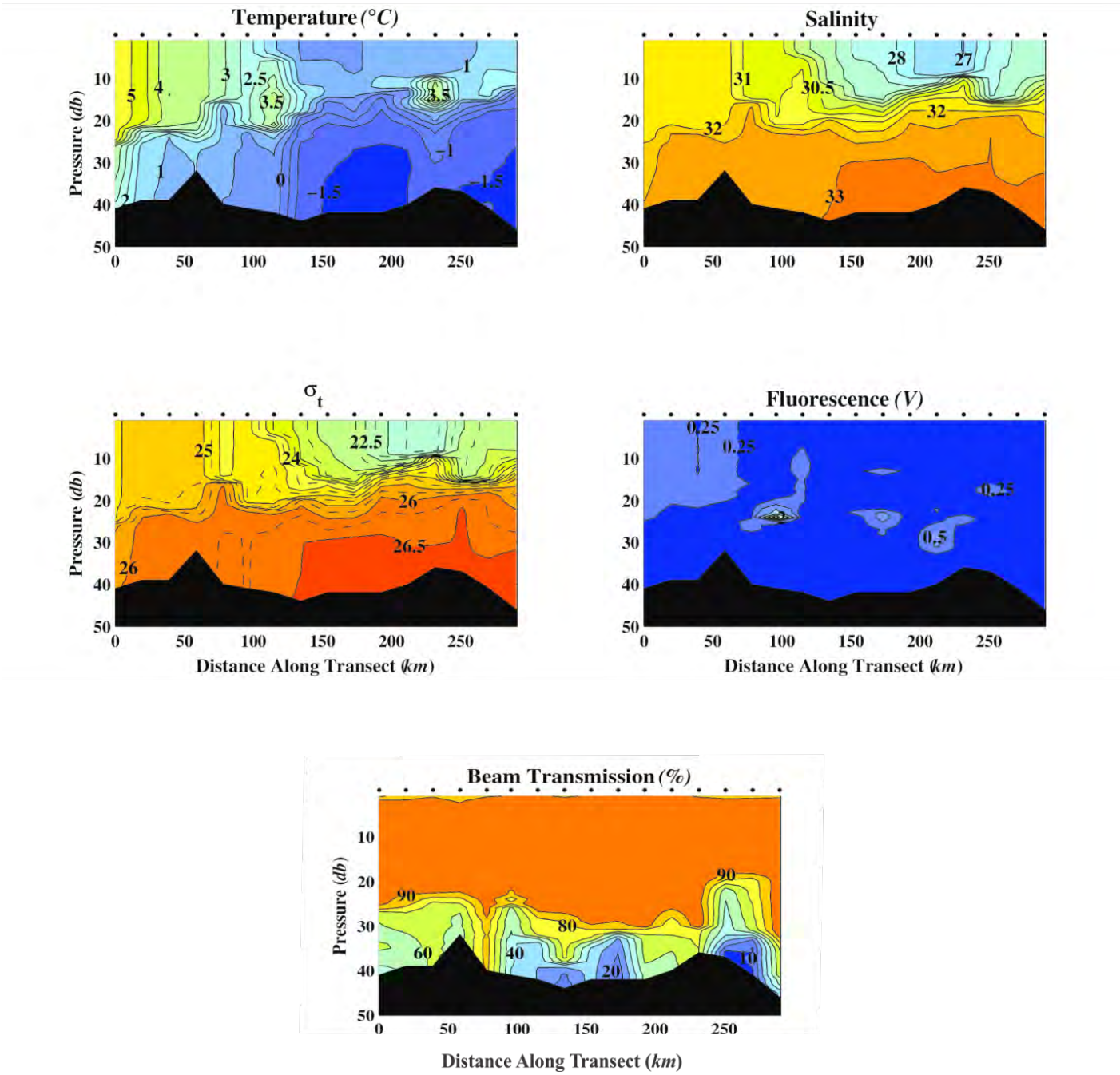

Figure 36. Southwest-northeast (T34-3) section (per **Figure 20**) of temperature, salinity, sigma-t, fluorescence and beam transmission from the 31 August - 3 October 2012 survey.

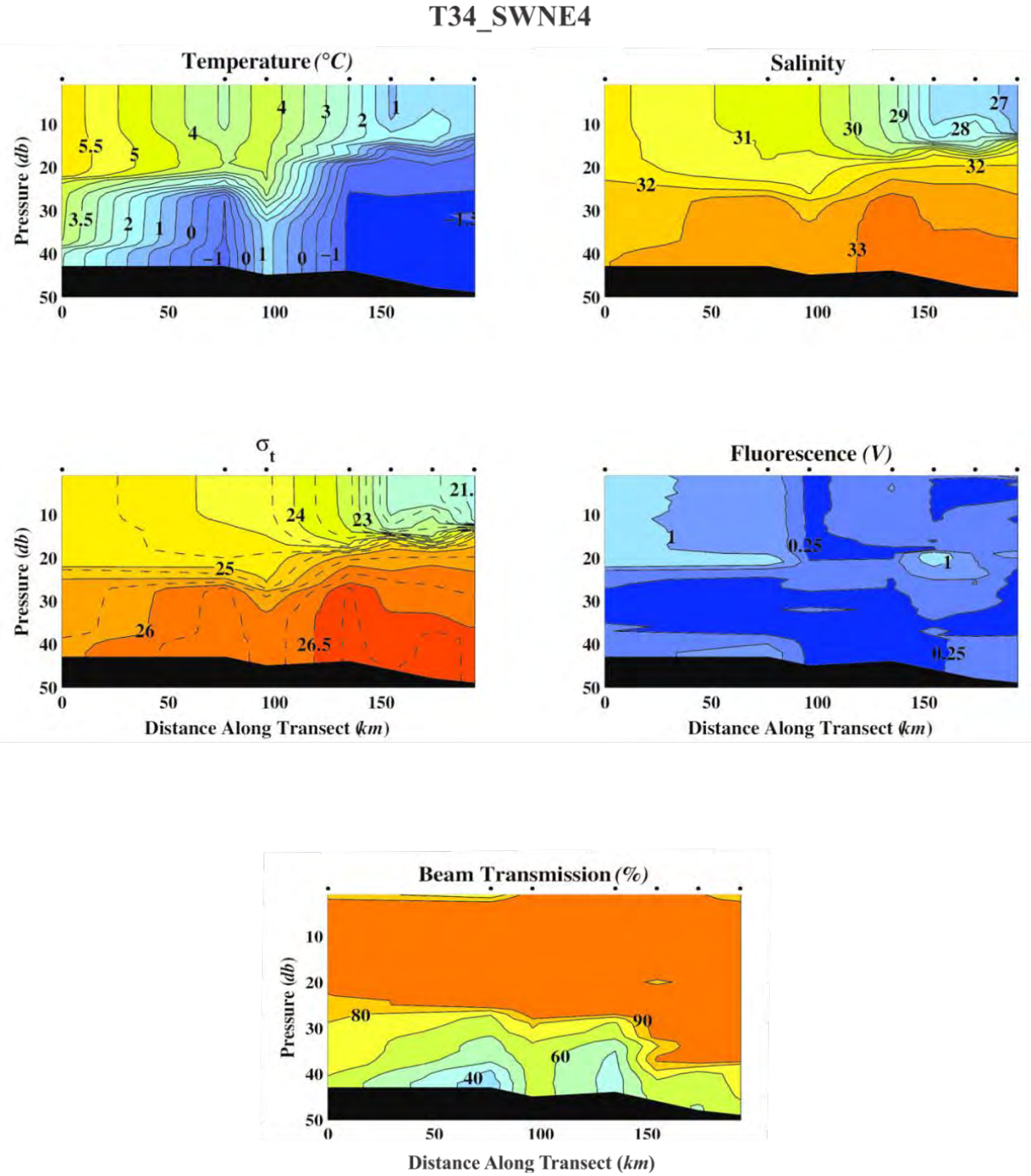

Figure 37. Southwest-northeast (SWNE4) section (per figure 23) of temperature, salinity, sigma-t, fluorescence and beam transmission from the 31 August - 3 October 2012 survey.

We conclude this section by examining the horizontal distributions of temperature and salinity averaged over the upper 10 m (**Figure 38**) and the bottom 5 m (**Figure 39**). The surface maps indicate that during the first cruise warm, moderately saline water was present in Klondike. It had not penetrated very far northward by the time of the second cruise. In fact the surface temperatures and salinities actually decreased in Statoil and the southern half of Burger during the second cruise as meltwater encroached on these areas. Presumably this was due to increasing strength of the winds from the northeast. The meltwater formed a west-east thermohaline front along about 71^{o} 30'N. The maps suggest that this front trended northward to at least 72 ^{o}N along ~165 ^{o}W (although the data in this region is somewhat sparse). On the other hand bottom temperatures increased and salinities decreased in Statoil and the southern half of Burger between the two sets of cruises, indicating that the winter waters were slowly being replaced at these locations by BSW. However, the changes were much smaller than those which occurred in previous years. As apparent in the bottom salinity distribution on T34 (lower right, **Figure 39**) a considerable amount of dense winter water resided around Hanna Shoal. Moreover the coldest water extended as a tongue from the northeast side of Hanna Shoal into the northeast corner of Burger, before curving back toward the east side of Statoil. This cold tongue appears to be associated with the gentle, north-south oriented trough along the east side of Hanna Shoal (**Figure 2**), which then extends into the northeast side of Burger.

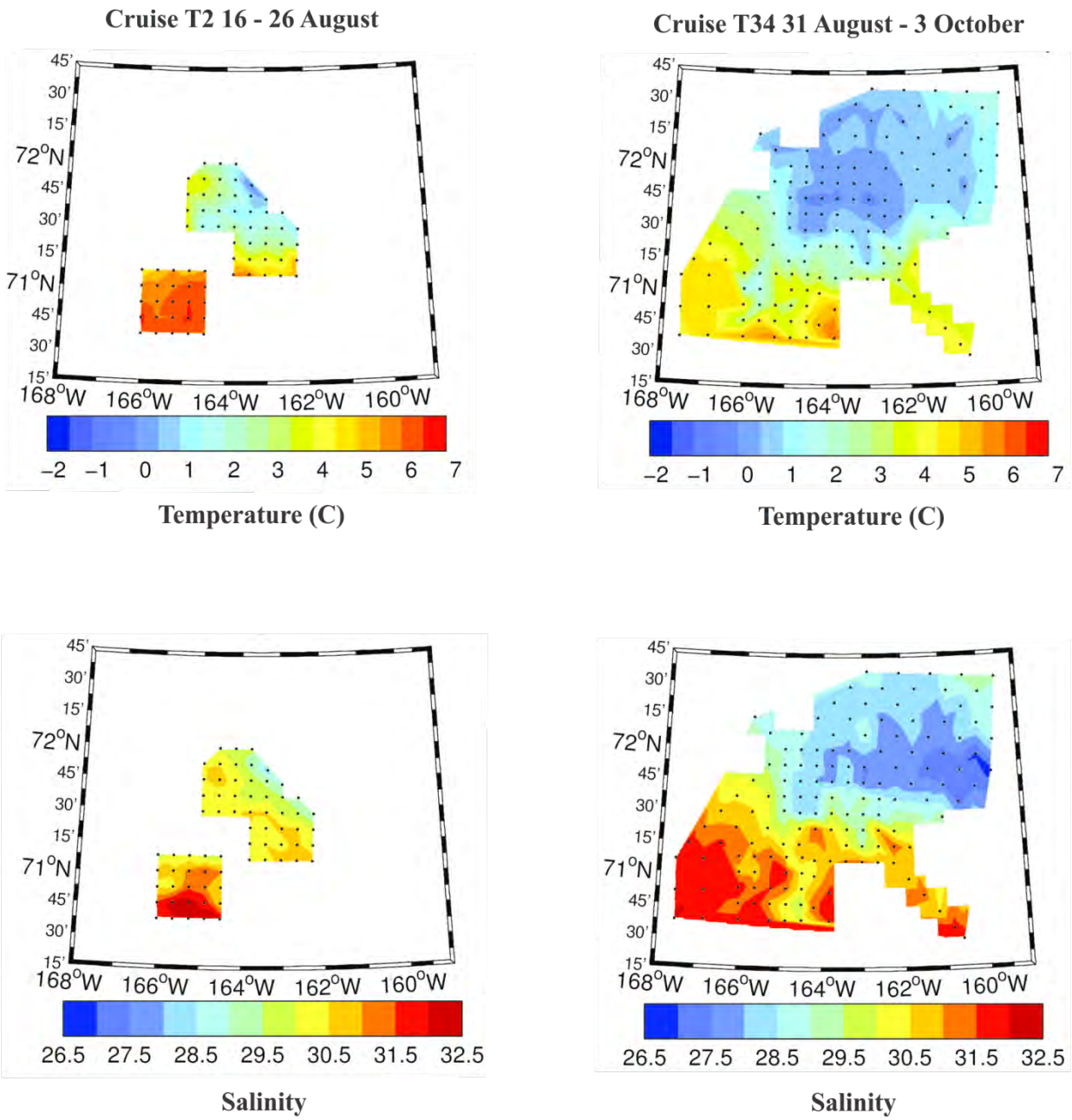

Figure 38. Average temperatures (top) and salinities (bottom) over the uppermost 10 m of the water column for Cruises T2 (left) and T34 (right).

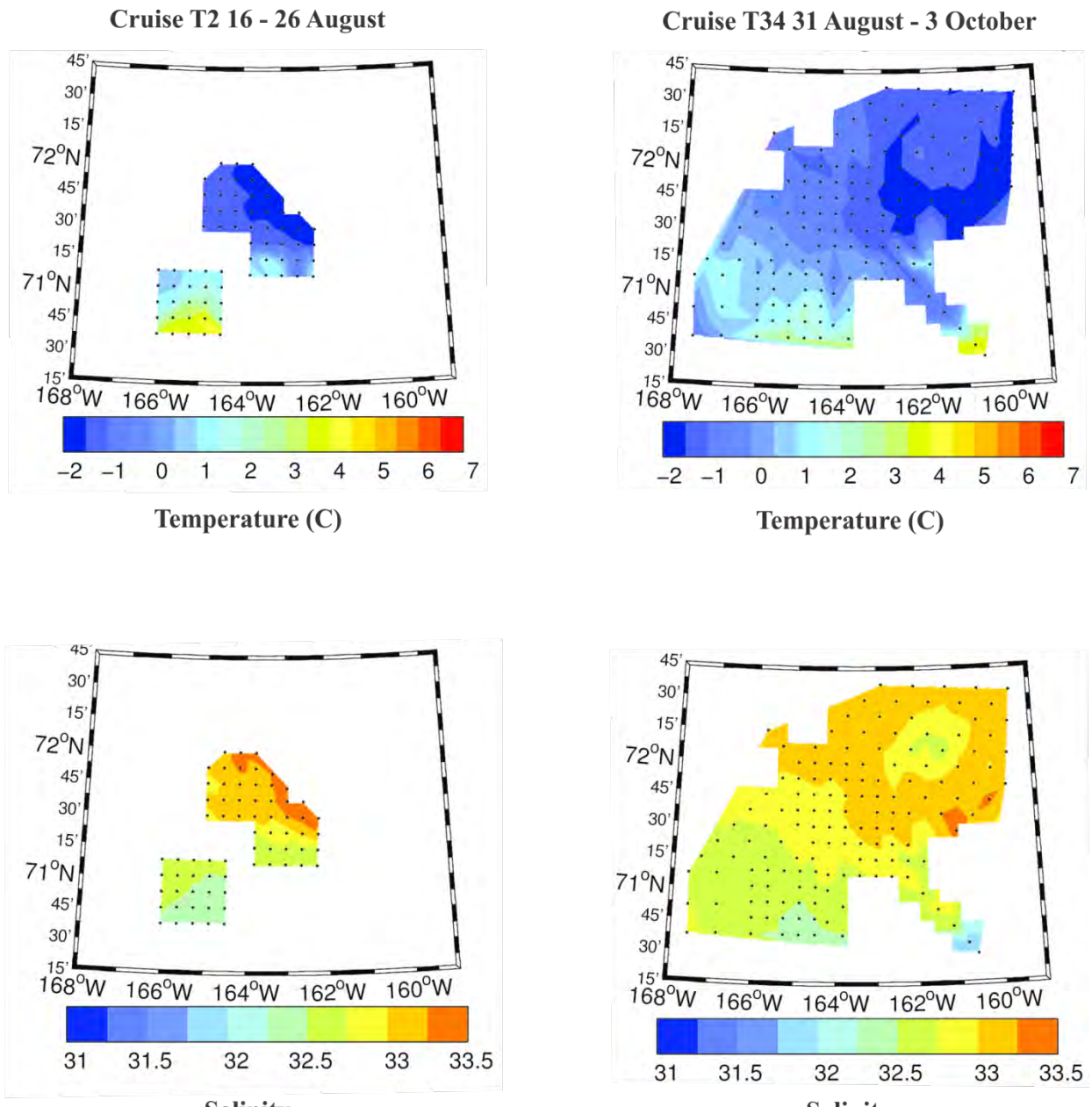

Figure 39. Average temperatures (top) and salinities (bottom) over the bottom 5m of the water column for Cruises T2 (left) and T34 (right).

Surface Velocity Maps

We present a subset of surface current maps gathered from shore-based high frequency radars (HFR) over the 2012 season. The maps should be regarded as approximate since the data are still undergoing quality control and editing. Moreover, the coverage in August is spatially gappy due to power issues at Pt. Lay and/or ice interference, or low ocean wave energies. Nevertheless these data provide a qualitative overview of several circulation features.

As previously noted, during most of August the winds were from the south. The current maps during much of this month (**Figures 40 – 41**) indicate that the flow over the northeastern Chukchi shelf was generally to the northeastward along the coast and eastward between 70^{o} 30'N and 71^{o} 30'N and between 163^{o} and 166^{o} W. The HFR maps are in general agreement with the vessel-mounted ADCP data collected between 10 – 25 August (**Figure 42**). The observed circulation pattern appears to be typical during periods of either low winds or winds from southerly quadrants (Weingartner et al., 2013). The surface flow field would enhance the northward movement of summer waters from the Bering Sea and the retreat of meltwater across the northeastern shelf.

Beginning in late August the southerly winds collapsed and northeasterlies began to develop (**Figure 6**). We speculate that this wind transition was accompanied by enhanced mesoscale activity associated with meanders along meltwater fronts across which the surface circulation is convergent. (Several of these frontal systems are inferred based on patterns of surface flow convergence as indicated by the yellow curves on several of the current maps.) By August 31 (**Figure 44**, top panel) the northeasterly winds were sufficiently strong that the shelf circulation had reversed and the flow, being largely toward the southwest, would have enhanced southward advection of ice and meltwater. Throughout much of September, however, the flow was variable, being occasionally southward or northward over the shelf, or variable as exemplified in **Figures 45 and 46**. The circulation front inferred on September 20 (e.g., **Figure 45**, top panel) indicates flow convergence (delineated by a yellow curve) clearly with a westward flow north of the front and eastward flow south of the front. The front's position in **Figure 45** agrees with the position of the front based on the SWNE3 and the T34-3 transects (**Figure 35** and **36,** respectively) and the surface distribution of salinity and temperature (**Figure 38**). In aggregate these all suggest that the front was present along ~71^{o} 30'N and between 160^{o} and 162^{o} W. As suggested by the yellow curve on the September 25 map (**Figure 46**, bottom panel), the eastern portion of the 20 September front had migrated northward to ~71^{o} 45'N by the 25th and was detectable along about 72^{o}N on 3 October (**Figure 47**, bottom panel). Some care should be taken in interpreting this as frontal migration. It is conceivable that during the conditions noted, the front broadened (became weaker) and vertical mixing was enhanced by the strong winds from the northeast. When these winds relax the front can reform, although frontal reformation may occur at a new location.

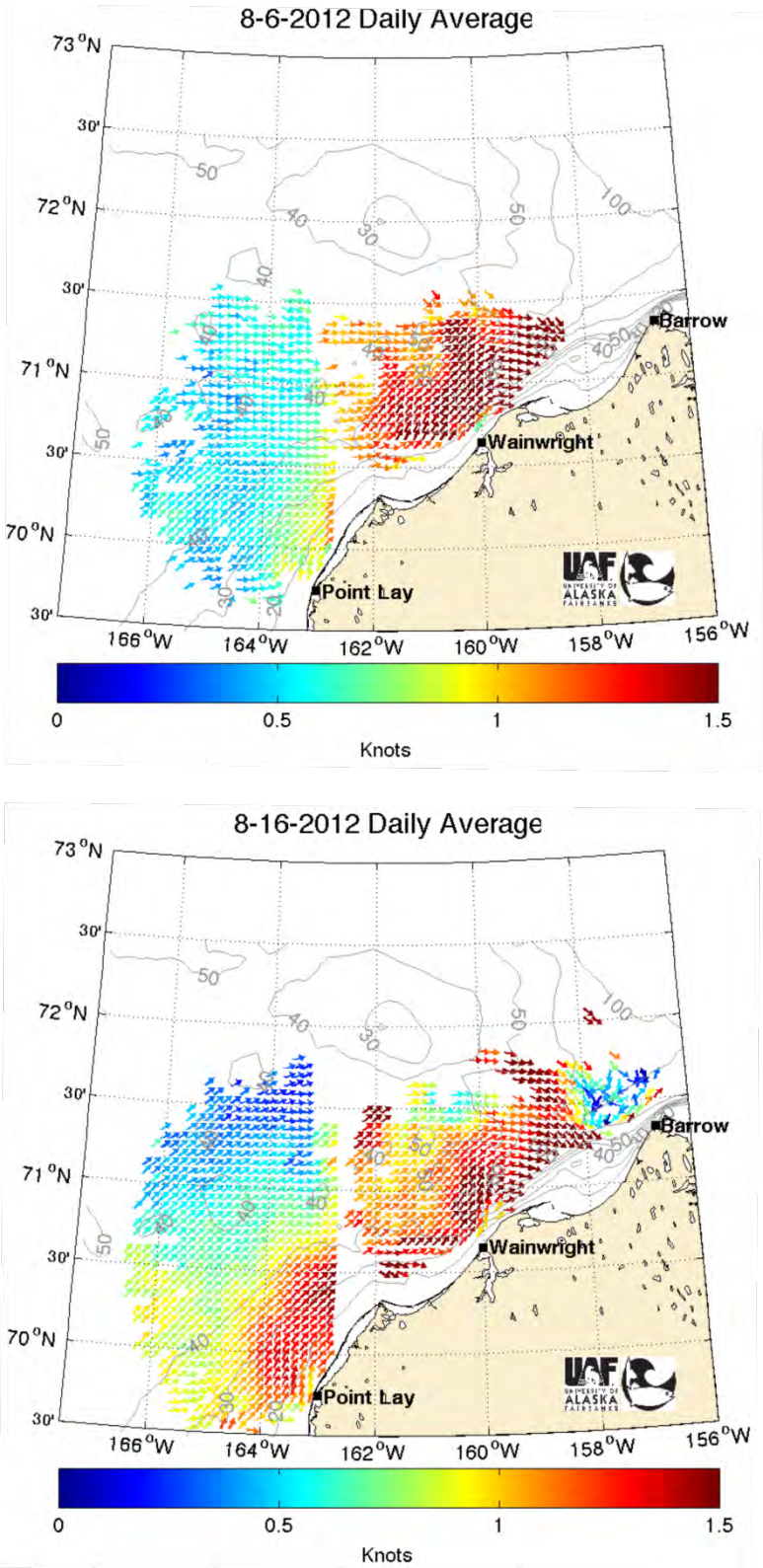

Figure 40. Mean daily surface currents derived from HFR for 6 and 16 August.

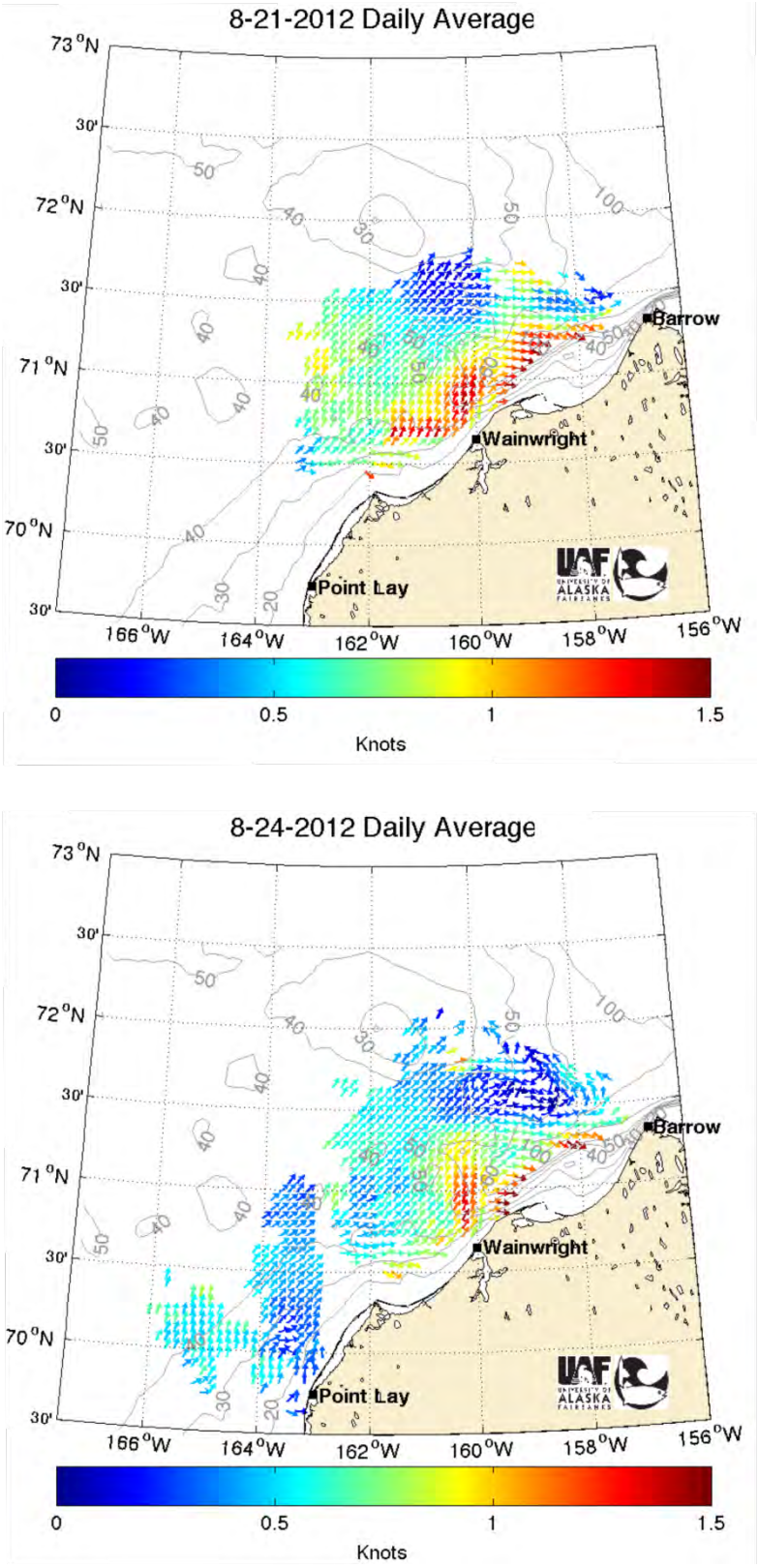

Figure 41. Mean daily surface currents derived from HFR for 21 and 24 August.

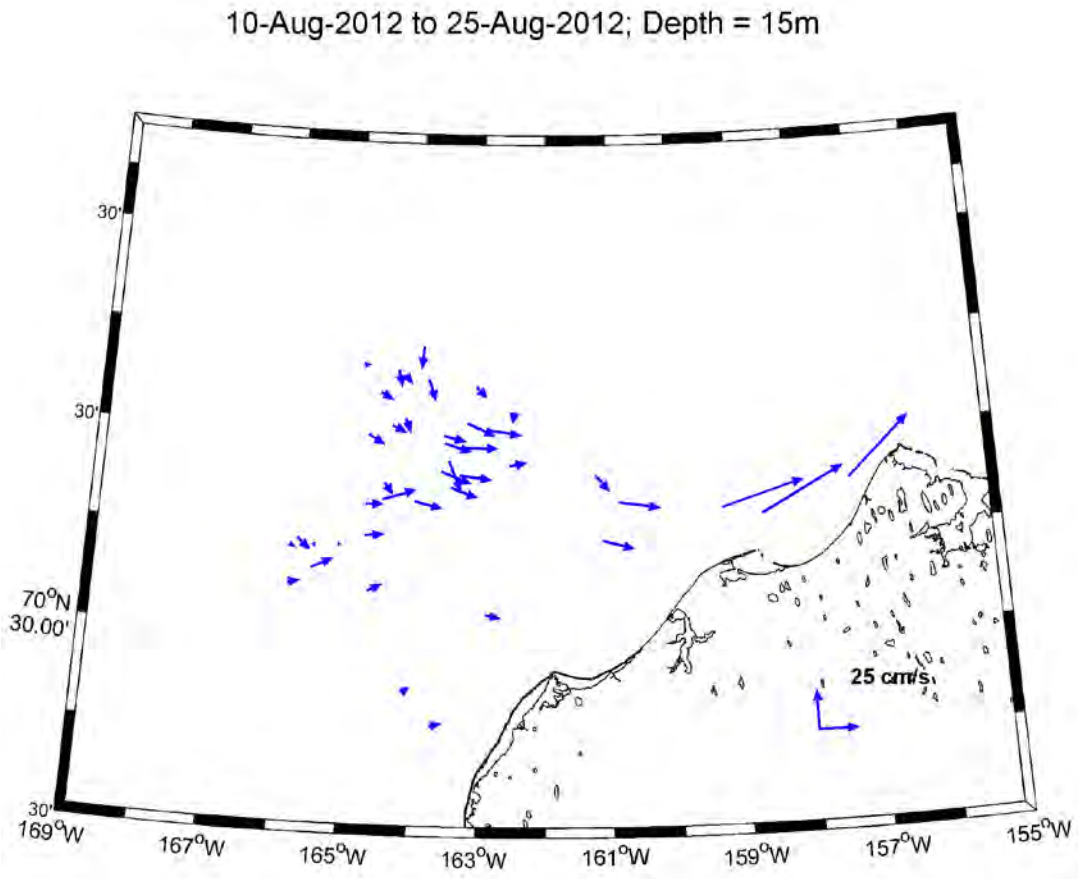

Figure 42. Vessel-mounted ADCP data based on all good ensembles averaged over 6-hour periods in August 2012.

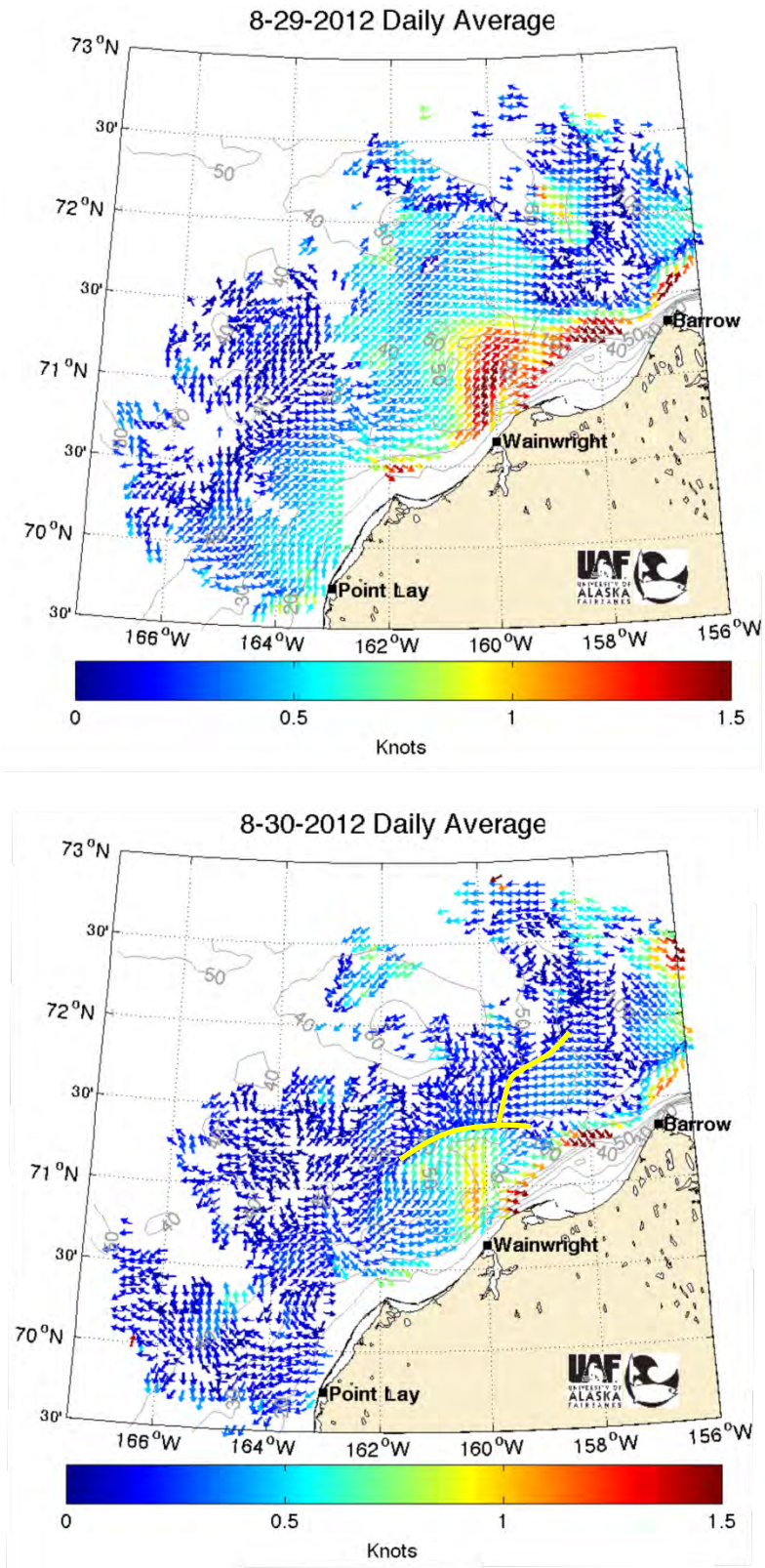

Figure 43. Mean daily surface currents derived from HFR for 29 and 30 August. The yellow curves (bottom panel) are inferred fronts.

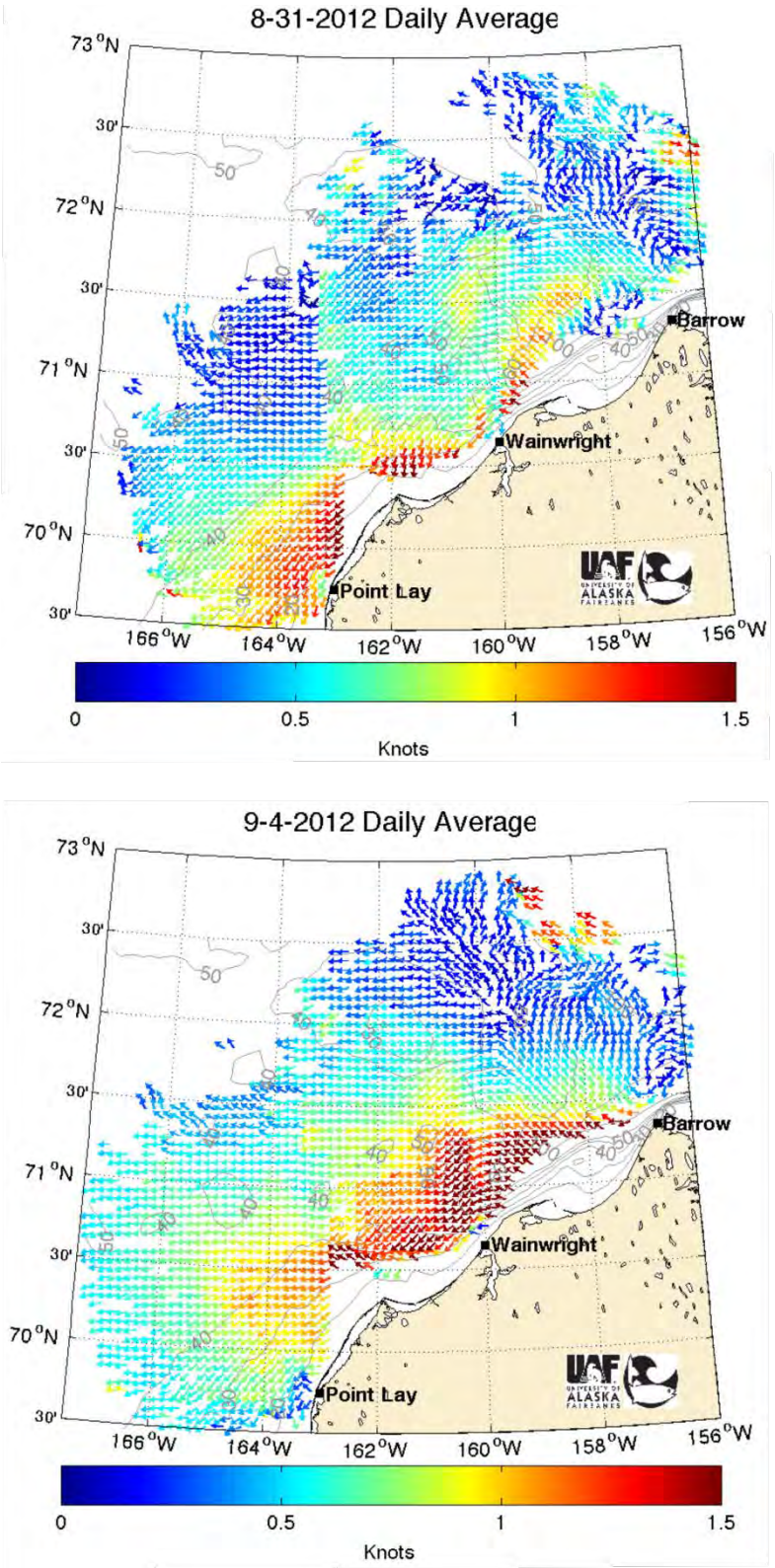

Figure 44. Mean daily surface currents derived from HFR for 31 August and 4 September.

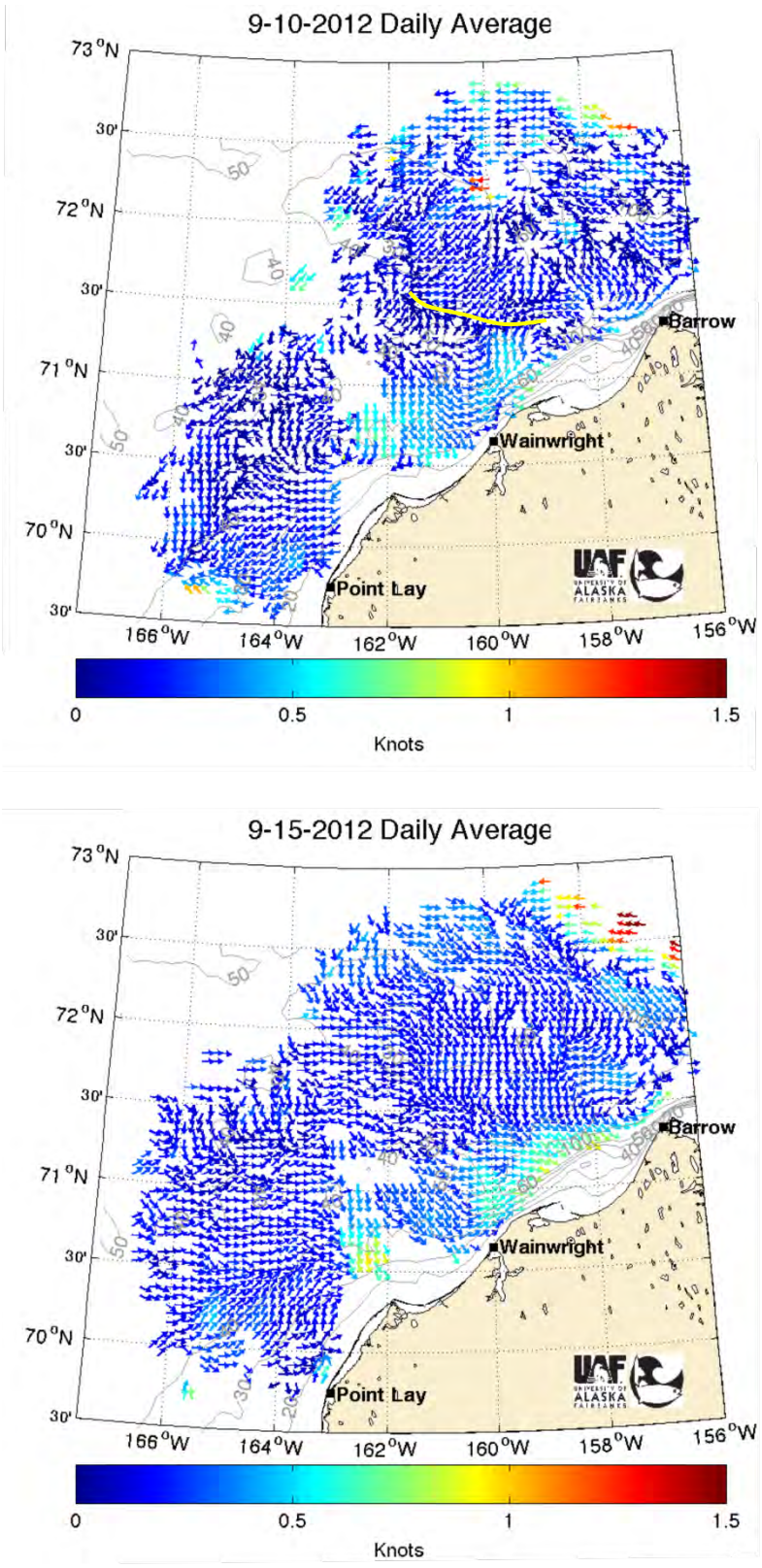

Figure 45. Mean daily surface currents derived from HFR for 10 and 15 September. The yellow curve (top panel) is an inferred meltwater front.

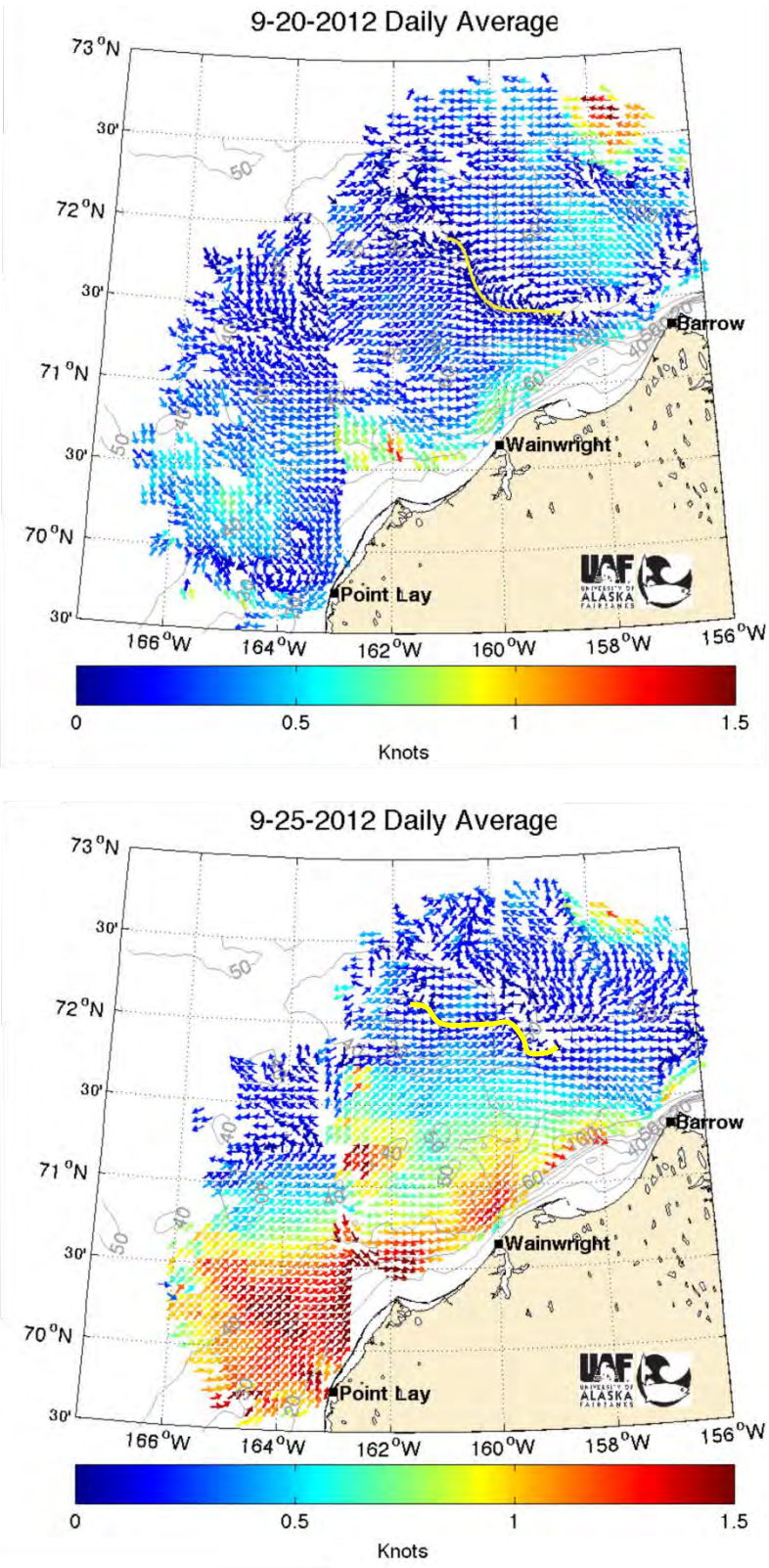

Figure 46. Mean daily surface currents derived from HFR for 20 and 25 September. The yellow curves are inferred meltwater fronts.

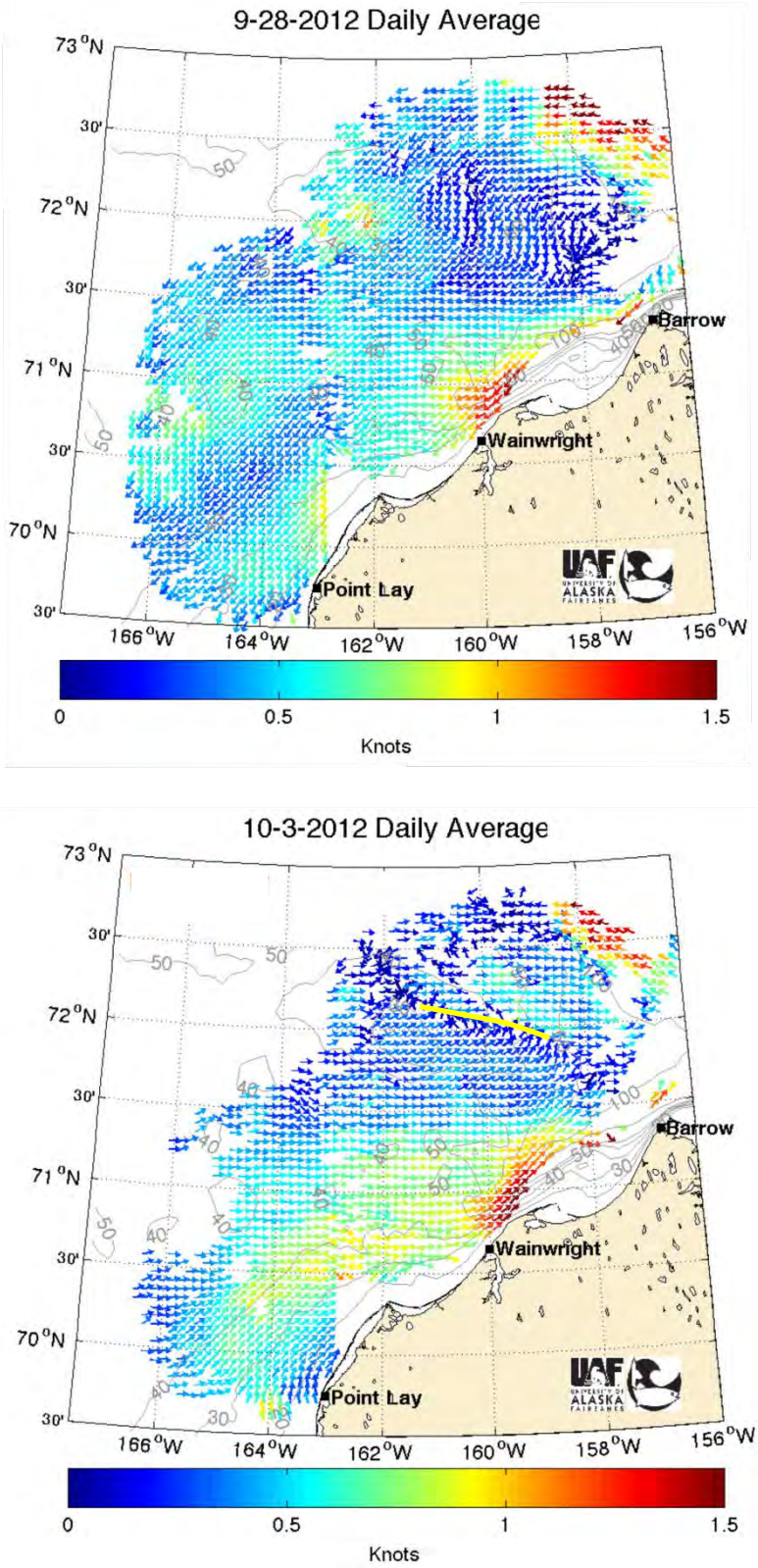

Figure 47. Mean daily surface currents derived from HFR for September and 3 October. The yellow curve (bottom panel) is an inferred meltwater fronts.

Discussion and Conclusions

The salient feature of the 2012 survey was the extent and persistence of sea ice in the northeastern Chukchi Sea. The ice persistence was a regional feature and limited to the northern Chukchi shelf, even though record ice retreat occurred over the Arctic Ocean in summer-fall 2012. We suggest that ice persistence in the Chukchi Sea was related to the grounding of large multi-year ice floes on Hanna Shoal during the preceding winter. Once grounded, these floes probably coalesced into a much larger ice sheet as first-year ice was advected against the grounded sheet and subsequently deformed. Attachment and deformation would increase the volume and area of the ice on Hanna Shoal. Consequently, ice retreat and melting proceeded slowly in the summer of 2012 compared to previous years. Moreover, as stated in earlier reports, Hanna Shoal serves as a reservoir for meltwater on the northeastern Chukchi shelf, since the circulation here is isolated by the shoal bathymetry from the rest of the shelf. The extensive ice cover in 2012 undoubtedly increased the volume and temporal extent of meltwater available to the shelf throughout summer and fall.

The meltwater, with salinities ranging from 27 – 30 was generally confined to the upper 15 m of the water column and overlaid very dense winter waters having salinities $\geq$32.5, and, in some areas, approaching 33.5. This resulted in a very strongly stratified "2-layer" water column, which persisted well into fall. This contrasts with many of the previous years, in which stratification weakened in fall as more of the moderately stratified BSW is advected over the shelf and displaces the 2-layer structure. This replacement was more limited in 2012 and largely confined to Klondike, southern Burger, and to a lesser extent in the western portion of Statoil.

The reasons for this sluggish replacement are not completely clear. The winds in August were from southerly quadrants, which should enhance northward transport of Bering waters. Indeed the surface currents estimated from shore-based radars suggested that the northward flow of surface waters was vigorous and fairly steady through August yielding a surface circulation pattern in broad agreement with inferences drawn from models and prior observations. For example, the tongue of ice retreat along the NW side of Hanna Shoal (**Figures 9 – 13**) for the period of 29 July to 30 August was consistent with northward warm water advection through the Central Channel, which presumably then proceeds clockwise around the north side of Hanna Shoal. This is also consistent with our findings that the water properties in the Central Channel and south of the regions encompassed by melt and winter waters were quite similar to previous years surveyed, suggesting that the inflow from Bering Strait was not anomalously cold.

The large volume of meltwater over the shelf was accompanied by an extensive and prominent meltwater frontal system. This front was approximately zonally-oriented and extended from Statoil eastward to Barrow Canyon (with the latter observations made by P. Winsor, personal communication). The front was a convergence zone and was evident in the surface current maps on occasion. When evident the flow was southwestward on the north side of the front and northeastward on the south side. The dynamics of this circulation are beyond the scope of this report, however we suggest the following conceptual model. On both sides of the front the circulation is governed by barotropic pressure gradients (e.g., one in which the pressure gradient is uniform over depth). These pressure gradients reflect the mean pressure gradient between the Pacific and Arctic oceans as well as time-varying sea surface slopes established by sea level slopes associated with the regional winds. The absence of strong horizontal density gradients,

except in areas occupied by meltwater fronts, supports that assumption of barotropic pressure gradients being the dominant component of the shelf pressure field. In general, we believe that the pressure field tends to propel a vertically-uniform eastward flow over the shelf south of Hanna Shoal as suggested by Spall's (2007) model (**Figure 1**). The density field associated with a zonally-oriented meltwater front, as encountered in 2012, would induce westward along-front flow that opposes the flow established by the barotropic pressure gradient. In addition to the barotropic and density-driven pressure fields, the local winds also affect the circulation. In the weakly stratified waters south of the front the momentum input to the ocean is diffused throughout most of the 40 m deep water column. By contrast, in the heavily stratified areas north of the front, the same momentum is confined to the shallow mixed layer (~10 m) and may be sufficient to overcome (and oppose) the flow induced by the barotropic pressure field.

Several of the hydrographic sections imply that Bering summer waters, having a density intermediate between the meltwater and winter water, subduct along the front and then penetrate laterally into the pycnocline. Hence the warm Bering summer waters may not be directly contributing to lateral ice melt. Rather the subducted flow may be a mechanism by which heat is transferred laterally below the ice and subsequently made available to the underside of the ice by vertical mixing. This suggests that ice melt arises through a complicated advective-diffusive balance, whose attributes are dictated by the strength and position of the front, the pycnocline, and the properties of the Bering waters.

The front(s) also appeared to be highly mobile as reflected by changes in both the meltwater distribution and its signatures in the surface current maps. Meltwater (ice-edge) fronts are known to be dynamically variable and are often accompanied by meanders and eddies spawned by frontal instabilities. Although winds are an important source of current variability on the Chukchi shelf, the instabilities would add an additional level of both temporal and spatial variability to the circulation. As a consequence, the shelf circulation in summer 2012 may have been more variable than in previous years.

Although an extensive comparison among years will not be made here, it is worth noting a couple of the large differences between 2011 and 2012. The summer and fall of 2011 were characterized by a near absence of meltwater in the survey area, due to a rapid ice retreat early in the season. This was associated with weak shelf stratification and with the stratification being mainly due to vertical temperature gradients. In 2012, the late ice retreat in conjunction with the copious amounts of meltwater maintained the stratification well into fall and the stratification was established by vertical salinity gradients. In addition, the winter waters in 2012 were generally more saline (denser) than those in 2011. The reasons for this are unclear. It may be that denser water formed in winter 2011-2012 than winter 2010-2011. This could have occurred if the grounded ice on Hanna Shoal promoted polynya formation on the lee side of the ice throughout winter. These regions of open water are capable of forming large volumes of frazil ice that are then swept downwind leaving very salty waters behind and within the polyna. If this process occurred repeatedly through the winter of 2011-12, then we might expect denser waters around Hanna Shoal compared to 2011. On the other hand it may well be that the densest fractions of winter water were quickly removed in summer 2011 and therefore were not evident at the time of those surveys.

References.

Coachman, L. K., Aagaard, K., Tripp, R.B., 1975. Bering Strait: The Regional Physical Oceanography, Univ. of Washington Press, Seattle, 172 pp.

Mesinger, F., and 19 Coauthors, 2006. North American regional re-analysis, *Bull. Amer. Meteor. Soc.*, 87, 343–360.

Pickart, R.S., Weingartner, T., Pratt, L.J., Zimmermann, S., Torres, D.J., 2005. Flow of winter-transformed Pacific water into the western Arctic. Deep-Sea Research, Part II 52: 3175 - 3198.

Shroyer, E. L., Plueddemann, A.J., Wind-driven modification of the Alaskan coastal current. Journal of Geophysical Research, accepted.

Spall, M. A., 2007. Circulation and water mass transformation in a model of the Chukchi Sea. *Journal of Geophysical Research* 112, C05025,doi:10.1029/2005JC002264.

Spreen, G., Kaleschke, L., Heygster, G., 2008. Sea ice remote sensing using AMSR-E 89 GHz channels. *Journal of Geophysical Research* 113, C02S03, doi:10.1029/2005JC003384.

Walsh, J.J., McRoy, C.P., Coachman, L.K., Goering, J.J., Nihoul, J.J., Whitledge, T.E., Blackburn, T. H., Parker, P.L., Wirick, C.D., Shuert, P.G., Grebmeier, J.M., Springer, A.M., Tripp, R.D., Hansell, D.A., Djenedi, S., Deleersnijder, S., Henriksen, K., Lund, B.A., Andersen, P., Müller-Karger, F.E., Dean, K., 1989. Carbon and nitrogen cycling within the Bering/Chukchi seas: Source regions for organic matter affecting AOU demands of the Arctic Ocean. Progress in Oceanography 22, 277-359.

Weingartner, T., E. Dobbins, S. Danielson, P. Winsor, R. Potter, and H. Statscewich. Hydrographic variability over the northeastern Chukchi Sea shelf in summer-fall 2008–2010. 2013a. Continental Shelf Research. http://dx.doi.org/10.1016/j.csr.2013.03.012

Weingartner, T., P. Winsor, R. Potter, H. Statscewich, and E. Dobbins. 2013b. Application of High Frequency Radar to Potential Hydrocarbon Development Areas in the Northeast Chukchi Sea. *Final Report to the* U.S. Department of the Interior Bureau of Ocean Energy Management, Alaska Outer Continental Shelf Region, ConocoPhillips, Inc., and Shell Exploration & Production Company (Contract No: M09AC15207 as part of the BOEM Alaska Environmental Studies Program). 162 p.

Weingartner, T., Aagaard, K., Woodgate, R., Danielson, S., Sasaki, Y., Cavalieri, D., 2005. Circulation on the North Central Chukchi Sea Shelf. Deep-Sea Research, Part II 52: 3150-3174, doi:10.1016/j.dsr2.2005.10.015.

Winsor, P., Chapman, D. C., 2004. Pathways of Pacific Water across the Chukchi Sea: A numerical model study. *Journal of Geophysical Research* 109, C03002, doi: 1029/2003JC001962.

Woodgate, R.A., Aagaard, K., Weingartner, T. J., 2005a. Monthly temperature, salinity, and transport variability of the Bering Strait through flow. Geophysical Research Letters 32, L04601, doi:10.1029/2004GL021880.

Woodgate, R. A., Aagaard, K., Weingartner, T. J., 2005b. A year in the physical oceanography of the Chukchi Sea: Moored measurements from autumn 1990-1991, Deep-Sea Research Part II, *52*(24-26), 3116-3149.